# Experimental Study for High Sonoporation Efficiency

（ソノポレーションの高効率化に向けた実験的研究）

张 祎伟

Experimental Study for High Sonoporation Efficiency
ソノポレーションの高効率化に向けた実験的研究

张 祎伟

# Experimental Study for High Sonoporation Efficiency

（ソノポレーションの高効率化に向けた実験的研究）

Yiwei Zhang

A dissertation Submitted in Partial Fulfillment
of the Requirements of the Degree of

Doctor of Philosophy

The University of Tokyo

Department of Bioengineering
Supervisor: Prof. Yoichiro Matsumoto

2013

# Contents

Chapter 1. Introduction....1
1.1 Background....1
1.1.1 Targeted delivery....1
1.1.2 Delivery systems and vehicles....2
1.2 Ultrasound and acoustic cavitation....3
1.2.1 Ultrasound induced bioeffects....3
1.2.2 Acoustic cavitation....5
1.3 Sonoporation-mediated delivery....6
1.3.1 Sonoporation....6
1.3.2 Mechanism studies....10
1.3.3 Parametric studies....12
1.4 Scope of this thesis....13
Chapter 2. Change of microbubble concentration during ultrasound exposure....17
2.1 Introduction....17
2.1.1 Bubble oscillation and collapse....17
2.1.2 Ultrasound contrast agent (UCA)....22
2.1.3 Light absorbance and concentration....24
2.2 Experimental materials and methods....26
2.2.1 Ultrasound exposure system....26
2.2.2 Burst wave and parameters....28
2.2.3 Laser diode system....29
2.2.4 Exposure protocols....31
2.3 Results and discussions....31
2.3.1 Calibration of concentration and light absorption....31
2.3.2 Acoustic pressure....32
2.3.3 Influence of intensity....35
2.3.4 Influence of pulse duration....42

2.3.5 Influence of PRF ....49
2.4 Summary ....52

Chapter 3. Bubble behavior analysis from cavitation noise ....55
3.1 Cavitation noise ....55
3.1.1 Broadband noise source ....55
3.1.2 Noise spectrum ....57
3.1.3 Two ‘phases’ of cavitation ....59
3.2 Experimental methods ....60
3.2.1 Data collecting unit ....60
3.2.2 Data processing ....64
3.2.3 Irradiation protocols ....66
3.3 Results and discussions ....68
3.3.1 Visible noise ....68
3.3.2 Parametric influence on noise emission ....72
3.4 Summary of bubble behavior ....88

Chapter 4. Ultrasond-mediated delivery *in vitro*: parametric studies on sonoporation efficiency ....91
4.1 Introduction ....91
4.1.1 Delivery via sonoporation *in vitro* ....91
4.1.2 Difference between cell statuses ....91
4.2 Materials ....92
4.2.1 Cell line ....92
4.2.2 FITC-Dextran ....93
4.3 Methods ....95
4.3.1 Irradiation protocol of attachment status ....95
4.3.2 Cell preparing for suspension status ....96
4.3.3 Irradiation protocol of suspension status ....96
4.3.4 Flow cytometry and viability analysis ....97
4.4 Results and discussions ....99
4.4.1 Influence of intensity ....99

4.4.2 Influence of irradiation time ..... 102
4.4.3 Influence of pulse duration ..... 109
4.4.4 Influence of PRF ..... 111
4.5 Correlation between bubble and cell behaviors ..... 113
4.6 Therapeutic ratio ..... 115
4.7 Summary ..... 119
Chapter 5. Conclusions and future directions ..... 121
Bibliography ..... 123
List of Figures ..... 131
List of Tables ..... 135
Biography ..... 137
Publications ..... 139
Acknowledgements ..... 141

# Chapter 1. Introduction

## 1.1 Background

### 1.1.1 Targeted delivery

Difficult diseases, such as cancer, cardiovascular illness, and genetic disorders, have always been the hottest spots in research and clinical fields. Through years, many new therapeutic drugs and medical devices related to gene therapy are invented and developed, aiming to cure these largest obstacles to a healthy human life [1] [2] [3] [4]. In conventional delivery systems, typically oral ingestion and intravascular injection, the medication is distributed throughout the body through the systemic blood circulation. For most therapeutic agents, only a small portion of the medication reaches the organ to be affected. Problems frequently occurring with many conventional drug delivery methods are [5]: poor solubility, insufficient *in vitro* stability (shelf life), too low bioavailability, too short *in vivo* stability (half-life), strong side effects, and lack of large scale production.

As a result, the need of effective administration of these pharmaceutical agents targeted directly to the diseased area is becoming more and more urgent. Such a manner of site-specific delivery, termed targeted delivery, aims to prolong, localize, target and have a protected drug interaction with the diseased tissue. Many of the pharmacological properties of drugs can be improved through targeted delivery because both safety and efficacy are protected [6] [7]. Obviously drug targeting to specific sites in the body requires different delivery systems depending on the delivery route selected [8]. But commonly, there are several key requirements that a targeted delivery system must fulfill: retain, evade, target and release [6]. To be more specific, the characteristics required are listed [5]:

1. Easy to produce
2. Applicable to as many drugs as possible
3. Physically stable

4. Being composed of well tolerated and simultaneously already regulatorily accepted excipients

5. Being able to be produced on large scale

6. Production lines should be able to be qualified and acceptable by regulatory authorities.

Towards these requirements, many delivery systems as well as drug carriers, also called vehicles are developed.

### 1.1.2 Delivery systems and vehicles

Due to the many requirements needed to be fulfilled, targeted delivery is becoming a multidisplinary science consisting of physics, chemistry, biology and pharmacology. Based on their own experience of research, strides from various fields have been made by scientists and researchers. A number of approaches aiming for targeted delivery are developed over the past years. A list of them is shown in Table 1.1 [9] [10] [11] [12] [13], classified basically on the main science which the method referred to. One thing needs to be pointed out here is that all these methods deliver drugs by means of manipulating drugs. Changing the size of therapeutic agents, such as reducing it to micro- or even nano-scale is not the topic here.

Table 1.1 Targeted delivery methods

| Chemical methods | Physical methods | Others |
|---|---|---|
| Liposome | Direct injection | |
| Polymeric micelle | Particle bombardment | |
| Biodegradable particle | Electroporation | |
| Carbon nanotube [14] | Magnetic sphere [15] | Virus [16] |
| Cell adhesion peptide [17] | Microfluidics | |
| Antibody | Microneedles | |
| | Thermal poration | |
| | Ultrasound-mediated method | |

The applications of chemical methods are often very specific. A certain kind of delivery method can usually be applied to a certain kind of drug or they delivery is confined to a certain area or a certain disease.

The category which ultrasound-mediated method belongs to is the physical group. Physical methods are more widely applicable compared to chemical methods. Each method has its own unique advantages and limitations; however, the ultrasound-mediated method, which was developed relatively recently [18], has several advantages over the other physical methods. Specifically, it is less invasive than the electroporation method since the ultrasound wave can propagate through soft tissue and reach the cells of internal organs [19] [20]. In addition, both spatial and temporal aspects of delivery can be controlled by adjusting the ultrasound parameters, transducers and acoustic waves, and in so doing, the desired area can be targeted and side effects can be reduced [19].

## 1.2 Ultrasound and acoustic cavitation

### 1.2.1 Ultrasound induced bioeffects

Ultrasound is a type of mechanical wave that has a frequency exceeding 20 kHz; it cannot be heard by human ears. The fundamental characteristic of the wave is that the particles of the medium oscillate about their equilibrium position, with the particle displacement from the equilibrium position. For fluids the displacement will be in the direction of propagation of the wave, so that the waves are longitudinal. The pressure amplitude of the longitudinal wave (also called compressional wave) is typically specified in Pascal, but kPa or MPa is more commonly seen in the medical field. Ultrasonic waves transport energy in the form of kinetic energy (particle motion) and potential energy (fluid compression). As a result ultrasonic waves can alternatively be characterized in terms of their energy density and the rate at which they transmit energy. The acoustic intensity of a sound wave ($W/cm^2$) is defined as the average rate of flow of energy through a unit area normal to the direction of propagation and is proportional to the square of the pressure amplitude. Ultrasound is one of the most widely applied clinical diagnostic tools and most of the therapeutic effects of

ultrasound have been developed during the long period when ultrasound served as one of the most reliable diagnostic technique. These effects have included techniques such as ablation of tissue or cancer (by high intensity focused ultrasound, HIFU), sonophoresis, hemostasis, and vascular occlusion [21] [22].

To better understand how ultrasound changes its role from diagnostic to therapeutic, the bioeffects induced by ultrasound: heating and cavitation, are introduced here. Heating and cavitation are the primary mechanisms of action underlying these therapeutic effects, all of which arise from the propagation of ultrasound waves in cells and tissues. Heating is a direct bioeffect induced by ultrasound and can be easily observed [23]. Energy is lost from the ultrasonic wave as it passes through tissue, largely as a result of visco-elastic absorption processes. Most of the acoustic energy so deposited is converted to heat, raising the tissue temperature and creating the thermal hazard under discussion. Although heating caused by ultrasound is highly localized, limited in extent to the region within, and immediately adjacent to, the ultrasound beam, the intensities and powers used in present-day diagnostic ultrasound scanners are sufficient to raise the temperature of tissues, locally, by a few degree Celsius, from the absorption of ultrasound alone. Such a temperature raise can easily cause cell death and especially when it comes to HIFU (high intensity focused ultrasound), the heating is so severe that it will ablate tissue or cancer cells if designated.

Cavitation, compared to heating, is a much more complicated bioeffect and is stressed in the following section.

Besides heating and cavitation, a number of secondary physical effects can also be generated by an ultrasonic field [24]. These result from the nonlinear nature of acoustic equations that describe the wave behavior. As these are secondary effects they tend to increase in proportion to intensity and are generally relatively small in magnitude. The first of the secondary effects is radiation pressure, a steady (for a continuous wave) small pressure exerted on surfaces or media interfaces and acting in the direction of propagation of the wave. The second is a bulk movement of fluid away from the transducer in the direction of propagation known as acoustic streaming. Since the intensity of sound wave applied in ultrasound-mediated delivery is usually

not so high, influences from these secondary effects are not as substantial as from heating or cavitation.

### 1.2.2 Acoustic cavitation

Acoustic cavitation is the most important bioeffect related to the delivery via ultrasound. Here a brief introduction to the very phenomenon is given and detailed bubble dynamics will be illustrated in the next chapter.

When an ultrasound wave propagates in the liquid or liquid containing tissue, a mechanical strain is induced, where strain refers to the relative change in dimensions or shape of the body that is subjected to stress. The strain is significant near gas or vapor bubbles, hence the interest in ultrasound-induced cavitation. Acoustic cavitation, or to be more specific, ultrasonic cavitation, in a broad sense, refers to ultrasonically induced activity occurring in a liquid or liquid-like material that contains bubbles or pockets containing gas or vapor [25]. When a gas bubble in a liquid experiences the variations in pressure of an acoustic wave, its size is driven to change, expanding during the period of decreased pressure and contracting during the compression half-cycle of the wave. For low values of peak acoustic pressure, oscillations in bubble radius largely follow variations in pressure. As the peak acoustic pressure increases, a variety of different motions may be induced. Ultimately the bubble becomes unstable as it contracts, collapsing catastrophically under the inertia of the surrounding liquid. Consequently, there are two defined types of acoustic cavitation classified according to the bubble behavior: non-inertial and inertial [26]. Non-inertial cavitation, formerly called stable cavitation; occurs when a gas bubble in a liquid is forced to oscillate with only a relatively small to moderate increase and decrease of radius, when the pressure amplitude of the external acoustic field is not too high. So no matter what the name it is called, the most characteristic point of such a kind of cavitation is the oscillating of bubbles. Inertial cavitation, formerly called transient cavitation, occurs if the acoustic pressure amplitude is sufficiently high and above a threshold level. The bubble grows to its maximum radius and then collapse. Here again, no matter what the name this kind of cavitation it is called, the most characteristic point of inertial cavitation is the violent collapse of

the bubble after growth and oscillation.

Oscillating bubble can generate small-scale and boundary-associated steady and direct current flow [27] [28]. To differ it from the acoustic streaming generated by the acoustic filed itself, this kind of acoustic streaming is termed as microstreaming. The bubble oscillations induce on the surface steady shear stress attributed to microstreaming. The amplitude of the shear stress is small but when the bubble is adjacent to a cell, this shear stress can also cause changes to the cell.

Toward the end of the collapse of bubbles in cavitation, the predicted wall speeds and accelerations are high, and shock waves can propagate through the gas and be emitted into the liquid [24] [29]. Polytropic models of the collapse of a bubble containing homogeneous gas predict pressures in the range of hundreds of megapascals and temperatures in the range of thousands of degrees Kelvin when the volume is minimal [30]. These transient temperatures and the gas shocks are capable of generating free radicals by hydrolysis, which subsequently yield reactive chemicals. Electronically excited species, in turn, can cause the emission of a light flash, a phenomenon known as sonoluminescence.

Either from the mechanisms in non-inertial cavitation or inertial cavitation, these microscopic phenomena are found to be manipulatable in research as well as clinical fields. Acoustic cavitation is thus responsible for, or at least strongly related to, many therapeutic applications of ultrasound.

## 1.3 Sonoporation-mediated delivery

### 1.3.1 Sonoporation

The reason that ultrasound-mediated are capable of delivery therapeutic agents in cellular level is a phenomenon termed sonoporation, an effect of ultrasound on cells. Ultrasound-mediated gene delivery is considered to be closely related to acoustic cavitation. Cavitation and cavitation-induced activities can temporally increase cell membrane permeability through a process referred to as sonoporation; briefly, transient holes are induced in the phospholipid bilayer of the cell membrane, which allows large molecules to be transferred into the cell [20]. Ultrasound-mediated

delivery method is a very effective modality for drug delivery and gene therapy because energy that is non-invasively transmitted through the skin can be focused deeply into the human body in a specific location and employed to release drugs at that site [31].

The most characteristic symbol of sonoporation is a small hole on cell membrane [32] (seen in Figure 1.1). Direct observation of such pores is of course the most effective evidence of sonoporation. Considering the difficulty in direct observation caused by the small size of such pores, sonoporation can also be indicated by trapping large fluorescent molecules inside the viable cells (the molecules are excluded by viable cells and leak out of nonviable cells), and is different from the commonly noted permeabilization indicated by trypan blue or propidium iodide stains, which stain lysed, nonviable cells. An example of intracellular drug delivery is shown in Figure 1.2 [33]. Confocal microscopy showed that all of the molecules were transported into the cytosol of living cells when present in the media during sonication. Another successful delivery of plasmid DNA to a cell line is shown as an example of intracellular delivery via sonoporation, seen in Figure 1.3 [34]. This transfection was shown 2 days after sonication, showing that the damage to cell membrane was not lethal and cells survived after sonoporation.

As that listed in Table 1.1, another pore formation method using electrical field which is sometimes discussed together with sonoporation is electroporation, a significant increase in the electrical conductivity and permeability of the cell plasma membrane caused by an externally applied electrical field. Electroporation was first demonstrated by Neumann and colleagues in 1982 and has subsequently become a widely used technique. The voltage required for pore opening varies considerably and is dependent on cell size and shape, ranging from values of approximately 100 V/cm in large cells such as myotubes up to 1–2 kV/cm in small cells such as bacteria. [35]. Similarly as that in sonoporation process, the exact mechanism by which the plasmid enters the cell following electroporation is unclear. Technically electrodes are needed in electroporation and this method is thus invasive or sometimes mini-invasive while sonoporation is of course noninvasive. Mehier-Humbert has reviewed these two physical methods together and made a detailed comparison [36]. The efficiency of

electroporation is generally higher than sonoporation. For example for Jurkat lymphocytes (nonprimary cells) electroporation was superior to sonoporation in terms of transfection efficiency (15.83±3.5% vs 7.53±0.4%) [37]. However, for certain kinds of cells, the efficiency difference may be little. Toxicity and invasiveness from electrodes are limitations for electroporation while efficacy is the main limitation for sonoporation method. In sonoporation the cell viability usually drops with increasing efficiency, and in electroporation due to its nature of invasiveness such drop is even quicker [38].

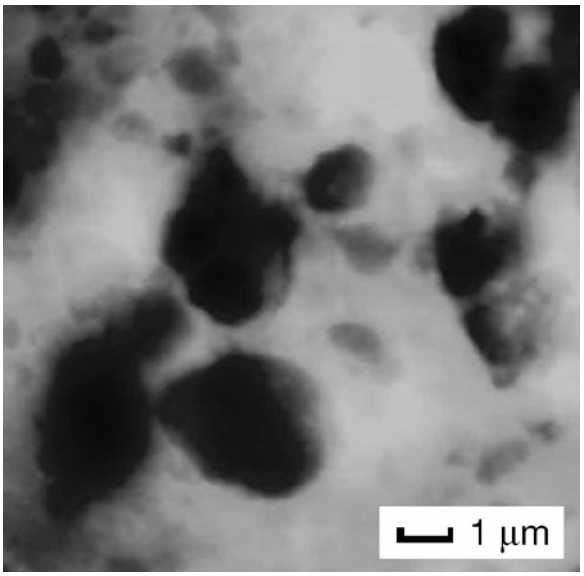


Figure 1.1 An atomic force microscopy image of pores on the cell membrane [32]

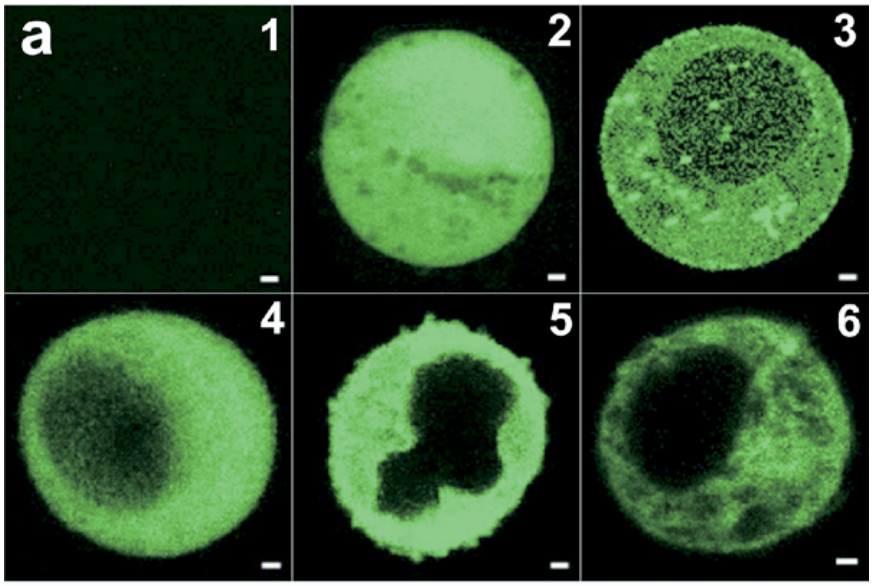


Figure 1.2 An example of intracellular delivery by ultrasound. (a) Confocal micrographs showing a nonsonicated DU 145 cell exposed to calcein (A1) and sonicated cells exhibiting uptake of calcein (A2), bovine serum albumin (A3) and 150 (A4), 500 (A5) and 2,000 kDa (A6) dextrans. Scale bars are 1 μm [33]

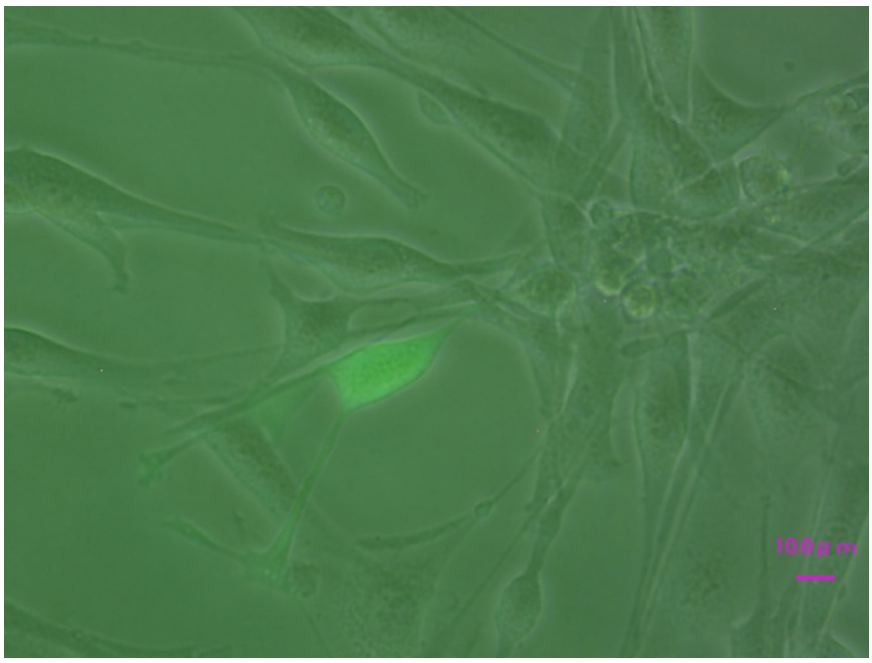


Figure 1.3 An example of intracellular delivery of plasmid DNA via sonoporation [34]

### 1.3.2 Mechanism studies

One of the earliest investigations on the use of ultrasound to enhance drug delivery was reported by Fellinger and Schmid in 1954 [39], when they enhanced the delivery of hydrocortisone ointment into inflamed tissue. In a more modern fashioned scientific research way, the studies on ultrasound enhanced uptake of drugs or gene expression dates back to as early as 1980s [40] [41]and gains more and more interest from 1990s [18] [42] [43]. Since then, a large variety of deliveries were achieved including, fluorescent markers [44], therapeutic drugs [45]especially anti-cancer drugs [46], short interfering RNAs [47], and plasmid DNAs [34]. Successful deliveries *in vivo* [48] implicated very good future of sonoporation-mediated method into a clinical application. Yet, a large obstacle to this advancement is the fact that till now the mechanism of sonoporation is not fully understood.

The first matter to be considered is where sonoporation happens. As known to all, the biological cell membrane is mainly composed of lipids, ion channels, and proteins. Its framework consists of a double layer of phospholipids (lipid bilayer). The cell membrane consists primarily of a thin layer of amphipathic phospholipids which spontaneously arrange so that the hydrophobic "tail" regions are isolated from the surrounding polar fluid, causing the more hydrophilic "head" regions to associate with the intracellular (cytosolic) and extracellular faces of the resulting bilayer. Both molecular simulations [49] [50]and direct visualization of pores following ultrasound exposure in experiment results [32] [51]have proved that sonoporation takes place in the lipid bilayer, and may possibly somehow related to the self-assembly of hydrophobic and hydrophilic parts in the bilayer [49]. The membrane is also responsible for the controlled entry and exit of ions like sodium, potassium, calcium. Calcium transients were found during sonoporation by Deng’s group and their results indicate the formation of nonspecific pores in the cell membrane by ultrasound-stimulated microbubbles and the generation of calcium waves in surrounding cells without pores [52].

The second matter here is how the pores on the biological membranes come into being. The current conception of the biological mechanism underpinning sonoporation is the formation of non-lethal and transient pores on the surface of cell

membranes in a manner that allows cell-impermeable molecules to enter the intracellular space, and subsequent resealing and/or repair of the pores. The formation of pores during sonoporation is strongly related to acoustic cavitation. The acoustical mechanisms underpinning sonoporation include effects associated with stable microbubble oscillation such as microstreaming [27] [28] [53] [54], and microbubble disruption in cavitation leading to the generation of shock waves [55]and microjets [56].

Steady oscillations of gas bubbles in liquid generate velocity gradients near a wall. The bubble oscillations induce on the surface steady shear stress attributed to microstreaming which may lead to sonoporation when cells are adjacent or attached to the wall. Models and methods for estimating acoustical microstreaming and the shear stress that is induced on a surface by the pulsations of a bubble have shown that the amplitude of the stress are in kilo Pascal order [28] [57] [58], relatively mild when compared to the value of shock waves from its inertial counterpart. Although the exact mechanism requires further investigation, shear stress on endothelial cells is likely to be translated into biological responses by interactions among the cytoskeleton, ion channels, and membrane receptors [59], thereby activating a chain of biochemical and genetic processes that allow the cells to adapt to flow, such as transients of calcium ions [60].

Violent collapse of bubbles leads to severe physical phenomena such as shock wave and high speed jetting during inertial cavitation [61]. Sudden collapse of cavitation bubbles leads to the formation of shock waves that are capable of disrupting the tissues and enhancing drug transport and collapsing bubbles near a wall experience non-uniformities in their surroundings that results in the formation of high-velocity microjets. The microjet can penetrate into the tissue or generate secondary stress waves in the tissue. Structural details of membrane disruption are not completely clear. Molecular dynamics simulation shows an option of explanation on how pores come into being from shock wave or high speed microjets [49] [50] [62]: some amount of water molecules was injected to the hydrophobic region of phospholipid bilayer and then in several nanoseconds, the bilayer-water system can spontaneously develop into a water-filled pore structure without any mechanical and

electrical forcing from outside, when the initial number of water molecules in the hydrophobic region exceeds a critical value.

### 1.3.3 Parametric studies

Low delivery efficiency has always been one of the major issues of ultrasound-mediated delivery. The solution requires a thorough consideration because the complexity of an ultrasound-mediated delivery system comes from various aspects. The ultrasound wave, even from a commercial diagnostic system, itself has many parameters, such as intensity, the duration of exposure, and burst settings. Influences from gas bubbles, such as type and concentration also need to be considered. Since cavitation happens in liquids, the type of medium also counts. The types of cells and tissues surely matter.

A number of studies have aimed at understanding the influence of parameters on sonoporation efficiency and cell viability and also optimizing parameters for a proper balance [44] [63] [64] [65] [66]. Similar results were found: with higher intensity and larger total energy exerted higher delivery efficiency and lower cell viability were expected. The relationship was not quite strict since plateau was found for almost each parameter examined. An example of our previous results is shown in Figure 1.4 [34]. For the parameters studied, the overall trend for the data is that increases in transfection efficiency are associated with decreased cell viability.

The criteria for a tradeoff between delivery efficiency and cell viability may differ by the cases applied. But the most basic rule is that higher efficiency and higher viability are preferred. Finding the optimized arrangement of parameters will not only enhance therapeutic effects but also reduces side effects.

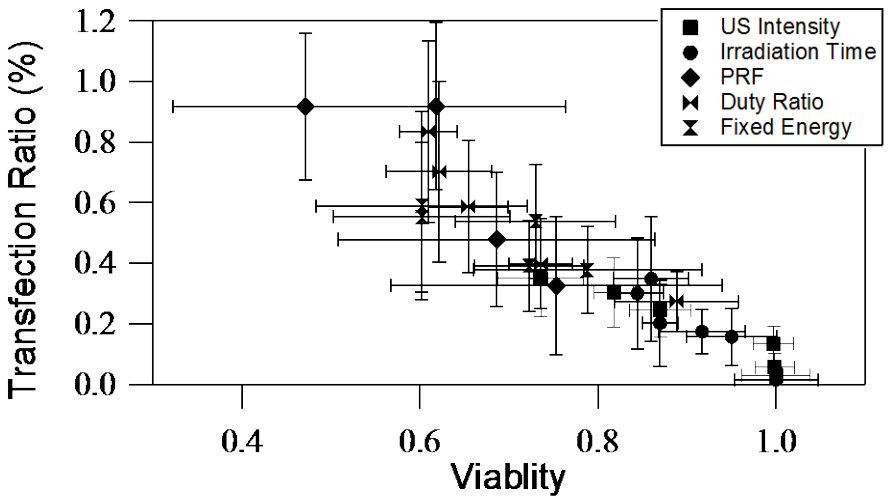


Figure 1.4 An example of parametric studies on sonoporation efficiency and cell viability, PRF stands for pulse repetition frequency [34]

## 1.4 Scope of this thesis

Studies to date have proved sonoporation-mediated delivery method has a bright future as a targeted delivery tool, indicating further treatments for cancer, gene therapy and several other difficult diseases. To accelerate its applying to clinical process, more knowledge on sonoporation mechanism is needed, which will in turn gives instructions on how to improve the delivery efficiency.

A sketch of the research topics of this dissertation is shown in Figure 1.5. Towards higher delivery efficiency from sonoporation, experimental studies from two sides were carried out. The overall aim is deeper understanding of sonoporation mechanism and thus methods to improve sonoporation efficiency.

The first side deals with microbubble behavior. Understanding the oscillation and collapse from artificially added agents as well as cavities in the medium is the object of this part. Towards this end, bubble behavior under ultrasonic wave is studied from two aspects: concentration change and cavitation noise. Concentration changes indicate facts on bubble collapse while broadband noise analysis provides more facts on both bubble oscillation and explosion from both artificially added bubbles and cavities inside the medium.

The second side deals with intracellular delivery in the presence of artificially added microbubbles. Markers are delivered into cultured cell lines in *vitro*. Results of delivery efficiency and cell viability are obtained for cells irradiated both in attachment and suspension status.

What's more, because the experimental conditions for the two sides of studies are totally identical, the relationship between bubble behavior and intracellular delivery results can then be correlated. So with mechanism understanding of sonoporation from bubble radial motion, as the dissertation titled, experimental arrangements for high sonoporation efficiency is achieved.

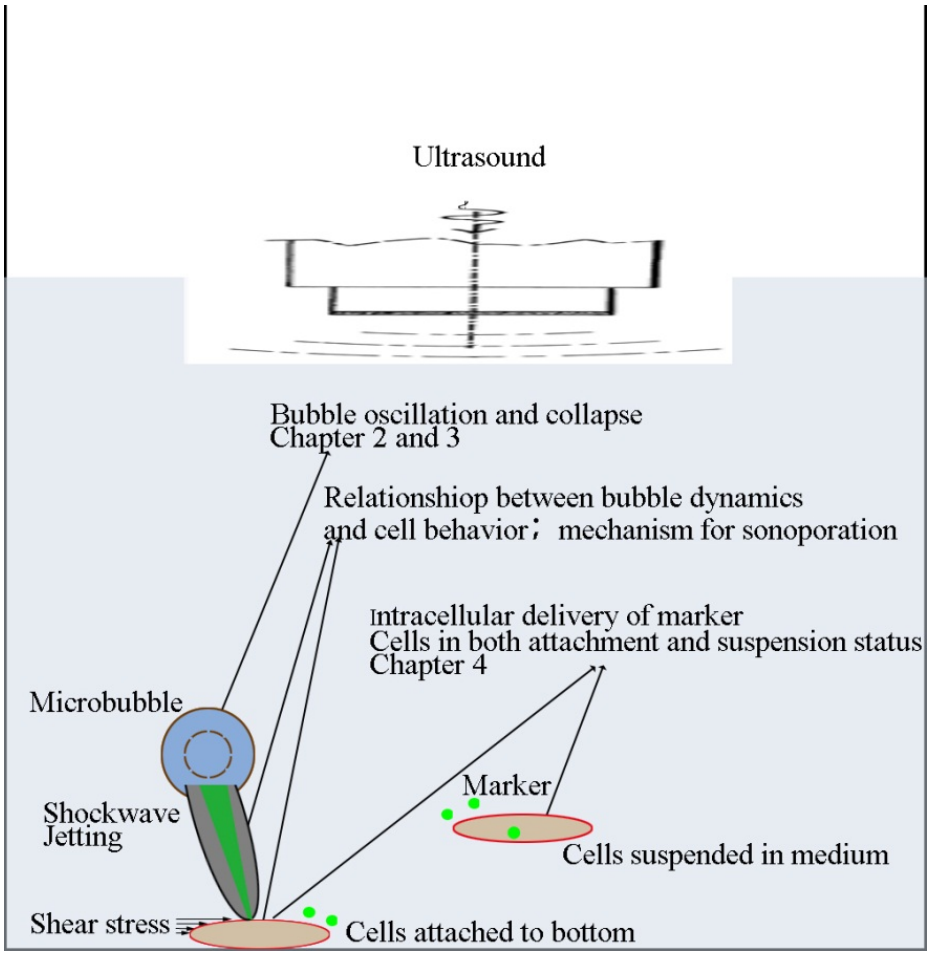


Figure 1.5 Sonoporation studied in this dissertation, mainly two parts: bubble behavior including concentration change and broadband noise, and cell behavior including marker uptake and cell viability

By chapters, chapter 1 is an introduction to the topic. It begins with backgrounds such as targeted delivery and acoustic cavitation, proceeds with the conception of sonoporation. Sonoporation related research is briefly reviewed, and finally ends with a guide of this dissertation.

Chapter 2 and 3 are the experimental part on bubble behavior. Chapter 2 focuses on the bubble concentration change during irradiation. It begins with an introduction to bubble oscillation and collapse, proceeds with experimental methods and materials, which are also partly used in chapter 3, and finally ends with the experimental results and discussions. The results part includes the acoustic field measuring as well as the microbubble concentration change during cavitation. Chapter 3 focuses on the broadband noise from cavitating bubbles. It begins with an introduction to noise spectra and frequency domain analysis of cavitation, proceeds with data collecting as well as processing units and methods, and finally ends with the results and discussions.

Chapter 4 is the experimental part on intracellular delivery, including an introduction to materials and methods and results and discussions of both delivery efficiency and cell viability and finally ending with the relationship between results from bubbles and cells.

Chapter 5 concludes this dissertation and looks forward to future experimental topics.

# Chapter 2. Change of microbubble concentration during ultrasound exposure

## 2.1 Introduction

### 2.1.1 Bubble oscillation and collapse

As described in Chapter 1, sonoporation process is highly cavitation related. Cavitation typically begins with the formation of liquid-free zones, which is bubbles, and ends with the implosion of these bubbles, so better understanding of bubble dynamics is of vast importance to better comprehension and manipulation of sonoporation. The phenomenon of acoustic cavitation was introduced in Chapter 1, but cavitation was first noticed in hydrodynamic area, for example, flows through Venturi nozzles. Hydrodynamic cavitation is cavitation in flowing liquids and pressure change comes from the flow. The studies of bubble dynamics, including its radial movements and final collapse, during cavitation dated back to the same time as hydrodynamic cavitation was studied. The cavitation referred to in this thesis is another type of cavitation: acoustic cavitation, which occurs in a static or nearly static liquid [67]. The pressure change is artificially applied from an oscillating source. Though having different sources of pressure change, the bubble behavior during both two types of cavitation is much the same.

A typical life cycle of a cavitating bubble consists of three periods: inception, oscillation and collapse [25]. Cavitation inception is not the topic of this chapter and thus not discussed here. In an acoustic field matter is alternately subjected to pressure and tension, so are bubbles formed. Behavior of bubbles under this alternate pressure change is quite complicated, so to make it easier to understand here the discussion begins from a single bubble case. The radial oscillation of a single bubble (Radius: $R$) during a pressure field is governed by the Rayleigh-Plesset equation, originated by Rayleigh in 1917 and developed by Plesset [68].

$$R\ddot{R} + \frac{3}{2}(\dot{R})^2 = \frac{1}{\rho}\left\{p_i - p_\infty - \frac{2\sigma}{R} - \frac{4\mu}{R}\dot{R}\right\} \quad (2\text{-}1)$$

Where $p_i$ is the pressure in the gas at the bubble wall; $p_\infty$ is the pressure at infinity; $\sigma$ is the surface tension constant; and $\mu$ is the coefficient of the liquid viscosity.

Although Rayleigh-Plesset is a very simplified model, it can still reveal basic facts of a bubble radial behavior under alternating pressure. In an acoustic field with low intensity the bubbles response in a relatively mild way, which may appear to be 'stable'. When bubbles expand and contract, without growing to the process of implosion, the activity is so called stable cavitation, or non-inertial cavitation [69]. The counterpart of stable cavitation is transient cavitation, or inertial cavitation. The most characteristic point of inertial cavitation is the violent collapse of the bubble after growth and oscillation. The bubble undertakes several oscillations, expands to a maximum size, and then rapidly collapses. Such collapse is a high-energy event and can generate a wide range of destructive effects such as high pressure and temperature, shock wave.

In experiments the real situation is that microbubbles with shells will behave under the acoustic field. Such bubble motion is much more complicated. Various works have showed how to add shell properties or other items to make the bubble radial motion more accurate [70]. Here a modified model from Prof. Ferrara's group is briefly introduced and the detailed derivation should be found in reference [71]. With a conventional Rayleigh-Plesset style derivation, a shelled model is added and the model is Equation 2.2. Where the shell is denoted by the subscript *s* and liquid is denoted by *l*. The inner and outer of a shelled bubble are denoted by the subscript number 1 and 2, respectively. $T_{rr}$ and *t* are radial component of the stress tensor and time respectively.

$$\begin{aligned}\rho_s R_1 \ddot{R}_1 \left[1+\left(\frac{\rho_l-\rho_s}{\rho_s}\right)\frac{R_1}{R_2}\right] \\ +\rho_s \dot{R_1}^2\left[\frac{3}{2}+\left(\frac{\rho_l-\rho_s}{\rho_s}\right)\frac{4{R_2}^3-{R_1}^3}{2{R_2}^3}\frac{R_1}{R_2}\right] \\ =P_s(R_1,t)-P_s(R_2,t)+P_1(R_1,t)-P_\infty(t) \\ +T_{s,rr}(R_2,t)-T_{1,rr}(R_2,t) \\ +3\int_{R_1}^{R_2}\frac{T_{s,rr}}{r}dr+3\int_{R_2}^{\infty}\frac{T_{l,rr}}{r}dr\end{aligned} \quad (2\text{-}2)$$

For ideal isothermal gas behavior assumption (the agent is filled with a high-molecular-weight perflurocarbon gas), denoting the equilibrium value with subscript 0, there is

$$P_g(R_1,t)=P_{g0}\left(\frac{R_{10}}{R_1}\right)^{3\kappa} \quad (2\text{-}3)$$

Combining Equation 2-2 and 2-3 and using the appropriate boundary conditions, a governing equation is obtained, expressed in terms of both the inner and outer radii. Such a governing equation is then soluble according to different shell properties.

Gaussian or “almost Gaussian” weighted sound waves are used as driving sound field. Figure 2.1 and 2.2 are simulation result from this model. Figure 2.1 shows the radial oscillations of a 2.5 μm radius agent with a 500 nm triacetin shell irradiate with a seven-cycle pulse at 2.5 MHz, 1.6 MPa. Holding the other parameters fixed, except for the shell thickness that is reduced to 5 nm, the subsequent agent response is shown in Figure 2.2.

In Figure 2.1, the maximum radial amplitude is 2.3 times of the equilibrium radius and the radial oscillation curve is relatively ‘smooth’. In Figure 2.2, the agent reaches a normalized radial maximum of 3.2, after the maximum positive pressure of the forcing pulse. The oscillation is more nonlinear with smaller secondary radial growth and collapse follows from the maximum. The influence of shell property on

bubble radial behavior is then obvious.

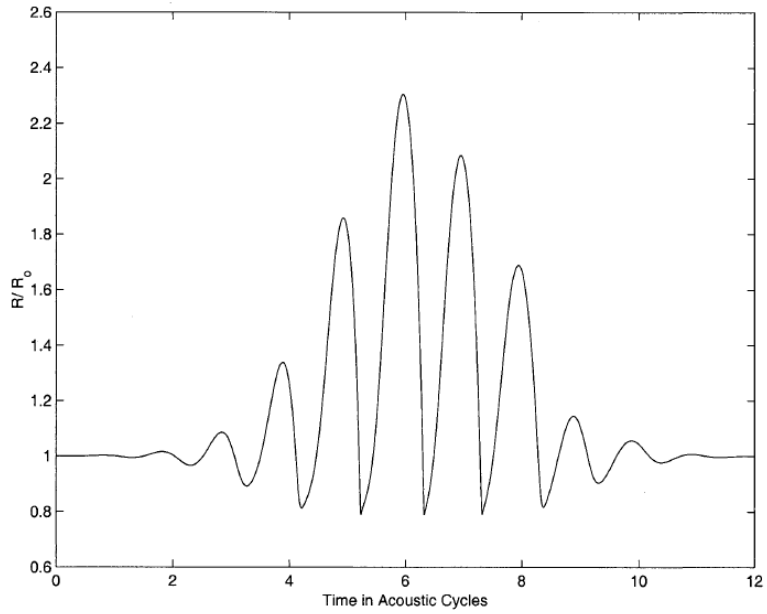


Figure 2.1 The radial oscillations for a 2.5 μm agent with a 500 nm triacetin shell driven at 1.6 MPa, 2.5 MHz [71]

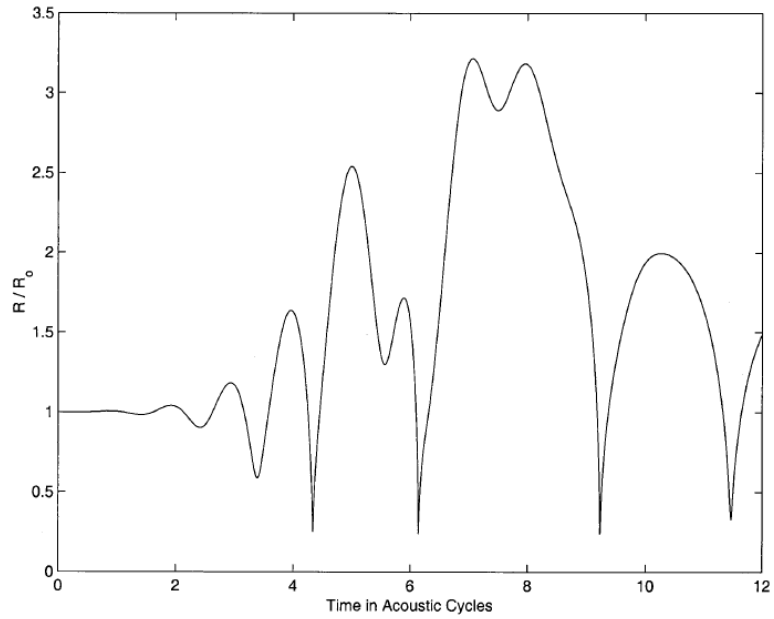


Figure 2.2 The radial oscillations for a 2.5 μm agent with a 5 nm triacetin shell driven at 1.6 MPa, 2.5 MHz [71]

Bubble behavior becomes much more complicated when it comes to the case of a large amount of bubbles. The complexity comes from several aspects. The first one is the distribution of bubble radius [72]. It is impossible that all the bubbles have the same value of radius. Usually, a normal distribution or a distribution close to normal is expected. For a given driving frequency, diameters of some bubbles are close to the resonant size while others are larger or smaller than resonant size. For a given intensity, stable and inertial cavitation will happen simultaneously. As the bubbles randomly suspend in the liquid, the degree of freedom and uncertainty of cavitation is much larger than the case of a single bubble. The second one is the ultrasound propagation in a bubbly liquid [73] [74]. When bubble population is large, the void fraction of the medium through which sound wave propagates must be considered. Scattering and reflecting of sound wave on gas-liquid boundaries make the prediction of bubble behavior more difficult. The least but not the last one is the interaction between bubbles. This is a very complicated topic even when there are only two or three bubbles [75], and becomes extremely complicated for a large population of bubbles [76].

One more factor that will add much complexity to bubble radial dynamics is cavitation inception. Cavitation inception is a very complicated topic and till now there are still much unknown about it. In our study artificially made bubbles with lipid shells are used, but inception of cavities in the liquid is still important. The existence of shelled bubbles will make the liquid easier to be torn out and also the gas contained in the shelled bubbles will form new cavities after collapse. All these points count for sonoporation process and will be studied.

Two aspects of bubble behavior are focused on in this dissertation: bubble concentration change due to bubble collapse and broadband noise emitted during cavitation. Here is this chapter; results of bubble concentration change are shown. No matter how complicated oscillation bubbles experienced, the collapse of bubbles with lipid shells will bring a drop to the total concentration since the lipid shell can’t repair itself, captured by a laser beam experimentally.

### 2.1.2 Ultrasound contrast agent (UCA)

Gas containing bubbles are artificially added to liquid in all the experiments carried out in this thesis except for those control groups. The size of these gas-filled bubbles is usually less than 10 micrometers so they are often called microbubbles. Such microbubbles are originally developed for contrast in ultrasonography because the echogenicity difference between the gas in the microbubbles and the soft tissue surroundings of the body is immense. It is due to this echogenicity difference that these microbubbles are defined as ultrasound contrast agent (UCA). The UCA applied in this thesis is Sonazoid$^{TM}$ (Daiichi Sankyo), a commercially available product in Japan.

Sonazoid$^{TM}$ consists of perfluorobutane gas (PFB, $C_4F_{10}$) microspheres stabilised by a membrane of hydrogenated egg phosphatidyl serine (HEPS). It is formulated as a powder for injection consisting of lyophilised sucrose entrapping HEPS stabilised PFB microspheres under a PFB headspace. The microbubble suspension sample was prepared according to the protocol provided by the manufacture by injecting 2 ml pure distilled water into each bottle of powder and then shaking for one minute. The stability of Sonazoid™ suspension solution after reconstitution is good, with no significant changes in physicochemical properties 2 h after reconstitution [77]. After preparation, a microscopic observation of microbubble solution is shown in Figure 2.3.

The microbubble diameters are no larger than 10 μm and the diameters differ. As mentioned before, the radius of microbubble is very important to its behavior in an acoustic field. The detailed measuring of diameters provided by the manufacturer is shown in following Figure 2.4.

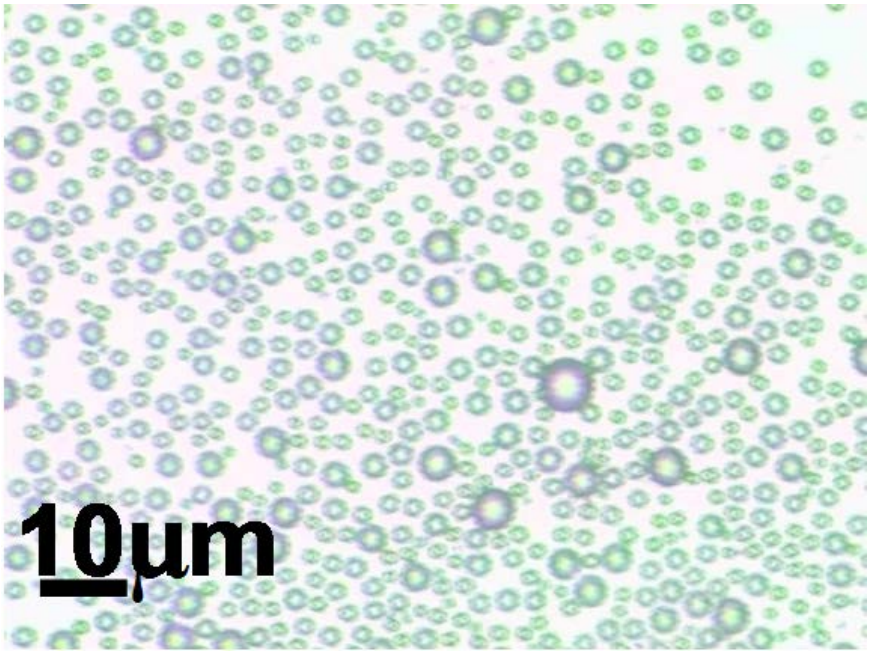


Figure 2.3 A microscopic view of Sonazoid™ suspension

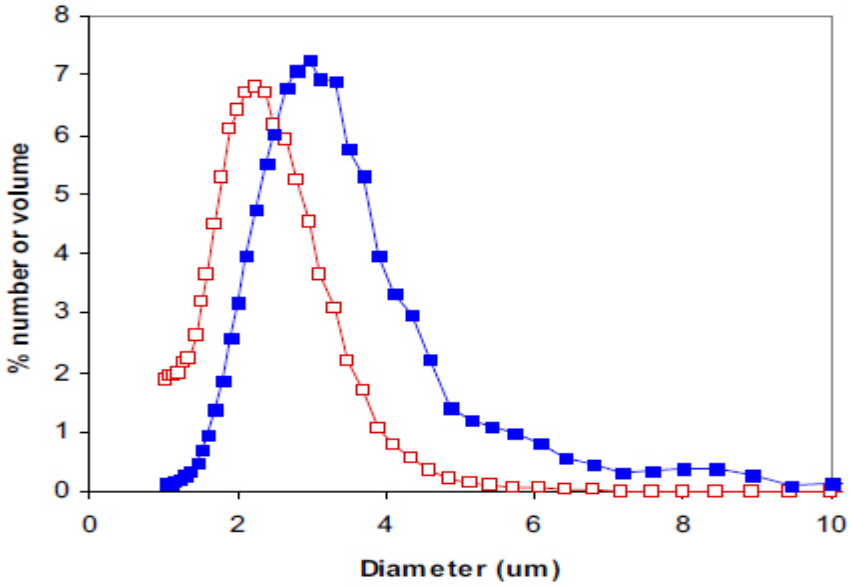


Figure 2.4 Number (open squares) and volume (filled squares) size distributions of Sonazoid™ suspension, data from manufacturer, GE Health [77]

The microsphere volume concentration in Sonazoid™ reconstituted product is 8.0 ± 0.6 μl. The spherical microspheres have a diameter typically ranged of 1 to 5 μm. The volume median diameter is 2.6 ± 0.1 μm and the number mean diameter is 2.1 ± 0.1 μm. Only less than 0.1% of the total number of microspheres has a diameter larger than 7 μm.

Using high magnification microscopy, the count of bubbles is measured and its relationship between bubble volume concentrations is given in the Table 2.1.

Table 2.1 Bubble volume concentration and density count

| Volume concentration (v/v %) | Count of bubbles/$mm^2$ |
|---|---|
| 0 | 0 |
| 0.1 | $2.0\times10^3$ |
| 1 | $1.4\times10^4$ |
| 10 | $1.7\times10^5$ |

In the most of our irradiation experiments, the volume concentration is chosen at 10%, corresponds to a density of $1.7\times10^5/mm^3$.

### 2.1.3 Light absorbance and concentration

Most solutions absorb electromagnetic radiation of some wavelength. Light absorption occurs when atoms or molecules take up the energy of a photon of light, thereby reducing the transmission of light as it is passed through a sample. Apparently, the proportion of the light absorbed will depend on how many molecules it interacts with.

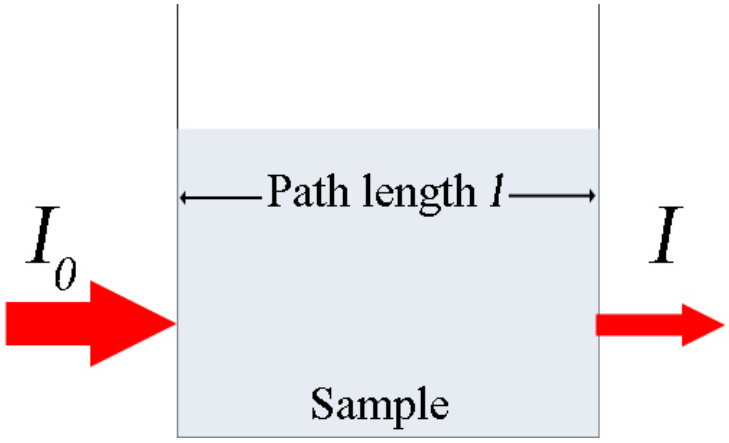


Figure 2.5 Diagram of Beer–Lambert absorption

Let's consider the case of a beam of light travels through a cuvette of width $l$ in which the sample is contained, as shown in the Figure 2.5 [78]. In our experiments, the transmitted light is captured on the same light path as incident light, so light captured may come from two sources: single scattering and multi scattering.

For the case of single scattering, absorbance of light $A$ for liquids is defined as:

$$A = -\log_{10} I/I_0 \qquad (2\text{-}4)$$

where $I_0$ and $I$ are the intensity (or power) of the incident light and the transmitted light, respectively. $I/I_0$ is also called the transmission (or transmissivity) of light.

Beer–Lambert law states that there is a logarithmic dependence between the transmission, $T$, of light through a substance and the product of the absorption coefficient of the substance, $\alpha$, and the distance the light travels through the material (i.e., the path length), $l$. The absorption coefficient can, in turn, be written as a product of either a molar absorptivity (extinction coefficient) of the absorber, $\varepsilon$, and the molar concentration $c$ of absorbing species in the material [79]. For liquids, the relations are written as:

$$T = \frac{I}{I_0} = 10^{-\varepsilon l c} \qquad (2\text{-}5)$$

This implies that the absorbance becomes linear with the concentration, which corresponds very well with the measured points Figure 2.9 without adding multi

scattering light item to the relationship. So in laser diode measuring the multi scattering light is very weak and omitted.

$$\varepsilon = \frac{lc}{A} \qquad (2\text{-}6)$$

Thus, if the path length and the molar absorptivity are known and the absorbance is measured, the concentration of the substance (or the number density of absorbers) can be deduced.

## 2.2 Experimental materials and methods

### 2.2.1 Ultrasound exposure system

A schematic diagram of the US exposure apparatus is shown in Figure 2.6. The system was comprised of two arbitrary waveform generators (model WF1974 and WF1944A, labeled A) and B) in the figure, NF Corporation, Yokohama, Japan), a 50 dB gain radio frequency amplifier (325LA, E&I, Rochester, NY, labeled C)), an oscilloscope (Wave Surfer 24 Xs-A, Lecroy, Chestnut Ridge, NY, labeled D)), and a custom-designed, single piezoceramic element plane transducer (13.5 mm diameter, Japan Probe, Yokohama, Japan, labeled E)) with a central frequency of 2 MHz.

One of the two synchronized signal from two channels of WF1974 is used for the trigger of oscilloscope and the other one is used to trig another waveform generator, WF1944A. Signal from WF1944A is the burst that will be amplified and then drive the transducer to vibrate. The ultrasound signal and the trigger for oscilloscope are then synchronized.

The E&I 325LA amplifier covers a frequency from 250 kHz to 150 MHz and its max linear power output is 25 W. The transducer is specially designed to fit the geometry of a commercial 24-well plate offered by BD Falcon (Bedford, MA, labeled F), the fit is shown in G)). The dimensions of the 24-well plate are depicted by six parameters, labeled from A to F. They are length, width, and height of the lid and plate. The values are 129.28, 85.14, 10.08, 127.63, 85.47, and 20.19 mm, respectively. The dimensions of a well, where the medium and bubbles are contained are shown in the following Table 2.2.

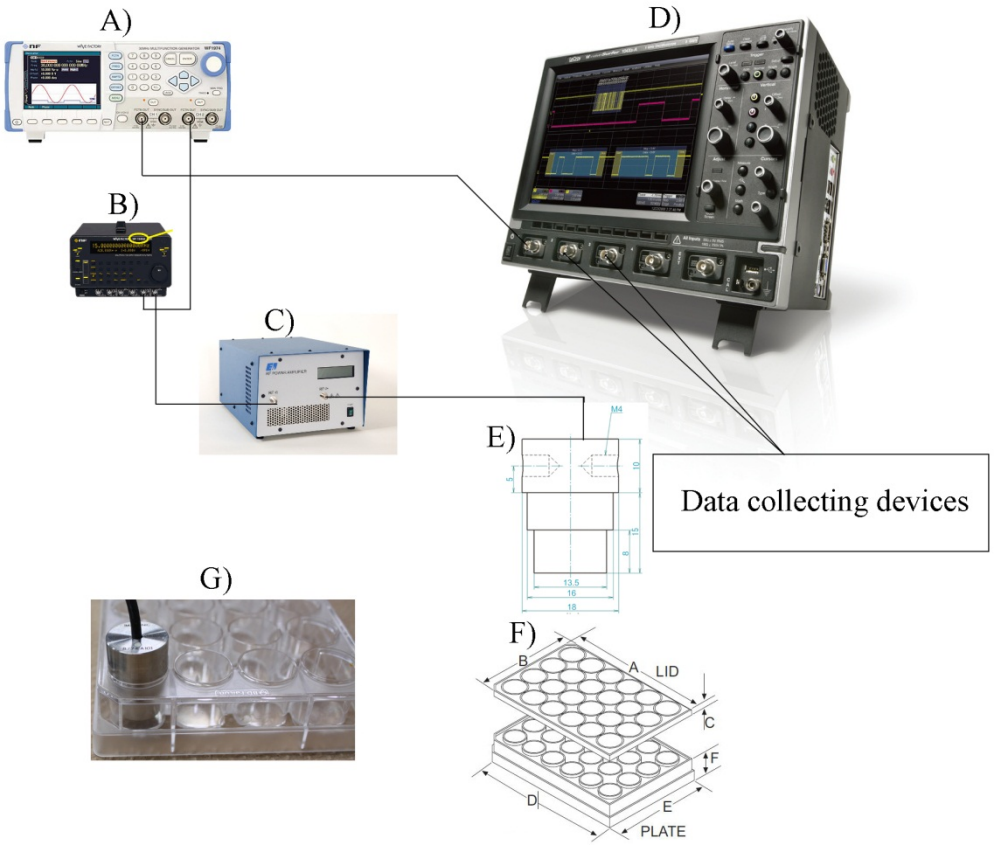


Figure 2.6 Diagram of ultrasound exposure system, all the pictures of instuments are provided by their manufacturers except for E) and G)

Table 2.2 Dimensions of a single well in the 24-well plate

| Parameter | Value |
|---|---|
| Top internal diameter | 16.30 mm |
| Bottom internal diamter | 15.49 mm |
| Depth | 17.98 mm |
| Bottom area | 1.883 $cm^2$ |

The oscilloscope saves signals as measuring units. It has 4 channels and 200 MHz bandwidth. For each channel, the maximal sampling rate is 2.5 GS/s and maximal save depth is 5 Mpts. The data saving frequency for a single channel is kept at 25 Hz during all experiments but the sampling points of each datum differ according to the experiment.

### 2.2.2 Burst wave and parameters

In almost all experiments, “burst” mode of ultrasound was applied. Since a 2 MHz transducer is used, the period of a cycle is 0.5 μs. A burst signal is composed of a mark component and a space component (both components are quantified by the number of cycles), as shown in Figure 2.7. The length of the mark component (also called pulse duration) divided by the total length of the pulse (pulse repetition period) is referred to as the duty ratio. The wave becomes continuous if there is only mark component.

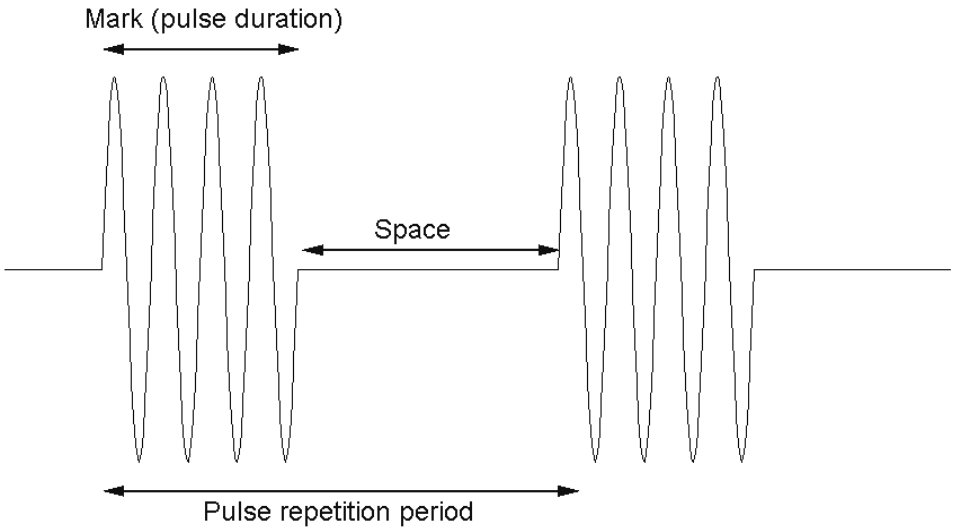


Figure 2.7 A chart of typical burst wave applied for most experimental cases

Variations in ultrasound intensity, pulse repetition frequency, pulse duration, and microbubble volume concentration were tested. The intensity of ultrasound is represented by the peak to peak acoustic pressure measured by a needle hydrophone. A list of parameters and their ranges is shown in Table 2.3.

Table 2.3 Parameters and ranges applied

| Parameter | Range |
|---|---|
| Intensity | 0-1.2 MPa |
| PRF | 50-50k Hz |
| Pulse duration | 0-500 μs |

### 2.2.3 Laser diode system

Laser diode system (670 nm, Beta-TX, Gwent, UK) was used to measure the change in concentration of microbubbles during irradiation. The laser beam goes through the 3-mm interval between transducer surface and well bottom surface and is then received by a diode sensor connected to an oscilloscope controlled by Matlab™ software in a PC. A sinusoidal wave with 1.1 kHz frequency was used for modulation to avoid noises. The laser emitting unit and the photo sensor are shown in the Figure 2.8. In (A), the left part is the laser unit and the right part is the diode unit.

As introduced the microbubble diameters are about 3 μm while the wavelength of red laser is 670 nm so naturally the microbubbles with lipid shells will reflect and scatter incident light. While cavity generated in the liquid are believed not to affect the light path based on two facts. One is the living cycle of a vapor cavity is short. It is difficult to capture any cavity information since the laser signal is modulated by a 1.1 kHz signal. The microbubbles can last for several seconds while the cavity may just response to ultrasound wave in microsecond order. The second one is that the size of cavity. Although there is no measured data, cavity is much smaller than microbubble. In our experiments it is validated that there is no significant difference between the transmitted light of two cases that only air contained in the well and liquid without microbubbles in the well. So it is confirmed that the measuring results from laser diode will only show information on microbubbles with lipid shells.


(A)

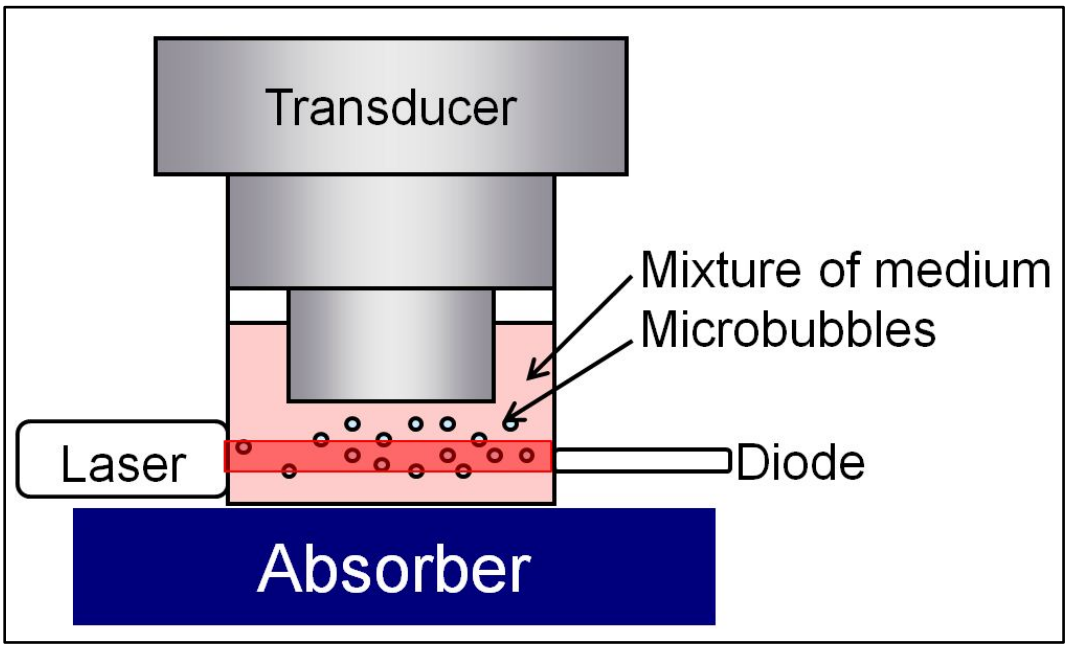


(B)

Figure 2.8 Laser diode units used to measuring the voltage of transmitted light. (A) is a photo of laser and diode unit, in which the left one is laser unit and the right one is diode unit; (B) is a diagram showing the position of this laser diode system, the diameter of laser beam is about 3 mm.

The voltage of the signal captured by the oscilloscope represents the magnitude of the transmitted light. Because the incident light is kept at the same, the voltage is then linearly related to transmission and exponentially related to absorbance.

The oscilloscope saves the signals from diode at a frequency of 25 Hz. The sampling frequency is set to be 500 kS/s and each datum contains 1 k sampling points, corresponds to a time length of 2 ms. Since the modulation frequency is 1.1 kHz, each saved datum contains 2 modulated cycles.

The saved data are processed by Matlab™. The peak to peak value of each saved 2 ms signal is averaged from 2 cycles contained in the signal. This peak to peak voltage value is converted to concentration value according to the calibration curve.

### 2.2.4 Exposure protocols

Sonazoid™ is mixed to Dulbecco's modified Eagle's medium (DMEM) supplemented with 10% v/v fetal bovine serum (FBS) and 1% v/v antibiotics (Penicillin-Streptomycin and L-Glutamine) by pre-decided volume concentration (in most cases, 10% microbubble). 0.8 ml of such mixture is injected to a well of 24-well plate placed on a sheet of sound absorbing material. The transducer is then injected into this well and ultrasound exposure begins. After irradiation, the mixture is drawn out using a pipette and the well is rinsed with water for 2 times before next test.

For control groups, the medium contains no microbubbles but only 0.8 ml DMEM medium. The exposure condition for each controlling case is identical as the corresponding test case.

## 2.3 Results and discussions

### 2.3.1 Calibration of concentration and light absorption

The Beer-Lambert law indicates the linear relationship between absorbance and concentration of an absorber of electromagnetic radiation. The calculation of the coefficients related in the linear relationship is difficult and not necessary. Measuring the absorbance of several solutions with known concentration can calibrate the linear relationship between absorbance and concentration. The voltages correspond to a set

of volume concentration of microbubbles (0, 0.5, 1, 2, 3, 4, 5, 6, 7, 8, 9, and 10%) were measured. The concentration-voltage dots plot is shown in Figure 2.9. The coefficients in Beer-Lambert law are then decided and the relationship curve is also drawn in the figure. All recorded voltage data can thus be converted to concentration data according to this calibrated curve.

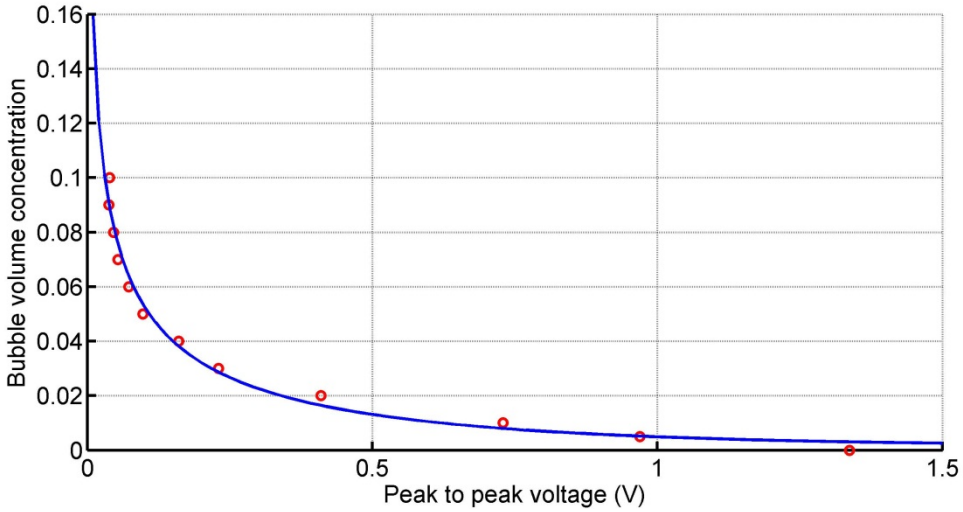


Figure 2.9 Fit curve of bubble concentration and intensity of transmitted light. Red dots are measured data with known concentration; blue curve is the fit curve calculated from Beer-Lambert law.

### 2.3.2 Acoustic pressure

The pressure field of the transducer was measured with a needle hydrophone (model 80-0.5-40, Imotec Messtechnik, Warendorf, Germany) at a fixed distance of 3 mm from the transducer surface; the distance between the transducer and the well-bottom surface was also 3 mm. The pressure field (peak-to-peak value, maximum value, minimum value) was recorded at 0.2 mm increments over a 15mm×15 mm surface perpendicular to the direction of beam propagation. The data in Figure 3A was obtained when the function generator output was 100 mV (peak-to-peak value). The measure acoustic pressure value is the peak positive value. Since the distribution is not very uniform, the intensity value was averaged over the circular transducer surface in all of the subsequent irradiation experiments.

Furthermore, because the plastic bottoms of plates could absorb and reflect incident waves, causing attenuation and reflection, and possibly forming a standing wave, measurements were done to confirm such absorption. First, the acoustic field was measured without plates and the hydrophone was placed 3 mm away from the transducer surface, as shown in right one of Figure 2.10. Then the needle hydrophone was positioned 3 mm away from plate bottom, which positioned between the needle hydrophone and transducer surface (6 mm away from the transducer surface), shown in the left one of Figure 2.10. The pressure field was recorded and shown in Figure 2.11. In Figure 2.11(B), the focus is the difference between two different situations; the acoustic pressure was normalized by the maximum value in both 2 situations. Since the difference in the sound fields of the two cases was negligible, neither attenuation nor reflection was considered.

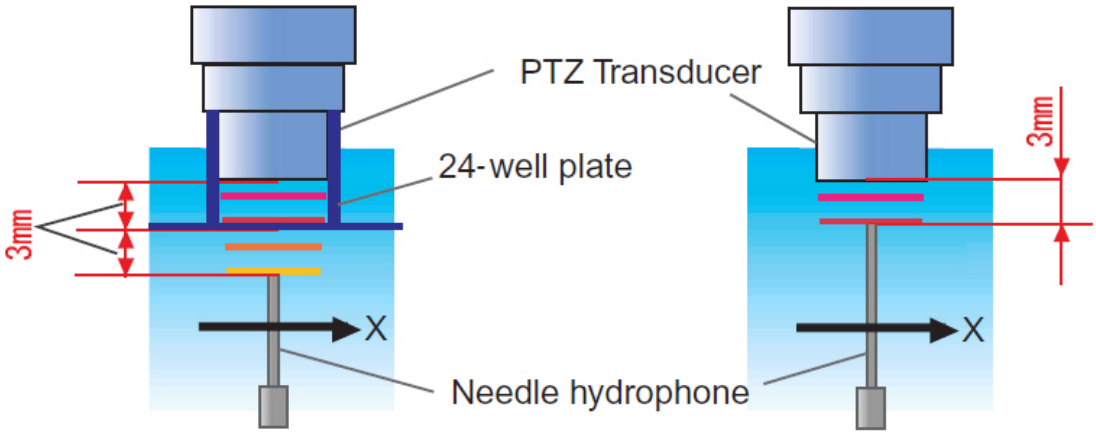


Figure 2.10 Hydrophone position for measuring ultrasound wave absorption and reflection

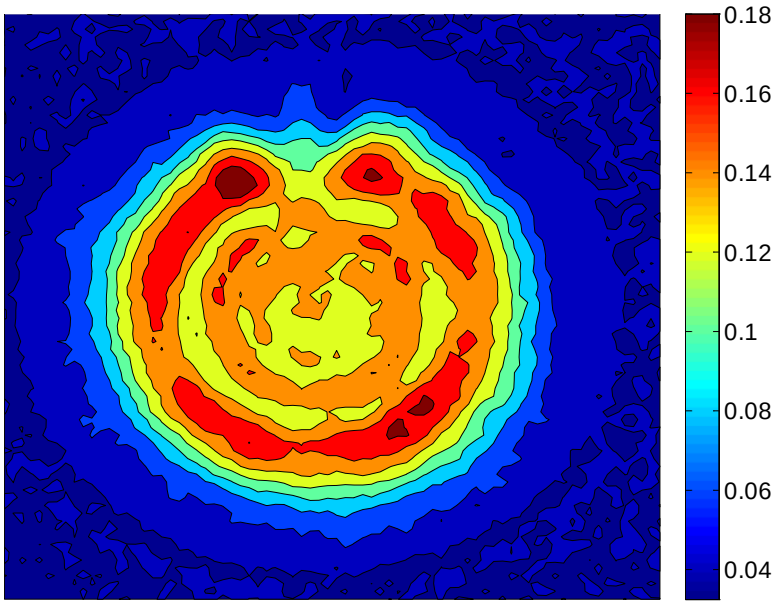


(A)

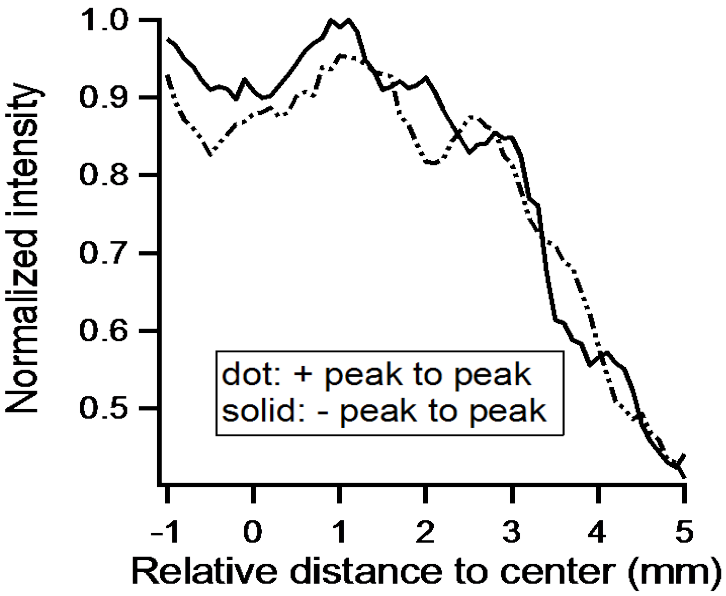


(B)

Figure 2.11 Acoustic pressure field measured with needle hydrophone. (A) Hydrophone placed 3 mm away from the transducer. The unit is Mega Pascal and the total area is 15mm×15 mm. (B) Hydrophone placed 6 mm away from the transducer. +: 24-well plate positioned between the hydrophone and the transducer; –: no 24-well plate positioned between the hydrophone and the transducer.

### 2.3.3 Influence of intensity

The influence of acoustic intensity on microbubble concentration was tested. The initial microbubble concentration is 0.1 (10% volume to volume, i.e. 0.08 ml microbubble solution and 0.072 ml DMEM). The concentration change details of microbubbles during irradiation of 8 intensities together with a control case were shown in Figure 2.12. The other parameters were set as: the irradiation time is 60s; PRF is 5 kHz and the pulse duration is 20 μs. Figure 2.12 (A) was the concentration change over time, (B) is the time took for each intensity case to reach a microbubble concentration of 0.015 (1.5%), and (C) is the minimum concentration reached for each intensity after 60 s irradiation.

There was slight drop of concentration in control case. Buoyancy and natural dissolving may be the reason since the laser beam went through the lowest position of the well. The bubble concentration did not reach 0.015 even after 60 s and the minimum concentration was still very large (> 0.8). Beginning with an intensity of 0.1 MPa, ultrasound was applied. At 0.1 MPa, the bubble concentration behavior was very similar to the case of control. The sound wave was too weak to cause any physical changes to the medium as well as the bubbles inside the medium. At 0.2 MPa, although the minimum concentration after irradiation was still larger than 0.015, indicating that majority of bubbles still existed after exposure, the microbubble concentration drop was larger than the control and 0.1 MPa case. So at 0.2 MPa, bubbles began to response to the compression and tension of sound wave and some bubbles which were unstable due to its large size of structure defects collapsed after exposure.

Starting from 0.3 an intensity of MPa, the bubble concentration change became more obvious. At 0.3 MPa, it took more than 50 seconds for the bubble concentration to reach 0.015 and the minimum concentration was about this value. The concentration drop during all 60 seconds exposure was quite even. Most bubbles were believed to oscillate and bubbles with radii around the resonant radius of the driving sound wave experienced stronger oscillation that lead to collapse. Here in this chapter, only the slow or quick drop of bubble concentration can be seen, the activities underlying such concentration change will be shown in next chapter by noise

emission. In this dissertation, this pattern of concentration change is defined as oscillation dominant.

The concentration changes of microbubbles from 0.4 MPa were again, dramatically different. At 0.4 MPa, the concentration dropped to 0.015 within less than 10 seconds and the minimum concentration at the end of exposure was about zero. The slope of the concentration change curve was very steep at the beginning 10 seconds and became almost horizontal after the sharp drop. Such change of microbubble concentrations indicated quick and violent collapse of bubbles, which will also be further proved with noise emission results in next chapter. The oscillation of bubbles was highly nonlinear and within 10 seconds, the majority of bubbles collapsed. Strong concomitant effects such as shock wave and high speed jetting were then expected. In this dissertation, this pattern of concentration change is defined as collapse dominant.

From 0.6 MPa to 1.2 MPa, the concentration changes were all similar to that of 0.4 MPa. The concentration dropped to 0.015 within less than 10 seconds and the minimum concentration at the end of exposure was about zero. The larger the intensity was, the less the time took for the concentration to reach 0.015. The slope of the concentration change curve was very steep at the beginning 10 seconds and became almost horizontal after the sharp drop. The larger the intensity was, the steeper the curve was at the beginning seconds. Still, quick and violent collapse of the majority of bubbles was believed to exist.

From 0.3 MPa, cavitation activities such as oscillating and collapse of bubbles became obvious. However, even with clear evidence of cavitation, there was still a great difference between 0.3 MPa case and 0.4 MPa case. To elucidate this difference, minor intensity increments were tested between these two intensities and the result were shown in Figure 2.13.

The concentration change of microbubbles at 0.32 MPa was quite close to that of 0.3 MPa in a not so steep way of concentration drop and over a long exposure time covering almost all 60 seconds of irradiation, which is oscillation dominant. Change of microbubbles at 0.38 MPa was more close to that of 0.4 MPa, as well as 0.45 MPa, which is collapse dominant. The bubble concentration dropped to a very low value

very quickly and then kept almost changeless. The concentration change patterns of 0.36 MPa and 0.38 MPa fell somehow between the former two. Such two different bubble concentration change patterns were also proved by the time took to reach 0.015 concentrations and the minimum concentration after exposure, shown in Figure 2.13 (B) and (C).

It is believed here that there is a cavitation pattern shift of cavitation, from oscillation dominant to collapse dominant, between these two intensities. When acoustic intensity increases from 0.3 MPa to 0.4 MPa, the cavitation changes from an oscillating dominant type to a collapse dominant type. Such cavitation pattern shift will be further validated in next chapter.

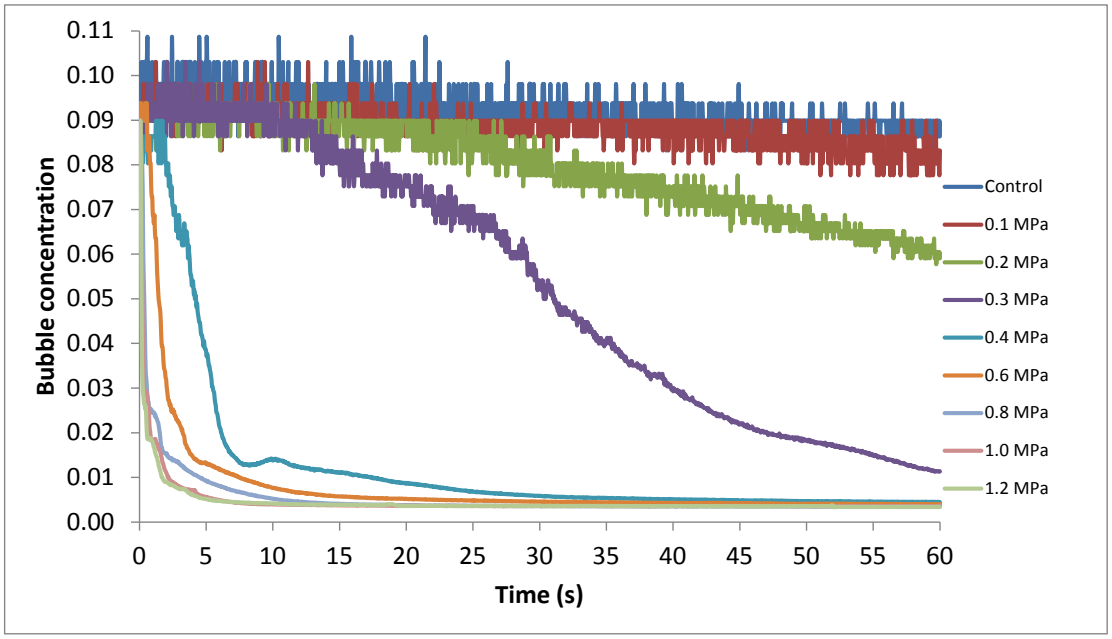
Bubble concentration
0.11
0.10
0.09
0.08
0.07
0.06
0.05
0.04
0.03
0.02
0.01
0.00
0
5
10
15
20
25
30
35
40
45
50
55
60
Time (s)
Control
0.1 MPa
0.2 MPa
0.3 MPa
0.4 MPa
0.6 MPa
0.8 MPa
1.0 MPa
1.2 MPa

(A)

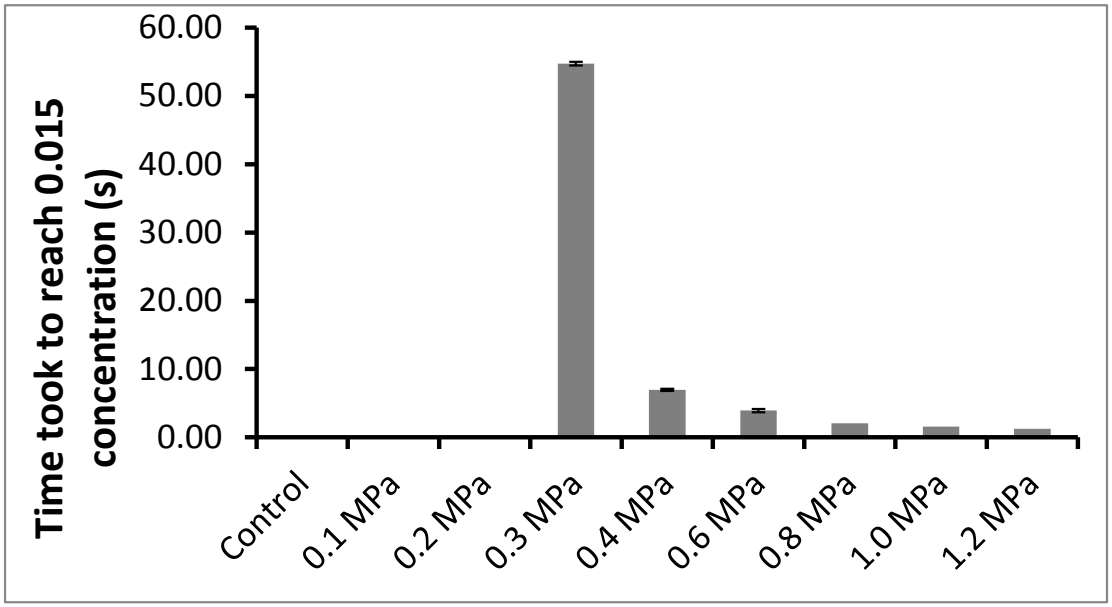
Time took to reach 0.015 concentration (s)
60.00
50.00
40.00
30.00
20.00
10.00
0.00
Control
0.1 MPa
0.2 MPa
0.3 MPa
0.4 MPa
0.6 MPa
0.8 MPa
1.0 MPa
1.2 MPa

(B)

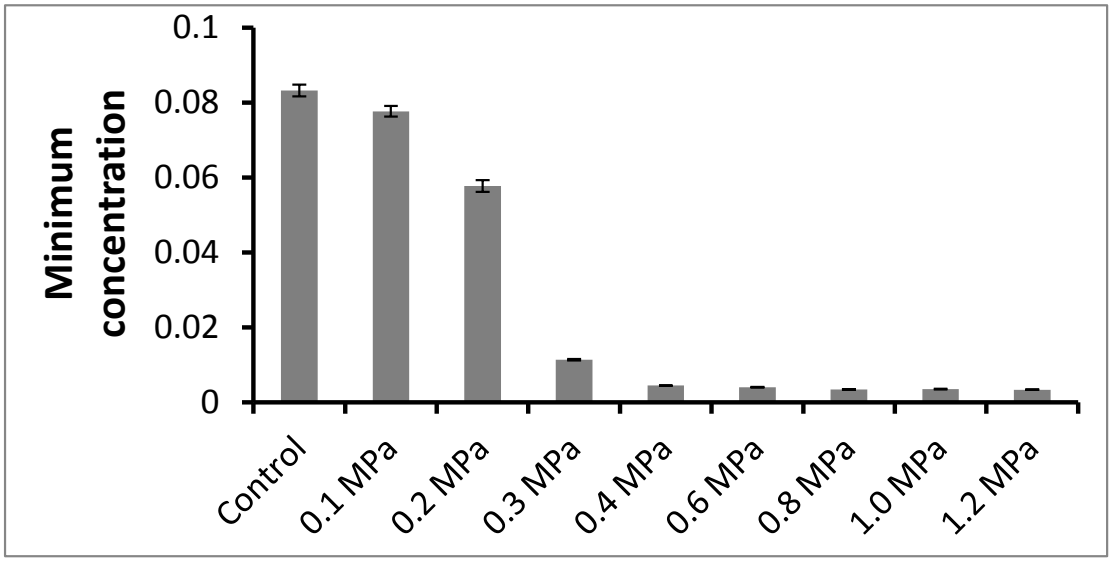


(C)

Figure 2.12 (A) Effects of ultrasound intensity on the microbubble concentration; (B) the time took for the microbubble to reach a concentration of 0.015; and (C) the minimum concentration of microbubbles during exposure. No ultrasound was applied in the case of control. The irradiation time is 60s; PRF is 5 kHz and the pulse duration is 20 μs. The data in (B) and (C) are averaged from three independent replicates and shown as the mean ± standard deviation.

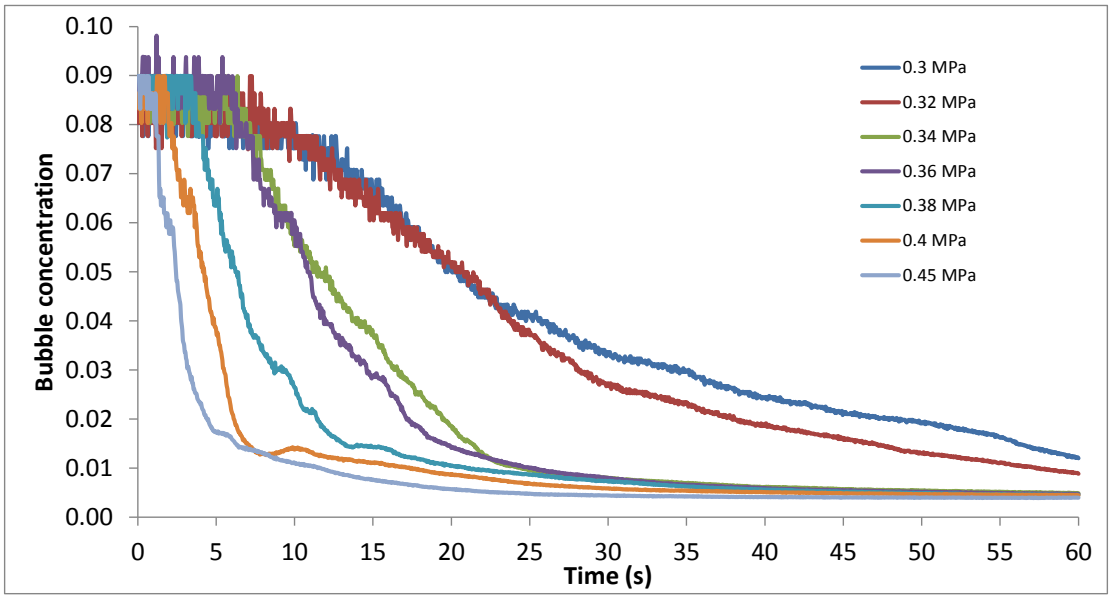
Bubble concentration
0.10
0.09
0.08
0.07
0.06
0.05
0.04
0.03
0.02
0.01
0.00
0
5
10
15
20
25
30
35
40
45
50
55
60
Time (s)
0.3 MPa
0.32 MPa
0.34 MPa
0.36 MPa
0.38 MPa
0.4 MPa
0.45 MPa

(A)

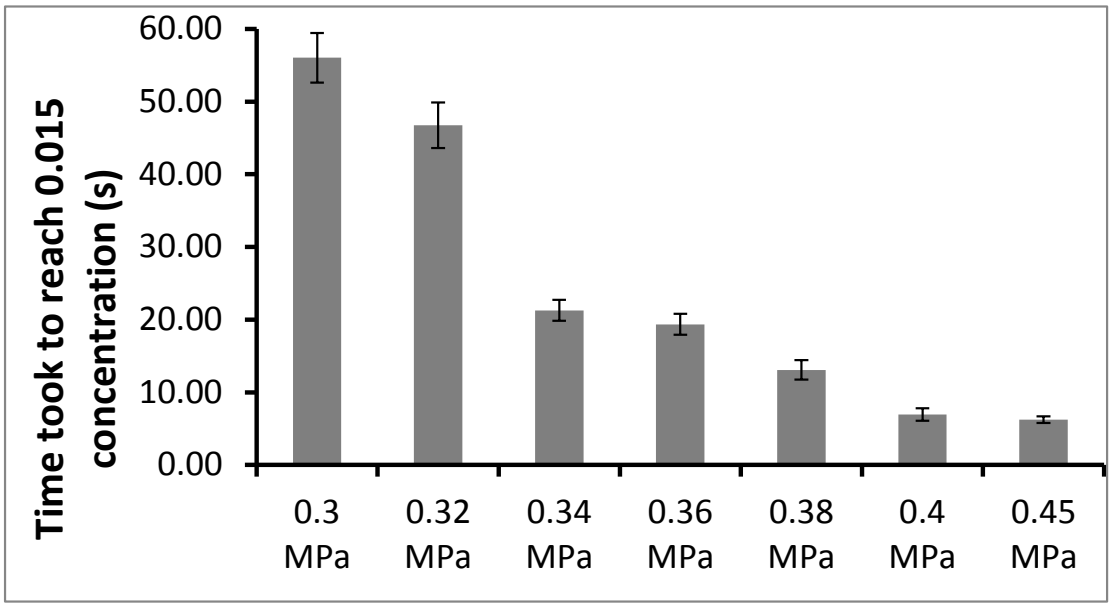
Time took to reach 0.015 concentration (s)
60.00
50.00
40.00
30.00
20.00
10.00
0.00
0.3 MPa
0.32 MPa
0.34 MPa
0.36 MPa
0.38 MPa
0.4 MPa
0.45 MPa

(B)

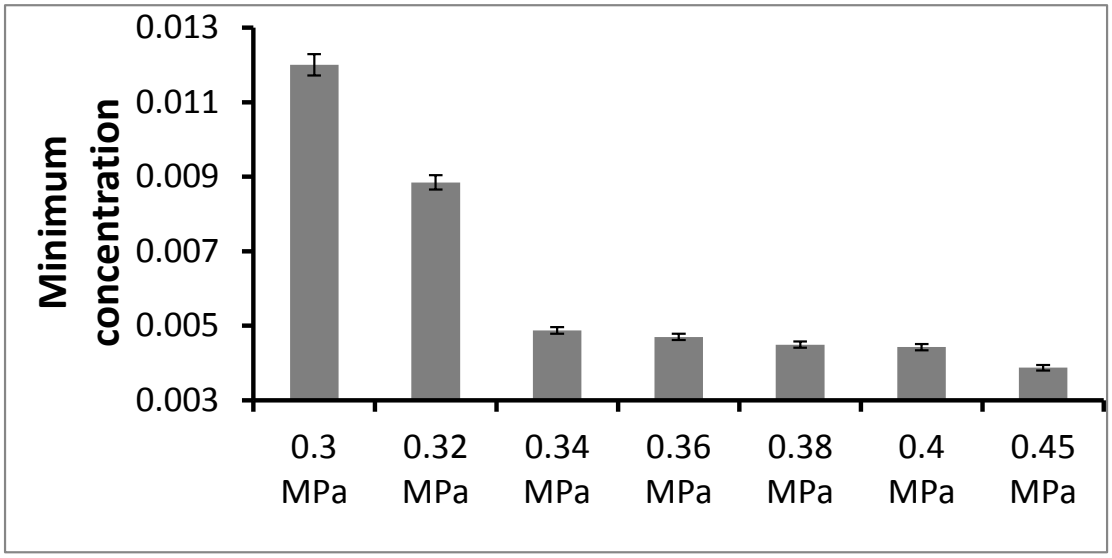


(C)

Figure 2.13( A) Effects of ultrasound intensity on the microbubble concentration with small intensity increments; (B) the time took for the microbubble to reach a concentration of 0.015; and (C) the minimum concentration of microbubbles during exposure. No ultrasound was applied in the case of control. The irradiation time is 60s; PRF is 5 kHz and the pulse duration is 20 μs. The data in (B) and (C) are averaged from three independent replicates and shown as the mean ± standard deviation.

### 2.3.4 Influence of pulse duration

The influence of pulse duration on microbubble concentration was tested at two different PRFs. The initial microbubble concentration is 0.1 (10% volume to volume). The concentration change details of microbubbles during irradiation of 4 pulse durations at 5 kHz PRF were shown in Figure 2.14. The other parameters were set as: the acoustic intensity is 0.8 MPa and the irradiation time is 60 s. At 5 kHz RPF, pulse durations of 5, 10, 20, and 50 μs correspond to duty ratios of 2.5, 5, 10, and 25%.

Overall, in all the cases the bubble concentration dropped very steeply. Within 8 seconds, the concentration reached or went even lower than 0.015, and the minimum concentration after exposure for all cases were around zero. With longer pulse duration, bubbles concentration dropped more quickly. It also took less time for bubble concentration to reach 0.015 with longer pulse duration. The minimum concentrations after exposure for all pulse durations were smaller with longer pulse duration, though the difference was minor since all these values are very small and close to zero.

The concentration change details of microbubbles during irradiation of 6 pulse durations at 500 Hz PRF were shown in Figure 2.15. The other parameters were set as: the acoustic intensity is 0.8 MPa; the irradiation time is 60 s; and the initial microbubble concentration is 0.1 (10% volume to volume). At 500 Hz RPF, pulse durations of 5, 10, 20, 50, 200, and 500 μs correspond to duty ratios of 0.25, 0.5, 1, 2.5, 10, and 25%.

At 5 μs pulse duration, it took more than 15 seconds for the bubble concentration to reach 0.015 and the minimum concentration did not reach 0.015. The concentration drop during all 60 seconds exposure was quite even. Then the bubble behavior did not present a collapse dominated way. Most bubbles were believed to oscillate and bubbles with radii around the resonant radius of the driving sound wave experienced stronger oscillation that lead to collapse. From 50 μs, the bubble concentration dropped to a very low value very quickly and then kept almost changeless. Within 7 seconds, the concentration reached or went even lower than 0.015, and the minimum concentration after exposure for all cases were around zero. The case of 10 and 20 μs were close to the cases after 50 μs. But the bubble concentration dropped to a very

low value relatively slowly and then kept almost changeless. It took longer time for these bubble concentrations in these two cases to reach to 0.015, or a value slightly larger than 0.015. Similarly, with longer pulse duration, bubbles concentration dropped more quickly. It also took less time for bubble concentration to reach 0.015 with longer pulse duration. The minimum concentrations after exposure for all pulse durations were smaller with longer pulse duration, though the difference was minor since all these values are very small and close to zero. With a lower PRF, the cavitation may not be collapse dominant when the pulse duration is too short even with an intensity of 0.8 MPa because there is not sufficient total energy.

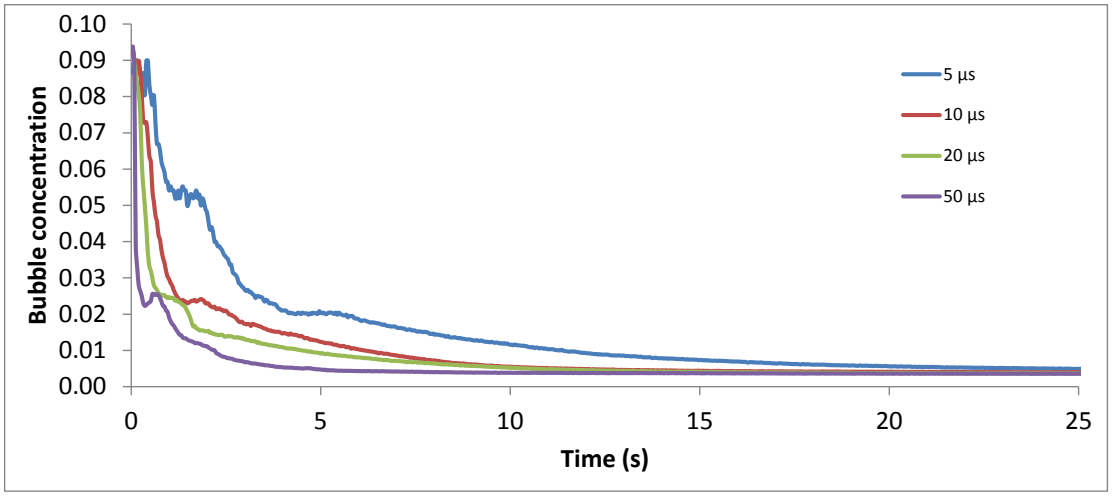
Bubble concentration
0.10
0.09
0.08
0.07
0.06
0.05
0.04
0.03
0.02
0.01
0.00
0
5
10
15
20
25
Time (s)
5 µs
10 µs
20 µs
50 µs

(A)

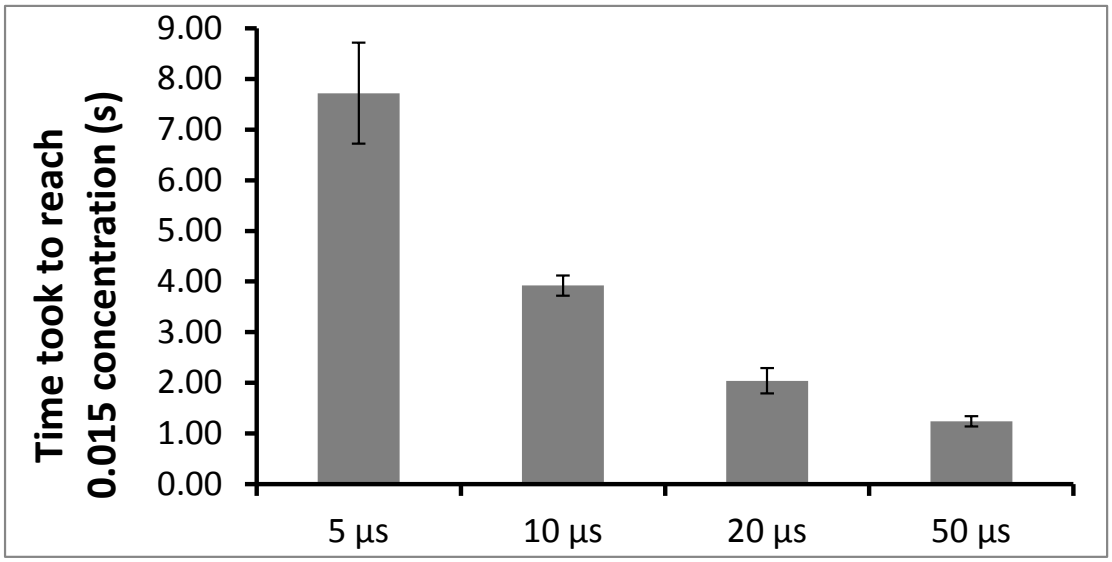
Time took to reach 0.015 concentration (s)
9.00
8.00
7.00
6.00
5.00
4.00
3.00
2.00
1.00
0.00
5 µs
10 µs
20 µs
50 µs

(B)

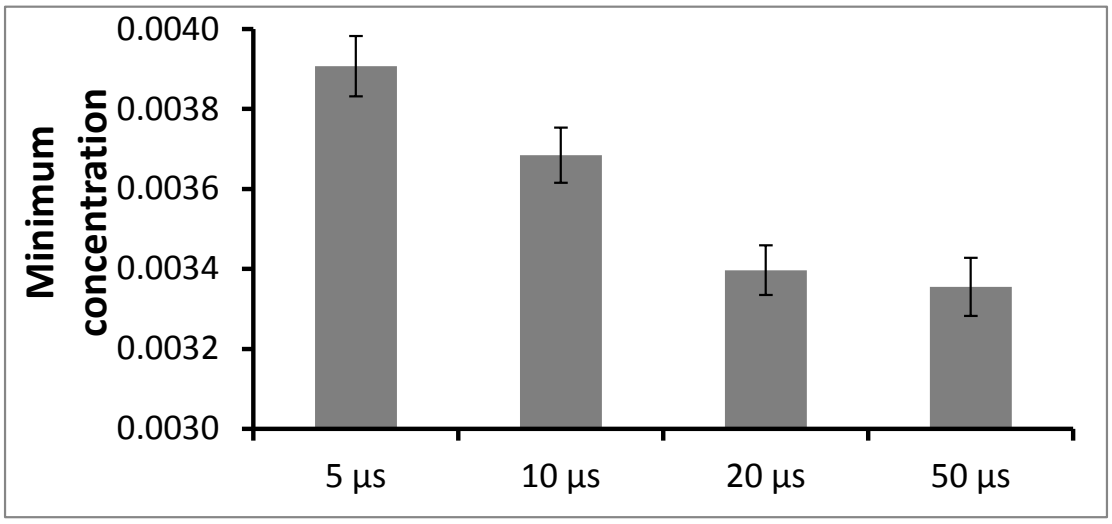


(C)

Figure 2.14 (A) Effects of pulse duration on the microbubble concentration, the data after 25 seconds were not shown; (B) the time took for the microbubble to reach a concentration of 0.015; and (C) the minimum concentration of microbubbles during exposure. The acoustic intensity is 0.8 MPa; PRF is 5 kHz and the irradiation time is 60 s. The data in (B) and (C) are averaged from three independent replicates and shown as the mean ± standard deviation.

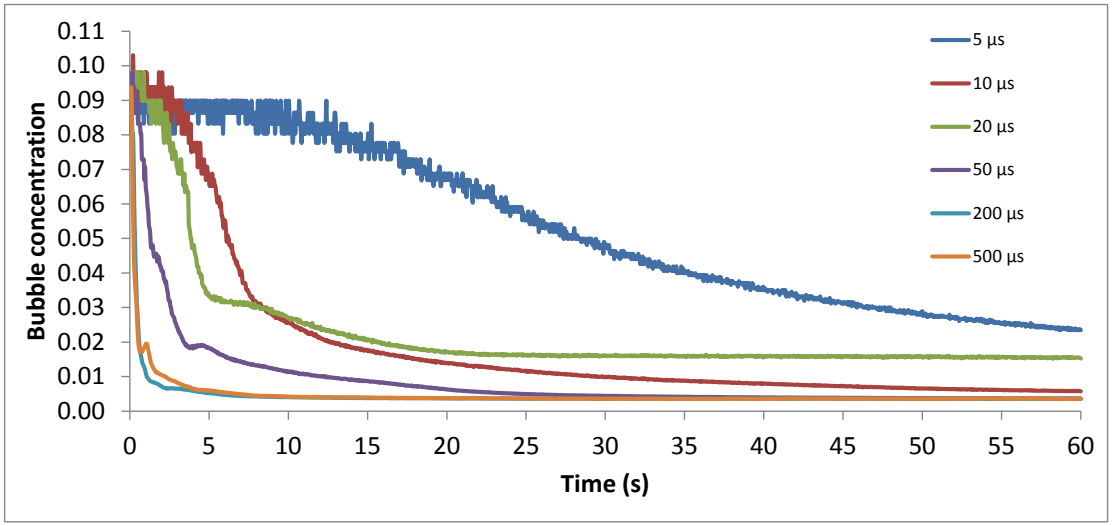
Bubble concentration
0.11
0.10
0.09
0.08
0.07
0.06
0.05
0.04
0.03
0.02
0.01
0.00
0
5
10
15
20
25
30
35
40
45
50
55
60
Time (s)
5 µs
10 µs
20 µs
50 µs
200 µs
500 µs

(A)

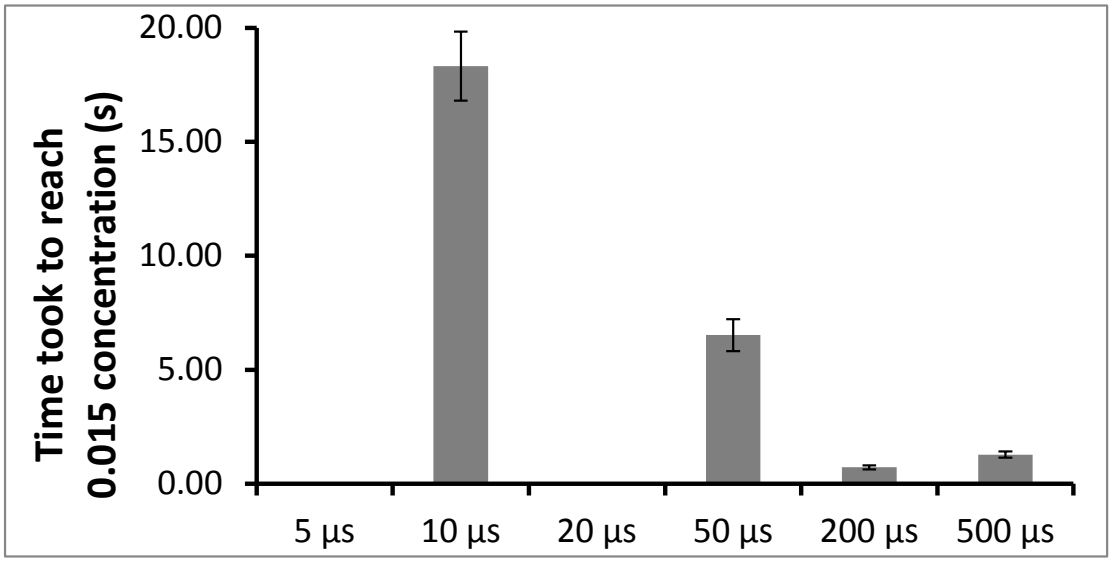
Time took to reach 0.015 concentration (s)
20.00
15.00
10.00
5.00
0.00
5 µs
10 µs
20 µs
50 µs
200 µs
500 µs

(B)

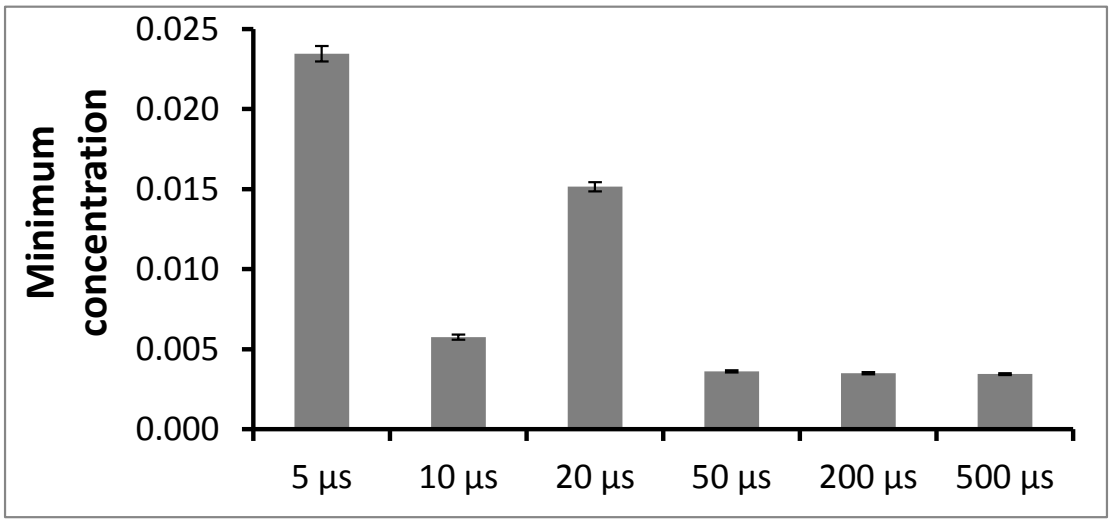


(C)

Figure 2.15 (A) Effects of pulse duration on the microbubble concentration with smaller PRF; (B) the time took for the microbubble to reach a concentration of 0.015; and (C) the minimum concentration of microbubbles during exposure. The acoustic intensity is 0.8 MPa; PRF is 5 kHz and the irradiation time is 60 s. The data in (B) and (C) are averaged from three independent replicates and shown as the mean +/- standard deviation.

Obviously changes in pulse length result in changing in the rest time of the wave. Here in the 2 series, with the same pulse length, the rest time are different as two series have different PRF values. To understand whether the pulse length or rest time counts for the bubble concentration change, a pulse scale comparison was carried out. Take the 5 μs case for example, the case with 5 kHz PRF will have ten times totaled number of wave pulses of the case with 500 Hz PRF. If the first 6 seconds of 5 kHz is picked out, the total number of waves will then be the same with the case with 500 Hz PRF during all 60 seconds irradiation. The comparison is then made based on the same total number of ultrasonic waves of 4 different pulse durations at 2 different PRFs, shown in Figure 2.16. The horizontal axis is scaled time. For the groups with longer rest time, the axis is the real time. But for the groups with shorter rest time, the axis is an enlarged and pulse scaled time, in other words, the 6 seconds real time is divided into 60 equal parts.

It is found that at 5 μs pulse duration, the difference in rest time causes difference in bubble concentration change: the case with shorter rest time has quicker bubble concentration loss. Beginning from 10 μs, there is no difference from rest time, even for the case of 50 μs pulse duration where the rest time multiplies by 13 times for two different PRFs. The reason is that during 5 μs ultrasound wave irradiation, the contrast agent may be still oscillating and the wave is not long enough to collapse the bubbles. The coming 5 μs irradiation will continue to act on the same bubbles so there is a gain like pattern of bubble behavior. While for pulse duration no shorter than 10 μs, the bubbles collapsed during one cycle. The next cycle will have no effect and only act on new bubbles. As a result, for bubbles, there is no memory of former pulse shot. Thus the difference from rest time is not found.

Then it is concluded that the bubble concentration loss comes from effect of pulse duration rather than rest time. What’s more, as discussed, beginning from certain pulse duration, the bubble concentration loss pattern becomes the same which is quick collapse dominant. So for contrast agent, the influence from pulse duration is not as strong as that from intensity.

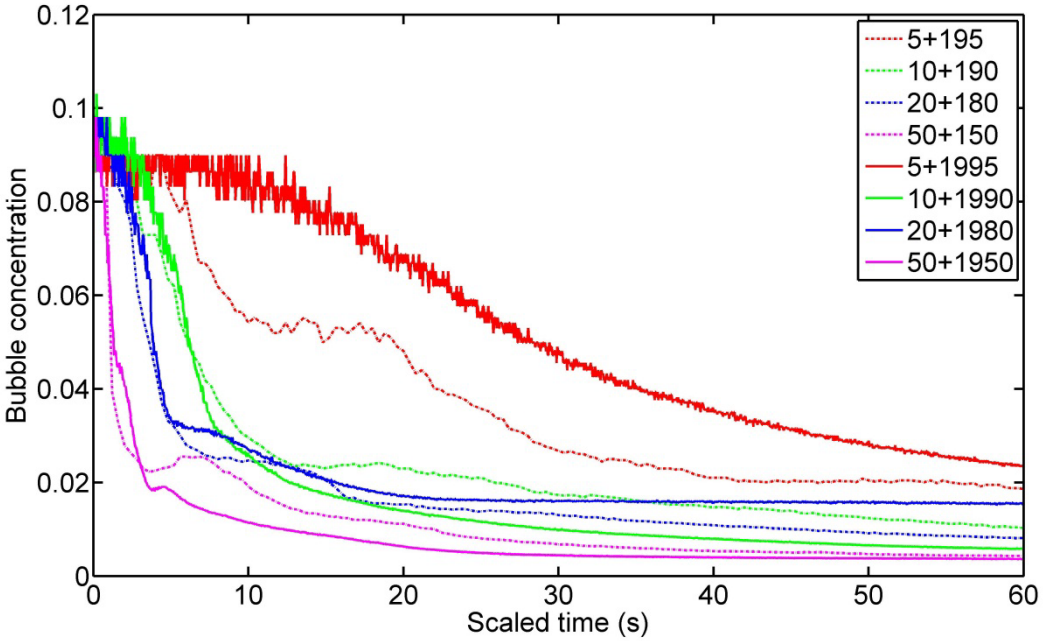


Figure 2.16 Pulse number scaled concentration change from different pulse lengths. The details of the waves are shown by the legend with μs unit. The acoustic intensity is 0.8 MPa; the duty cycle is kept at 10%; and the irradiation time is 60 s.

### 2.3.5 Influence of PRF

Burst settings, as introduced in Part 2.2.2, including pulse duration and pulse repetition frequency (PRF). Different burst settings have different total 'on' time of ultrasound and thus have different total energy.

The influence of PRF on microbubble concentration was tested. The initial microbubble concentration is 0.1 (10% volume to volume). The concentration change details of microbubbles during irradiation of 8 PRF values together with continuous wave case were shown in Figure 2.17. The other parameters were set as: the acoustic intensity is 0.8 MPa; the duty cycle is kept at 10%; and the irradiation time is 60 s except for the continuous case where the irradiation time is 20 s.

Overall, in all the cases the bubble concentration dropped very steeply. At an intensity of 0.8 MPa and 10% of duty ratio, in all cases within 4 seconds the concentration reached or went even lower than 0.015, and the minimum concentration after exposure for all cases were around zero. The difference between different PRFs

was not distinct, although as PRF decreased the concentration slightly dropped more quickly. So for all the PRF cases tested, violent collapse was here believed to be the dominant behavior. The majority of bubbles collapsed very quickly and fiercely. The further details of the influence of PRF on bubble radial dynamics will be discussed by their noise emission results.

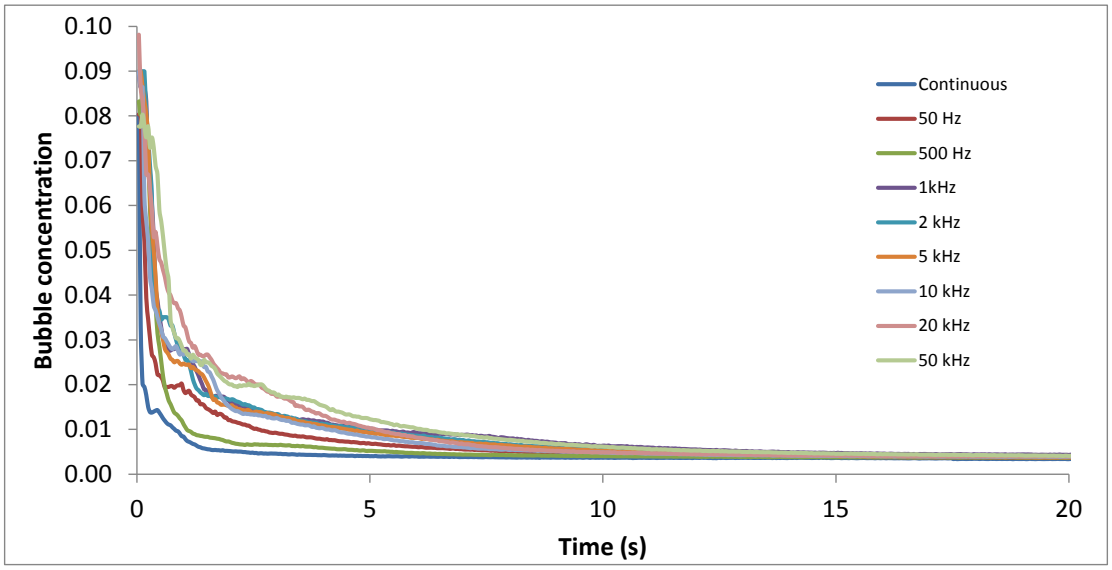


(A)

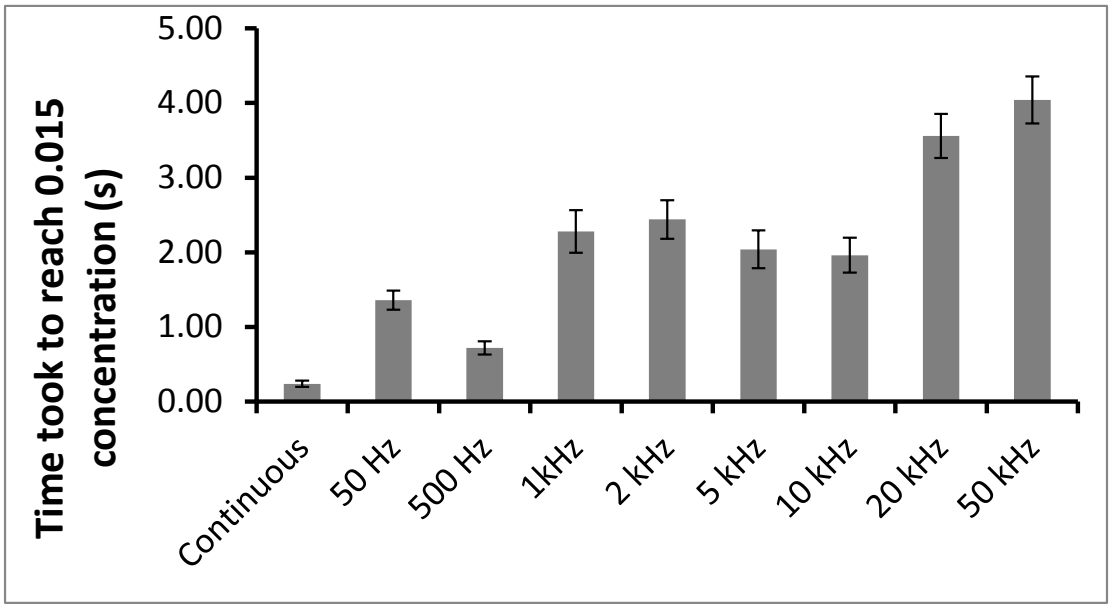


(B)

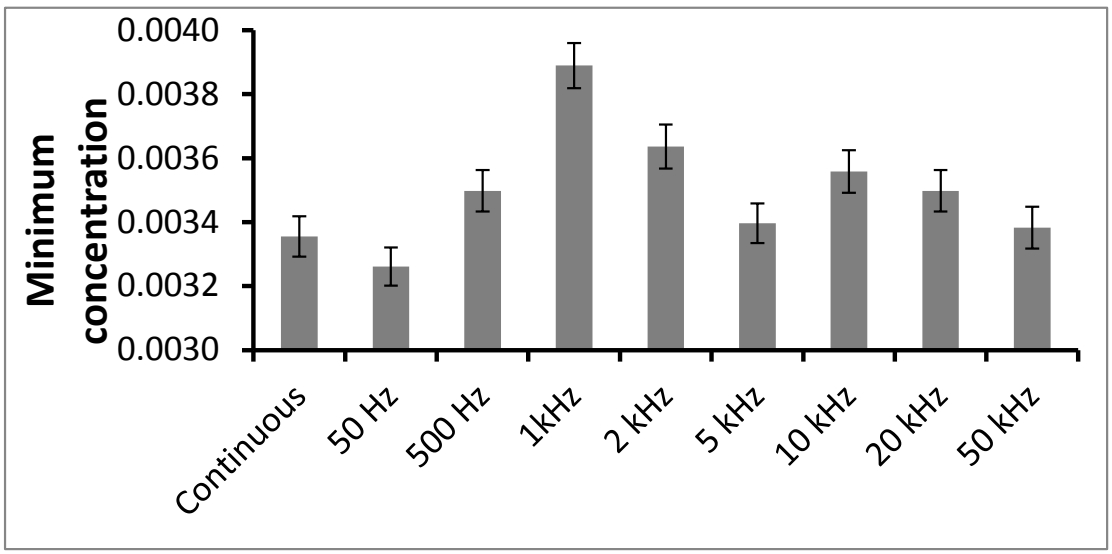


(C)

Figure 2.17 (A) Effects of PRF on the microbubble concentration, the data after 20 seconds were not shown; (B) the time took for the microbubble to reach a concentration of 0.015; and (C) the minimum concentration of microbubbles during exposure. The acoustic intensity is 0.8 MPa; the duty cycle is kept at 10%; and the irradiation time is 60 s. The data in (B) and (C) are averaged from three independent replicates and shown as the mean ± standard deviation.

## 2.4 Summary

Sonoporation is highly cavitation related so the study on sonoporation begins with bubble behavior in this dissertation. An ultrasound exposure system with full control over parameters was used to irradiate sound wave to microbubble containing liquid in a 24-well commercial plate. Using a laser diode unit, the concentration of microbubbles was measured during various exposure conditions. The influences of ultrasonic parameters, including intensity and burst settings, on change of microbubble concentration during irradiation were studied. The following conclusions are made:

- The plastic plate does not affect the propagation of sound wave. Reflection and absorption of waves from the plate are negligible for the following experiments. The planar distribution shows that the distribution of sound wave is not very uniform and the intensity for experiments is averaged value.

- There are two different patterns of bubble concentration change during irradiation: oscillation dominant and collapse dominant. For intensities less than 0.3 MPa, the bubble behavior is oscillation dominant; for intensities larger than 0.4 MPa, the bubble behavior is collapse dominant. There is a pattern shift of bubble behavior between these two intensities.

- For oscillation dominant bubble behavior, bubble oscillation and collapse coexist during all irradiation time while for collapse dominant bubble behavior, microbubble collapsed to a concentration near zero with in less than half of the irradiation time, differing from the settings.

- The influence of total energy related parameters are clear. With larger intensity and longer pulse duration, bubbles concentration dropped more quickly and the final concentration is smaller. With pulse duration changing, the influence from rest time is not obvious.

- With pulse durations no shorter than 10 μs, pulse duration rather than the rest time is the leading factor in a burst for its influence on bubble behavior.

- The influence of PRF on bubble concentration change is not as straight as intensities. With longer pulse duration, bubbles concentration dropped slightly more quickly.

- With 0.8 MPa acoustic intensity, all the burst setting cases tested present collapse dominant bubble behavior, which here means that the bubble concentration drops to less than 0.015 within less than 10 seconds, except for only one case with short pulse duration (5 μs, PRF=500 Hz).

# Chapter 3. Bubble behavior analysis from cavitation noise

The oscillation and collapse of microbubbles are introduced. Chapter 2 deals with the concentration change of microbubbles due to the collapse while this chapter focuses on the signals emitted while bubbles experience radial oscillation and violent collapse, aim at deeper understanding of the cavitation process and its relationship to further delivery process. With such understanding and summarizing the results together with that obtained in Chapter 2, bubble behavior with experiment settings for sonoporation delivery is summarized here .

## 3.1 Cavitation noise

### 3.1.1 Broadband noise source

As a bubble oscillates, itself becomes a sound source and emits sound waves. Such signals can be recorded and analyzed to obtain information on bubble radial dynamics. This tool is very effective since no matter what type of cavitation is bubbles experience radial oscillation or collapse. As shown in Figure 2.1 and Figure 2.2, the radial oscillation as well as the violent collapse of microbubbles will emit sound signals. A source list of emitted signals is shown in Figure 3.1 [80]. Bubble oscillation may show different patterns with different nonlinearity, which results a difference in emitted signal.

If the driven power is low, then the bubble simply pulsates in an approximately linear manner and the emitted signal is simply at the insonation frequency. However, the spectrum of the acoustic signal generated by bubbles cavitating in more powerful acoustic fields may contain broadband signals. Such type of emitted signal is often called broadband cavitation noise. An example of such broadband emission is shown in Figure 3.2 [81]. The driving frequency is 1 MHz, driving amplitude is 0.1 MPa, and the initial radius is 1.7 μm. The upper one shows a typical nonlinear bubble radius oscillation curve, and due to the oscillation the bubble in turn becomes a sound

source and emits signals, shown in the middle one. Changing the signals in the middle one from time domain to frequency domain, oscillation characteristics is shown in the lower one. Many frequency peaks can be seen since the oscillation is highly nonlinear. Such peak dotted spectrum represents harmonics, subharmonics and ultraharmonics of the insonation frequency [82]. A typical acoustic emission spectrum consists of peaks at specific frequencies that are harmonics or subharmonics of the driving ultrasound frequency, and broadband noise that spans the full frequency domain.

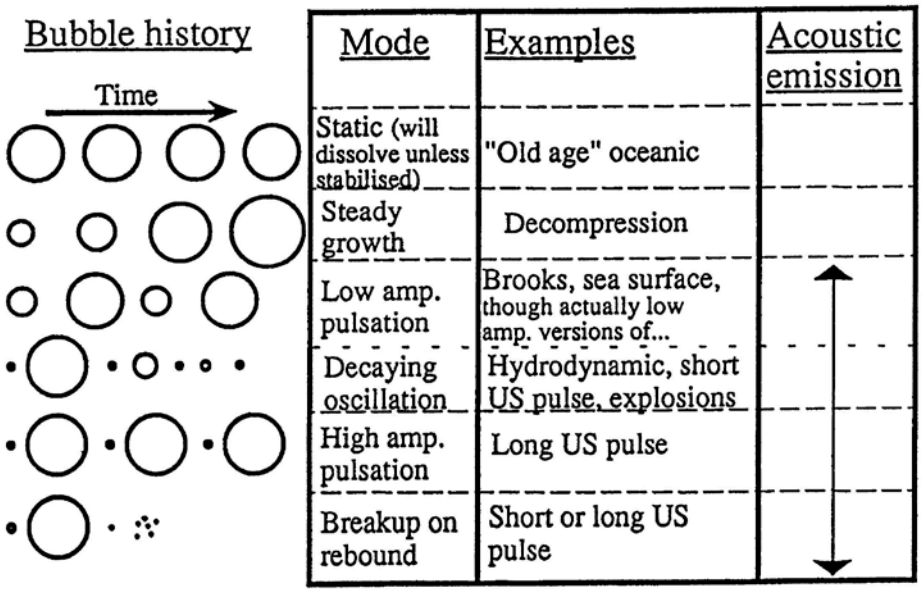


Figure 3.1 Sources of acoustic emission [80]

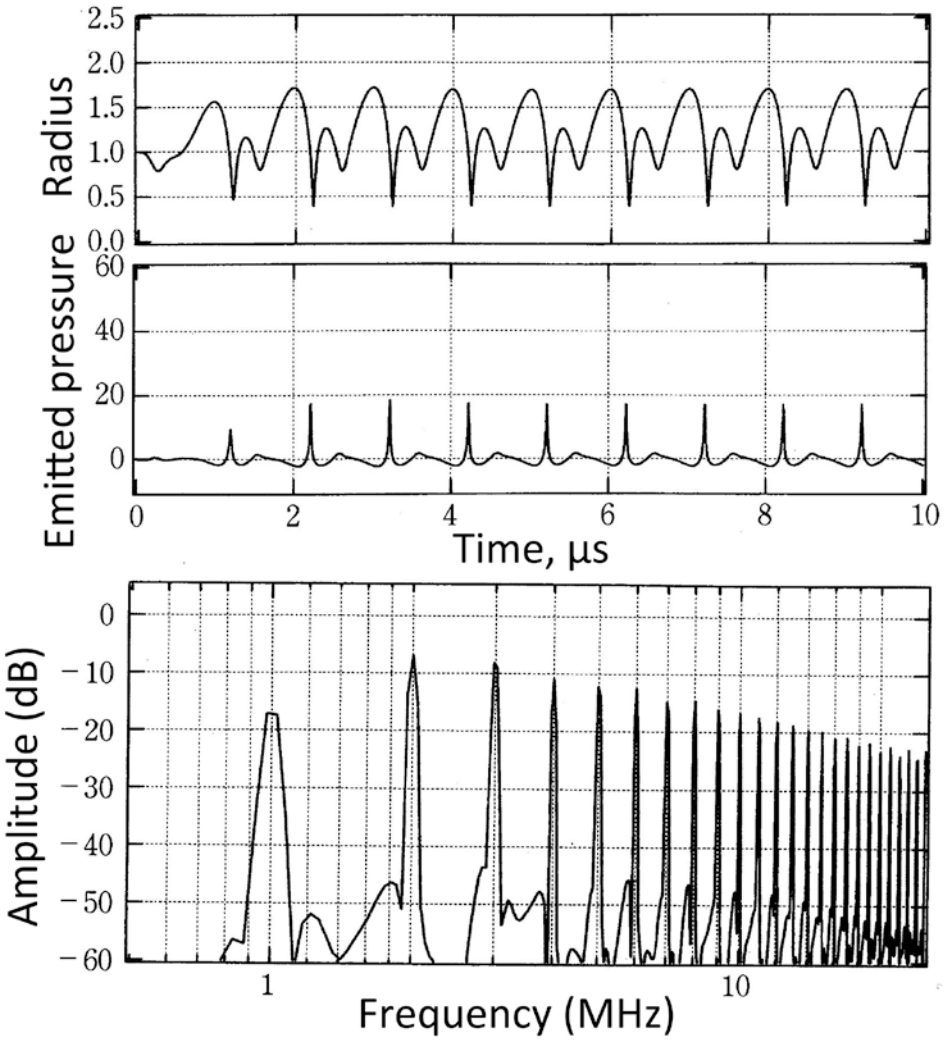


Figure 3.2 An example of broadband noise [81]. The upper one is the radius time curve, the middle one is the corresponding emitted sound signal due to the radial oscillation, and the lower one is the frequency domain characteristics of the signals.

### 3.1.2 Noise spectrum

Identifying the relationship between these emissions and cavitation dynamics are usually discussed separately based on whether the cavitation is stable or inertial, in other words, whether the bubbles keep oscillating or collapse, though realistically these two types often entangle with each other. In our research since direct measuring of bubble radius is not possible, they details of cavitation will be revealed by the analysis on the acoustic emissions during cavitation process.

Frequencies of both the harmonic (n*f*) and ultraharmonic ((2n+1)*f*/2) of the fundamental driving frequency '*f*' are generally believed to be related to stable cavitation; while frequencies of the subharmonic (*f*/n) and frequencies over a large range, in other words, broadband signals are somehow related to inertial cavitation [80] [82]. It is suggested that the broadband noise arises due to the emissions from rapidly changing bubble radii, whereas the subharmonic emissions originate from the prolonged expansion phase and a delayed collapse of oscillating bubbles. Both types of emissions have been reported in the case of transient cavitation, but there is growing support for using broadband noise as an indication of the onset of violent collapse in cavitation [83] [84] [85]. Here in this study, a frequency interval excluding any subharmonics or ultraharmonics is chosen to indicate details of inertial cavitation.

As the oscillation goes more nonlinear, the frequency domain becomes more complicated since half or even quarter of the frequencies will come out [86]. To make this total harmonics analysis easier to understand, Lauterborn gave a plot method showing the so called 'visible noise' [87], as shown in Figure 3.3. As intensity increased, the noise signal spectrum covered large range of frequencies. In other words, the spectrum changed from a peak lined style to a broadband style. The frequencies evolving process over other parameters, such as intensity, can be shown over time. Such evolving plot gives information on cavitation type transition as well as influences from parameters on cavitation. To understand more on cavitation and influences from parameters, similar plots are shown in this thesis.

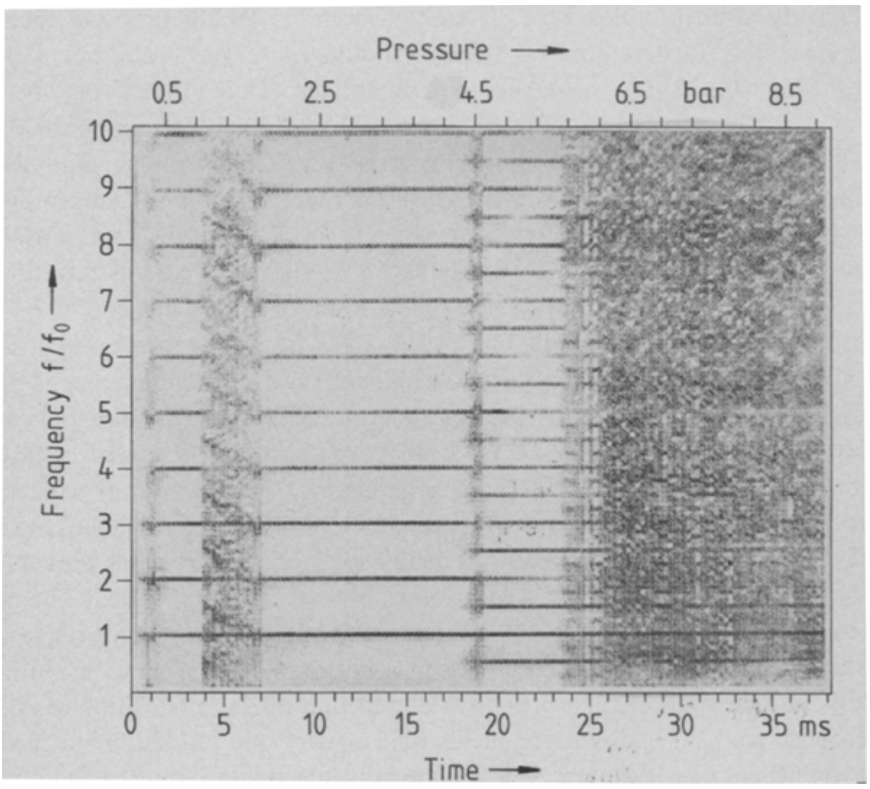


Figure 3.3 An example plot of ‘visible noise’ [87]

### 3.1.3 Two ‘phases’ of cavitation

As introduced in Chapter 2, gas bubbles with shell are added in all experiments. The collapse of these shelled bubbles resulted in the concentration drop, which is recorded by the laser diode method. However; even after the majority of shelled bubbles had collapsed, cavitation activities are still to be expected since there are cavities inside the medium. Here these two different phenomena are defined as two ‘phases’ of cavitation: shelled bubble cavitation phase and cavity cavitation phase. The latter escapes from the laser diode measuring and its details are analyzed with noise spectrum in this chapter.

The two ‘phases’ are discussed separately because the bubble oscillation and collapse behavior are different. Surface tension is a fundamental property of a fluid interface between gas and liquid phases. A newly formed cavity without encapsulation will dissolve spontaneously and nearly instantaneously as a consequence of surface tension at the gas-liquid interface. While to make a contrast

agent stable during circulation, the microbubble shell must be solid to eliminate surface tension and impart a significant permeation resistance.

Artificially added microbubbles no longer exist, or drop to a negligible concentration after violent collapse. The situation of cavities without shells is more complicated. Cavities may come into being during the rarefaction phase of the pressure wave. The collapse of shelled bubbles can also result in fragmentation of the bubble into smaller bubbles and/or dissolution of the encapsulated gas.

The details of difference between these two ‘phases’ are reviewed by Klibanov [88] and Ferrara [89]. In this chapter the focus is to prove the existence of such difference and correlates it to future different cell behavior.

No matter what analyzing methods are adopted, cavitation noises are studied here to relate the biological effects of ultrasound to both subharmonic and broadband emissions. Relationships between broadband noise levels and biological effects were discussed and correlation was proved [90] [91]. The cavitation noise results here discussed in our study will also be compared later to the intracellular delivery behavior of cells.

In this chapter, broadband noise were captured with the exact experimental conditions as done in Chapter 2 in order to obtain knowledge of bubble oscillations before or on the collapse process. Strong broadband signals emitted during collapse also give explanations to the collapse of artificially added contrast agents as well as cavities inside the medium.

## 3.2 Experimental methods

### 3.2.1 Data collecting unit

The exposure system is the same as introduced in part 2.2.1. To record the cavitation noise, the 24-well is partly immersed to water in a tank, and a focused hydrophone is placed near the transducer to collect signals, as indicated in Figure 4. The water inside the tank is degassed for more than 4 hours before experiment and a water bath unit keeps the temperature at 37 °C.

The focused hydrophone is customized by ELEMECH Electronics (Niigata,

Japan). Its central frequency is 2 MHz and responds flatly to a frequency range from 100 kHz to 10 MHz. The vibrating part is a PVDF membrane and the radius is 50 mm. The focal length is 45 mm. Signals from this hydrophone is amplified by an AG-2010 amplifier (ONDA, Seattle, WA) and then connected to the oscilloscope where these signals are saved, as shown in Figure 3.4. The hydrophone and the transducer are aligned in such a way that the highest points of the piezo material of the transducer and the PVDF membrane of the hydrophone are at the same height, and that the distance between two center points is the focus length of the focused hydrophone, which is, 45 mm.

The frequency of data saving to oscilloscope is 25 Hz. The sampling frequency is set to be 20 MS/s and each datum contains 1 k sampling points, corresponds to a time length of 50 μs.

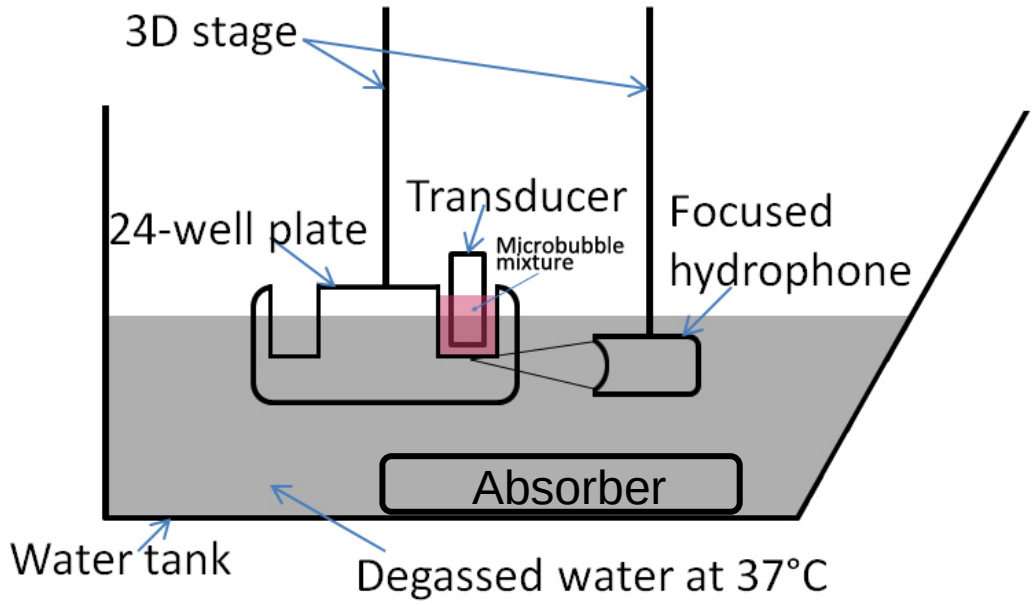
3D stage
Transducer
24-well plate
Microbubble mixture
Focused hydrophone
Absorber
Water tank
Degassed water at 37°C

(A)

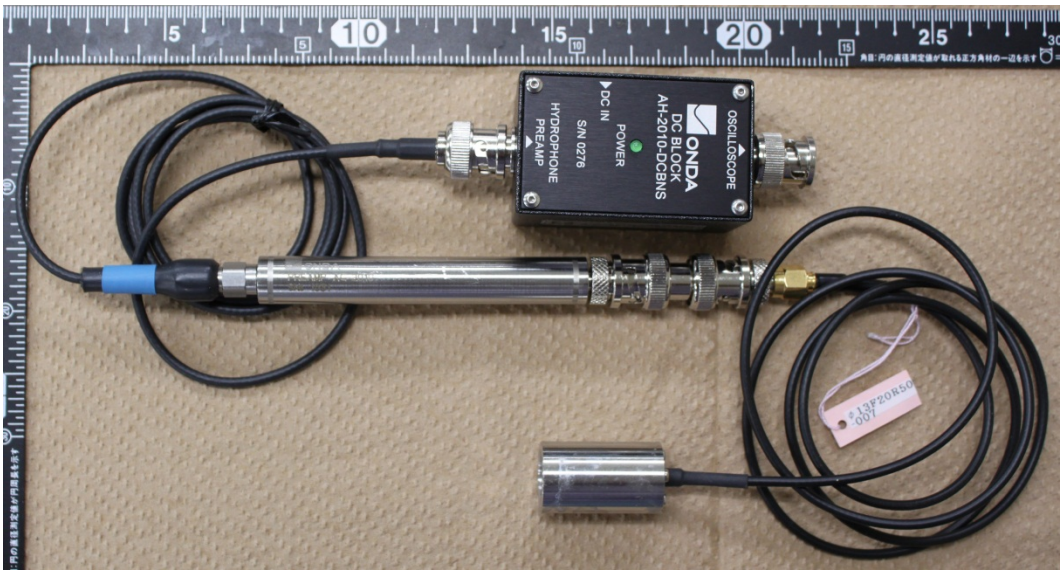
HYDROPHONE PREAMP
S/N 0276
DC IN
POWER
ONDA
DC BLOCK
AH-2010-DCBNS
OSCILLOSCOPE

(B)

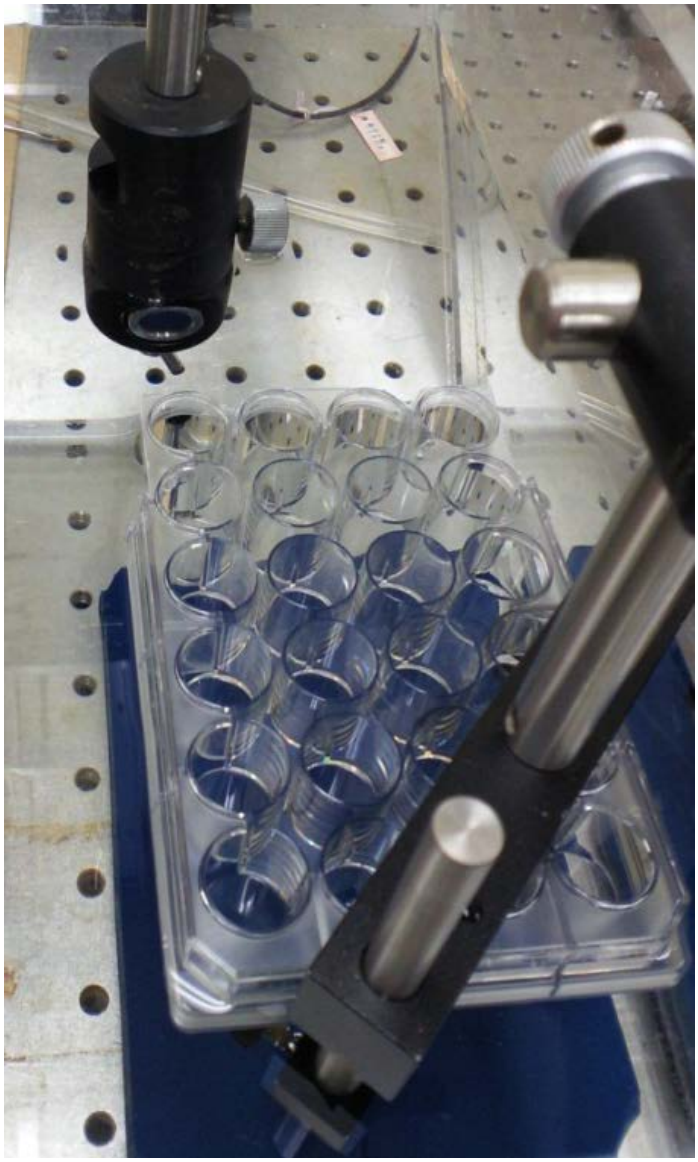

(C)

Figure 3.4 Experimental setup for cavitation noise recording system. (A) is the diagram plot; (B) is a photo of the system; and (C) is a photo of focused PVDF hydrophone and preamplifier, in which the lower unit is the focused hydrophone, the middle unit is the preamplifier, and the upper unit is the power supply for the preamplifier.

### 3.2.2 Data processing

For each datum, the sampling frequency is 20 MHz and each datum has a time length of 50 μs. The data is saving at 25 data per second. When pulse duration is 20 μs and PRF is 5 kHz, the datum contains the full mark part of the burst cycle for almost all cases, shown in Figure 3.5, A typical time domain signal shown in Figure 3.5 (A) which is recorded by the focal hydrophone and saved by the oscilloscope is then transformed to frequency domain by a FFT operation in Matlab™. Since the sampling frequency is 20 MHz, the frequency domain includes a range from 0 to 20 MHz. Dividing this range by the total number of sampling points, so the frequency increment is 20 kHz. Here the driving frequency is 2 MHz, any frequencies larger than 10 MHz are out of interest as they reveal little on bubble radial movements, and then here a frequency domain plot within 10 MHz is shown in Figure 3.5 (B).

Figure 3.5 (B) shows a typical frequency domain pattern. The scattering of the driving ultrasound signal makes the driving frequency, 2 MHz, the highest peak. To obtain more information of harmonics as well as broadband noise signals, limited magnitude of frequencies is also applied, indicated by the horizontal line. For example, here in Figure 3.5 (B) the maximum power value is 12.95 and in most cases a range of power less than 0.6 is shown.

Representative frequency values as well as intervals of frequencies are then chosen to show cavitation details. For example, harmonics frequencies such as 2, 4, and 6 MHz, intervals such as 0 to 1 MHz, and 2 to 3 MHz are plotted. For intervals there are 50 frequency values inside this interval and the averaged power magnitude is calculated. This averaged value represents the cavitation noise level for the very interval chosen. In 60 s irradiation, a total number of 1500 data were obtained for one case and the spectrum covers from 0 to 20 MHz. In some cases the data were averaged over time while in some other cases, the data were averaged over the frequency range.

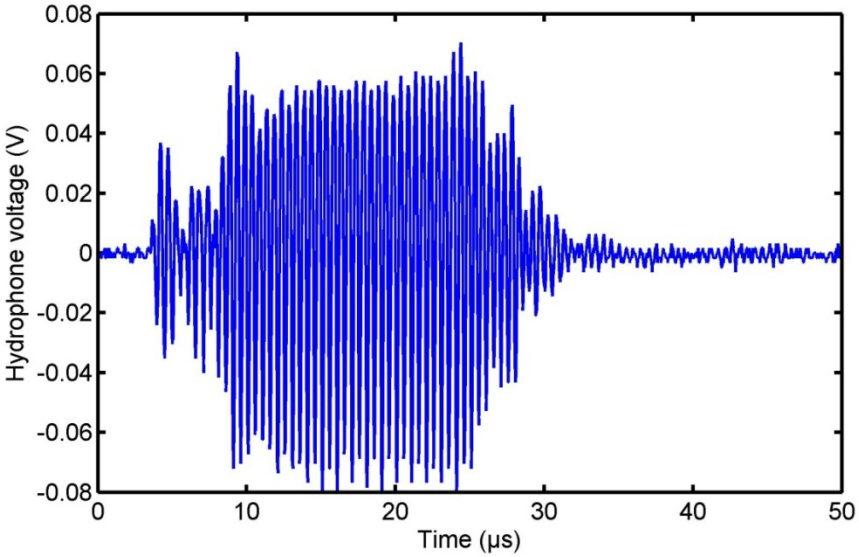


(A)

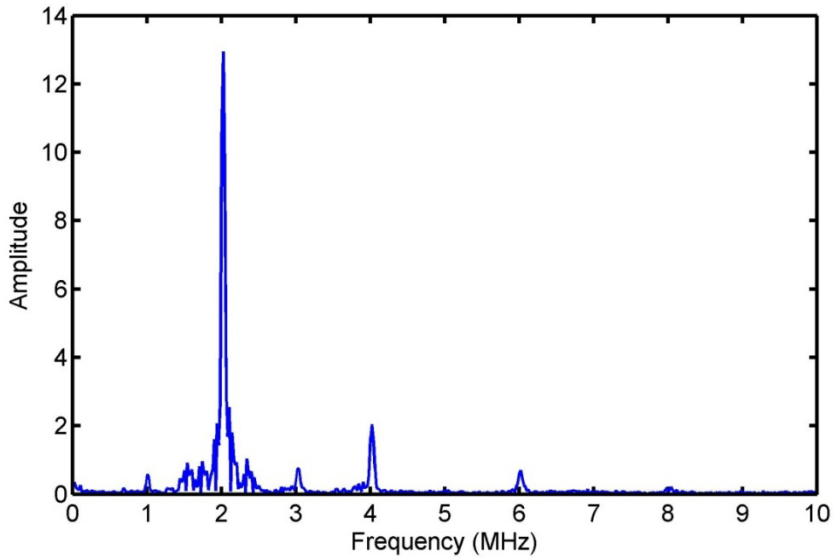


(B)

Figure 3.5 Noise spectrum processing method. The time domain signal (A) is obtained and then transformed to frequency domain in (B).

### 3.2.3 Irradiation protocols

For tested group, Sonazoid$^{TM}$ is mixed to Dulbecco's modified Eagle's medium (DMEM) supplemented with 10% v/v fetal bovine serum (FBS) and 1% v/v antibiotics (Penicillin-Streptomycin and L-Glutamine) by pre-decided volume concentration (in most cases, 10% microbubble). 0.8 ml of such mixture is injected to a well of 24-well plate placed on a sheet of sound absorbing material. The transducer is then injected into this well and ultrasound exposure begins. After irradiation, the mixture is drawn out using a pipette and the well is rinsed with water for 2 times before next test.

For control groups, the medium contains no microbubbles but only 0.8 ml DMEM medium. The exposure condition for each controlling case is identical as the corresponding test case.

Totally 23 experiment conditions were carried out for both control and test groups. The irradiation time for all cases is 60 seconds and the other details of each condition are shown in Table 3.1. Case 1 to case 8 together are defined as the intensity series; case 9 to case 15 together are defined as PRF series; case 16 to case 18 together are defined as pulse duration series at 5 kHz PRF; and case 19 to case 23 together are defined as pulse duration series at 500 Hz PRF.

Table 3.1 Experiment conditions

| Case number | Intensity (MPa) | PRF (kHz) | Pulse duration (μs) | Space (μs) | Duty ratio (%) |
|---|---|---|---|---|---|
| 1 | 0.1 | 5 | 20 | 180 | 10 |
| 2 | 0.2 | 5 | 20 | 180 | 10 |
| 3 | 0.3 | 5 | 20 | 180 | 10 |
| 4 | 0.4 | 5 | 20 | 180 | 10 |
| 5 | 0.6 | 5 | 20 | 180 | 10 |
| 6 | 0.8 | 5 | 20 | 180 | 10 |
| 7 | 1.0 | 5 | 20 | 180 | 10 |
| 8 | 1.2 | 5 | 20 | 180 | 10 |
| 9 | 0.8 | 50 | 2 | 8 | 10 |
| 10 | 0.8 | 20 | 5 | 45 | 10 |
| 11 | 0.8 | 10 | 10 | 90 | 10 |
| 12 | 0.8 | 2 | 50 | 450 | 10 |
| 13 | 0.8 | 1 | 100 | 900 | 10 |
| 14 | 0.8 | 0.5 | 200 | 1800 | 10 |
| 15 | 0.8 | 0.05 | 2000 | 18000 | 10 |
| 16 | 0.8 | 5 | 5 | 195 | 2.5 |
| 17 | 0.8 | 5 | 10 | 190 | 5 |
| 18 | 0.8 | 5 | 50 | 150 | 25 |
| 19 | 0.8 | 0.5 | 5 | 1995 | 0.25 |
| 20 | 0.8 | 0.5 | 10 | 1990 | 0.5 |
| 21 | 0.8 | 0.5 | 20 | 1980 | 1 |
| 22 | 0.8 | 0.5 | 50 | 1950 | 2.5 |
| 23 | 0.8 | 0.5 | 500 | 1500 | 25 |

## 3.3 Results and discussions

### 3.3.1 Visible noise

The sources of emission may be oscillation and collapse of shelled bubbles as well as cavities. Since the horizontal axis is time which covers a full range of irradiation, the contour provides information of evolvement of the frequency spectrum. As introduced, collapse is a temporal behavior lasting for only a short time while oscillation can last for longer time, or even over all the 60 s. To identify different sources of emission, in other words, different bubble behaviors, the spectra of both control and tested results for a single case are shown in Figure 3.6 and 3.7, by putting all the 1500 time steps' noise spectrum together. The experimental settings for the case shown are: case 15, 0.8 MPa intensity, 0.05 kHz PRF, and 10% duty ratio.

Figure 3.6 shows contour plots for control and tested cases while Figure 3.7 shows the value of frequency powers averaged over frequency intervals. To capture more details of spectra, the range of power magnitude in contour plot in Figure 3.6 does not include all the whole value range. In both Figure 3.6 (A) and Figure 3.7 (A), three broadband peaks around 1, 14, and 42 second are temporal, in other words, the broadband frequency power value increases and then decreases and after the peak the frequency power values restore after several seconds. Such pattern of change in frequency power shows that collapse of cavity happened in control case, without adding any contrast agents. Horizontally stable signals, such as strong signals around 3 MHz and 6 MHz last over all the 60 seconds, showing that oscillation of cavity also happened.

Adding of contrast agents brings large difference to noise spectra. The two later peaks appeared in both Figure 3.6 (A) and Figure 3.7 (A) disappeared after adding microbubbles into the medium, shown by Figure 3.6 (B) and Figure 3.7 (B). A peak appeared within the first 2 seconds. In Chapter 2, it has been shown that the bubble concentration drops to nearly zero within 2 seconds. So here the collapse signal in Figure 3.6 (B) also proves that the concentration drops measured by the laser diode unit in Chapter 2 are due to the collapse of bubbles. What's more, strong horizontally stable signals at more frequency values appear with microbubbles added, indicating

that stronger oscillation even with extremely low bubble concentration compared to control case.

For tested case, as shown by laser diode results, almost all of the bubbles collapsed after 2 seconds. However, there are dramatic differences between (A) and (B) in both Figure 3.6 and Figure 3.7 during 2 and 60 seconds. So the fact of adding microbubbles will influence bubble radial dynamics not only when they are in the medium but also after they have collapsed. Such influence may come from two factors. The first one is the collapse of shelled microbubbles will emit the gas contained within the shell, which will serve as new cavitation nuclei, making oscillation or collapse of cavity easier to happen. The other one is that debris of collapsed lipid shells will add impurity to the medium, which may also serve as nuclei.

One more thing shown in both Figure 3.7 (A) and Figure 3.7 (B) is that the majority of emitted signals fall into the frequency interval of 1.5 to 2.5 MHz. This frequency interval is chosen to compare emission levels between different cases in the follows sections.

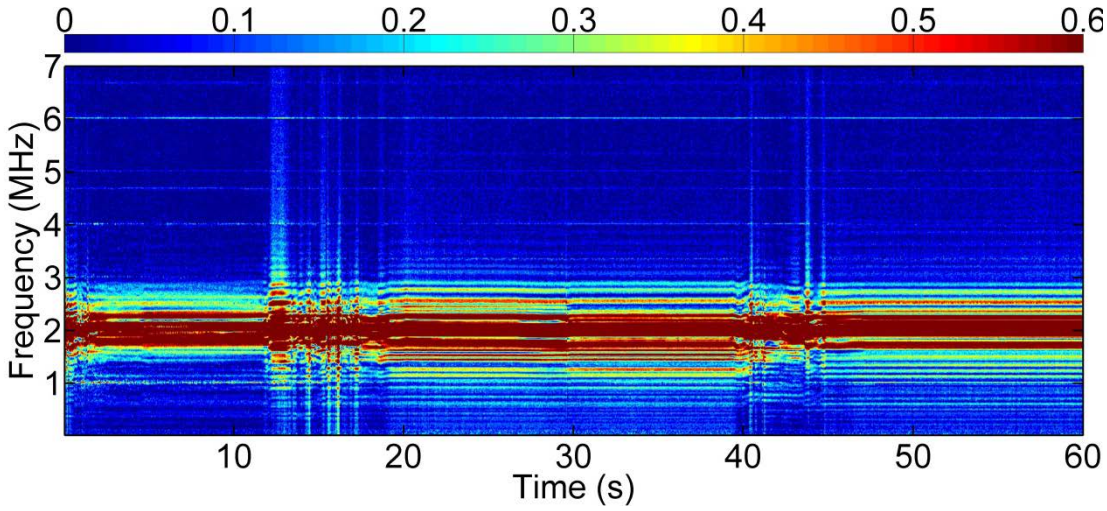


(A)

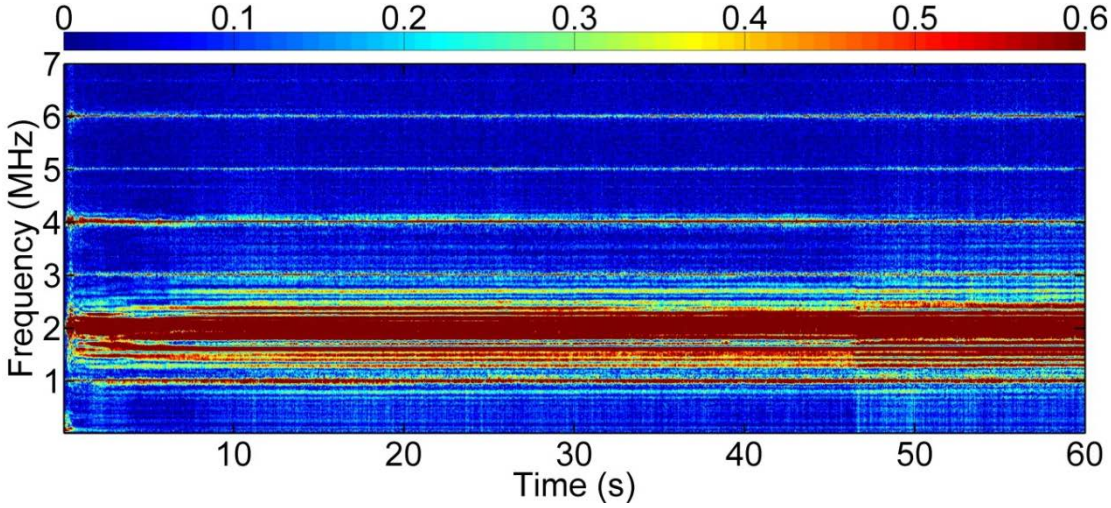


(B)

Figure 3.6 Cavitation noise spectrum contour of case 15 over the whole irradiation time. (A): control case without microbubbles; (B): tested case. The irradiation time is 60s; PRF is 0.05 kHz and the duty ratio is 10%. Color bar is the value of the power of frequencies after FFT with limited value range.

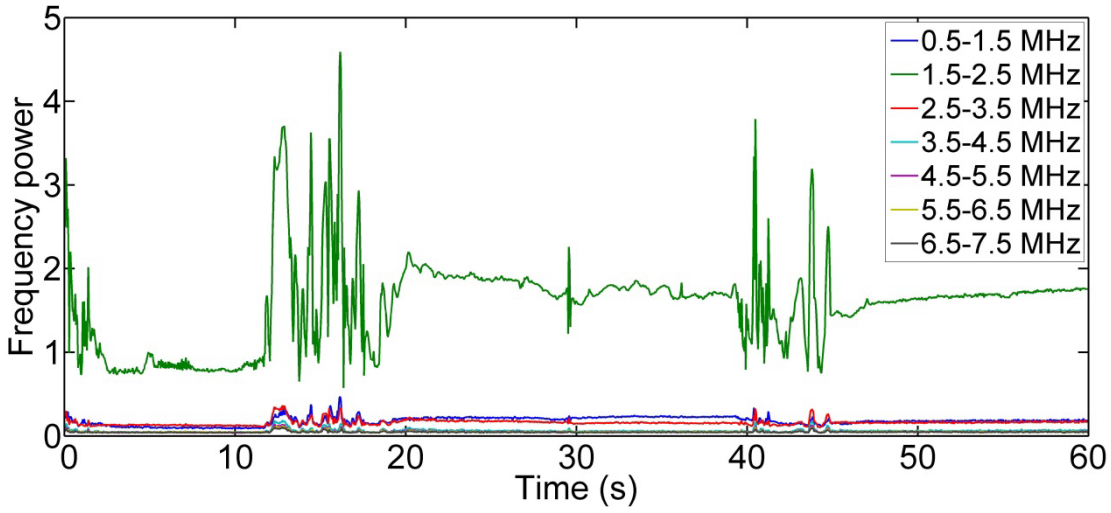


(A)

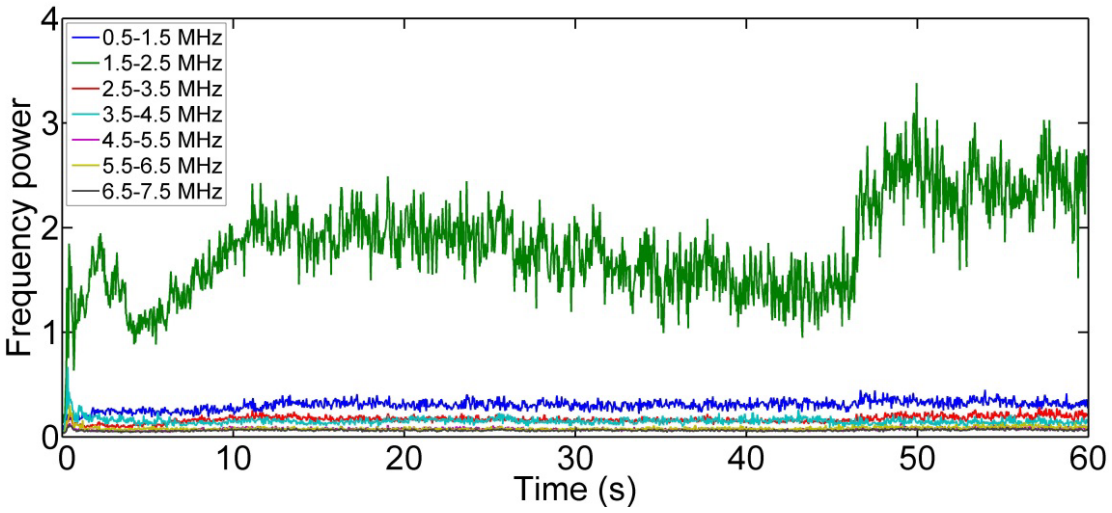


(B)

Figure 3.7 Averaged emission level of case 15 over the whole irradiation time. (A): control case without microbubbles; (B): tested case. The value of frequency power is averaged value over a frequency interval, indicating by the legend. The irradiation time is 60s; PRF is 0.05 kHz and the duty ratio is 10%.

### 3.3.2 Parametric influence on noise emission

Part 3.3.1 shows the noise spectra for a single case during whole irradiation time of 60 seconds. As listed in Table 3.1, there are total 23 cases tested, divided into 3 different series. The details of results are shown and discussed series by series in the following sections.

#### 3.3.2.1 Intensity series

In intensity series, 8 intensities from 0.1 MPa to 1.2 MPa were tested. The PRF is 5 kHz, the duty ratio is 10%, and the irradiation time is 60 seconds. At 0.1 MPa of intensity, no bubble activities are found by laser diode results. So here beginning from 0.2 MPa, noise spectra for 7 tested cases are shown in Figure 3.8.

Figure 3.8 (A) and Figure 3.8 (B) are contour plots of all 7 intensities, where Figure 3.8 (A) shows the first 10 seconds, i.e. from 0 to 10 seconds and Figure 3.8 (B) shows the third 10 seconds, i.e. from 30 to 40 seconds. Figure 3.8 (C) shows averaged emission level of 7 intensities represented by the interval of 1.5 to 2.5 MHz over all the 60 seconds irradiation time. Figure 3.8 (D) shows the frequency magnitude of 5 selected intensities, from 0 to 10 MHz, averaged over all the 60 seconds irradiation time.

In Figure 3.8 (A) during the first 10 seconds, no clear emission signals of either collapse of oscillation are captured in 0.2 MPa and 0.3 MPa cases. Beginning from 0.4 MPa, emission signals become apparent: from 6 second weak collapse signals and harmonics at $2f_0$ and 3 $f_0$ ($f_0$ is the driving frequency, i.e. 2 MHz) can be found. Beginning from 0.6 MPa, peaks of broadband frequency due to collapse, as well as horizontally stable frequencies of harmonics due to oscillation become clear. Ultraharmonic signals at 3/2 $f_0$ appear and then disappear from 1.0 MPa. Beginning from 1.0 MPa, the emissions become much broadband like, especially under the frequency of 4 MHz.

In Figure 3.8 (B), beginning from 0.4 MPa, horizontally stable frequency signals due to oscillation dominate the spectra. Similarly, ultraharmonic signals at 3/2 $f_0$ are apparent at only 0.6 MPa and 0.8 MPa. Beginning from 1.0 MPa, the emissions become much broadband like, especially under the frequency of 3 MHz. Under the

intensity of 1.0 MPa, there are only horizontal stable style emissions indicating that cavities are oscillating. Beginning from 1.0 MPa, the noise like broadband signals appear together with horizontally stable emissions, though with weak values, showing the happening of weak collapse of cavities.

As introduced in Figure 3.7, the main emission of noise falls into the frequency interval of 1.5 MHz to 2.5 MHz. In Figure 3.8 (C), the emission level increases as intensity increases only that the emission level of 1.2 MPa is smaller than that of 1.0 MPa. From 1.0 MPa, after 10 seconds, the emission curve is more jigsaws like, in other words, there are alternating increases and decreases.

In Figure 3.8 (D), both harmonic and ultraharmonic signals become much larger when intensity increases from 0.3 MPa to 0.4 MPa or larger. From 0.4 MPa, the the changes of harmonic signals at the frequencies of $2f_0$, $3f_0$, and $4\ f_0$ are not significant while ultraharmonic signals or broadband signals between harmonic frequencies increase as intensity increases.

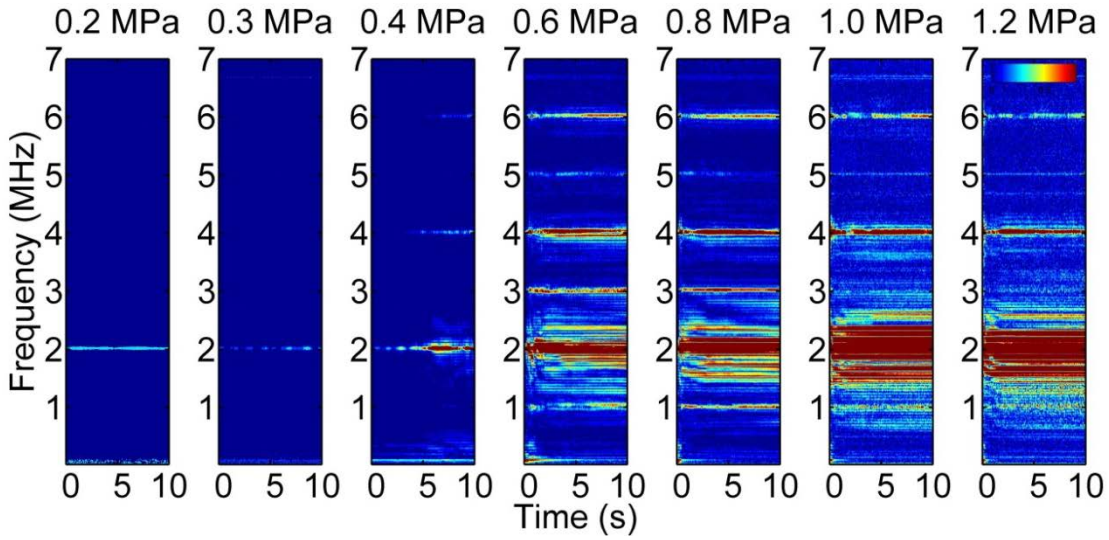
0.2 MPa
0.3 MPa
0.4 MPa
0.6 MPa
0.8 MPa
1.0 MPa
1.2 MPa
Frequency (MHz)
Time (s)

(A)

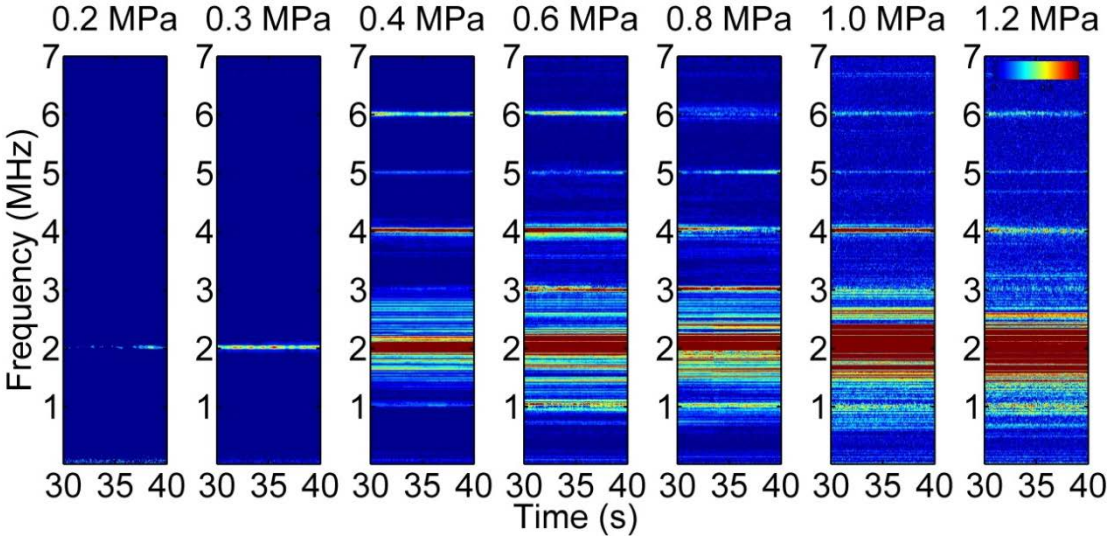
0.2 MPa
0.3 MPa
0.4 MPa
0.6 MPa
0.8 MPa
1.0 MPa
1.2 MPa
Frequency (MHz)
Time (s)

(B)

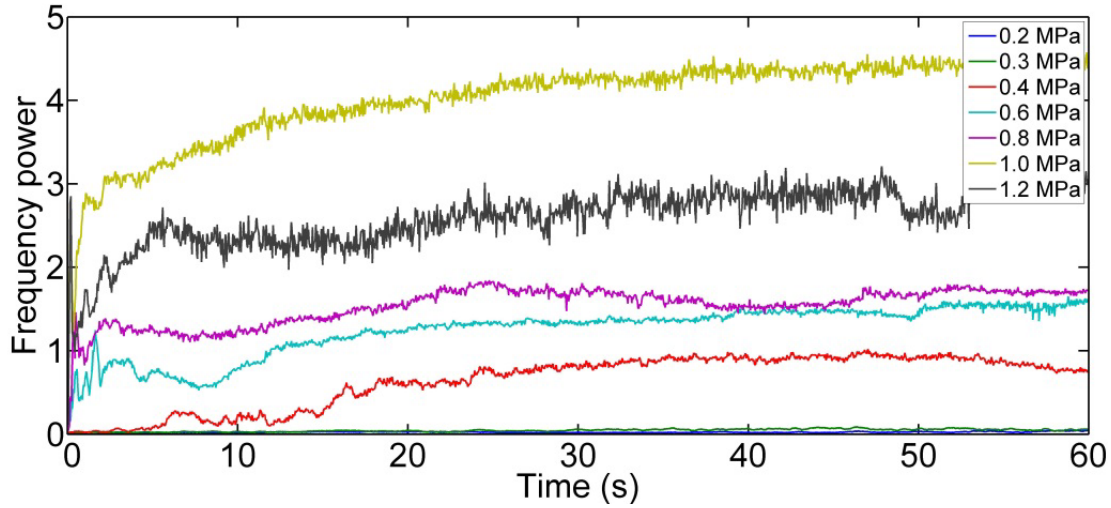


(C)

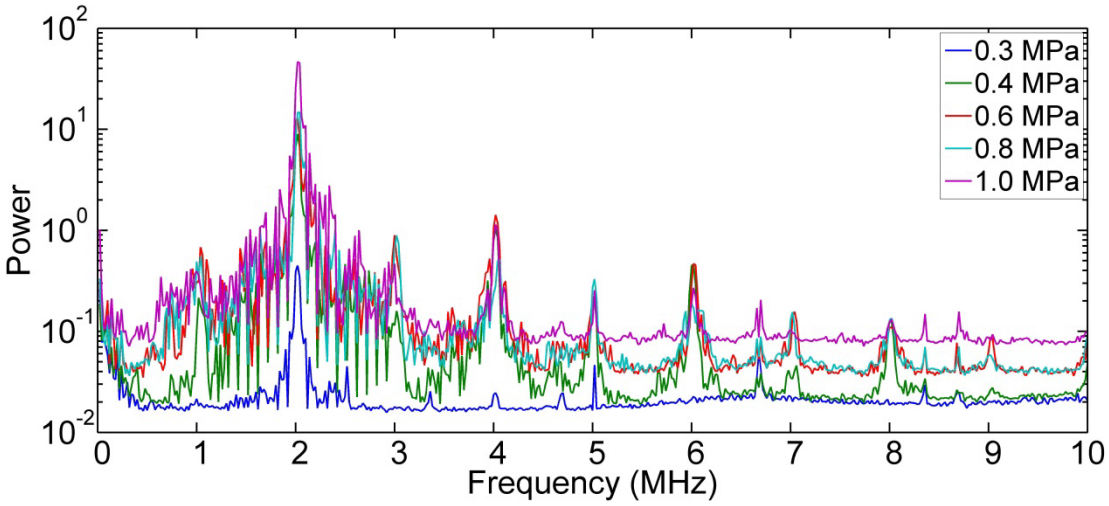


(D)

Figure 3.8 Influence of intensity on cavitation noise, (A) frequency contour during the first 10 seconds of irradiation; (B): frequency contour during the 3rd 10 seconds (from 30 to 40 second) of irradiation; (C): the noise emissions averaged over frequency interval of 1.5 to 2.5 MHz; (D): the noise emission spectra averaged over 30 to 40 second. The irradiation time is 60s; PRF is 5 kHz and the duty ratio is 10%. Color bar is the value of the power of frequencies after FFT with limited value range.

To discuss the influence of intensity on bubble behavior, the results from laser diode measuring will also be used.

Firstly, the difference between 0.3 MPa and 0.4 MPa is confirmed that shelled bubble changes from weak oscillation dominant to collapse dominant. For 0.2 MPa case and 0.3 MPa case, former threshold research has shown that the microbubble will begin to response with oscillations [92]. The results measured by laser diode have shown that at 0.3 MPa it takes more than 50 seconds for the bubble concentration to reach 1.5% while at 0.4 MPa the value is less than 10 seconds. Here in Figure 3.8 (A) and (B) the noise recorded at 0.3 MPa have only a peak frequency at driving frequency during both the first and third 10 seconds while the noise at 0.4 MPa show both collapse and oscillation behavior. The huge noise level difference between 0.3 MPa and 0.4 MPa in Figure 3.8 (C) also proves the change from weak oscillation dominant to collapse dominant.

Secondly, the intensity of collapse of shelled bubbles increases as intensity increases from 0.4 MPa. Beginning from 0.4 MPa, the concentrations of contrast agents drop to 1.5% within 10 seconds in all the cases. It has been prove that dramatic change of emission level comes from collapse behavior. In Figure 3.8 (C), it can be found that when intensity is above 0.4 MPa there are peaks of emission levels. While in Figure 2.12 (A), there are also extremely sharp drops of concentration. Since the sharp drop of bubble concentration comes from collapse, high level emission is expected. If the time when sharp drop of bubble concentration is labeled, then we can find the emission level peaks around this time. Such a peak of emission level can be used to evaluate the intensity of collapse process. The collapse behavior can be evaluated by the time it takes for bubbles or cavities collapse and the mount of emission during collapse. In other words, the quick the collapse is and the larger the emission is, the more violent the collapse is. Since the intensity of collapse mainly reveal itself by the quickness of collapse and the value of peak emission signal, to examine the difference in intensity of the collapse process, here a comparison between the collapse times as well as the peak emission signal value is done. In the first 10 seconds, the peaks of emission signals are the highest values of the emission while the emission level is still increasing sharply compared to afterwards, as

indicated by circles in Figure 3.9. The x coordinate value is the time it took to reach the peak emission level, the y coordinate value is the emission level value of the peak, and the values are compared in Table 3.2. As intensity increases, it takes less time for the emission from collapse of microbubbles to reach to the peak value and the peak value increases. The higher the intensity is, the more violent the collapse of shelled bubbles is. But the speed of increase decreases as intensity increases, in other words, such increase of collapse intensity plateaus gradually. The one exception here is the case of 1.2 MPa case. The time took to reach the peak is about the same as the 1.0 MPa case, showing that the intensity of 1.0 MPa is strong enough to collapse the microbubbles in extremely short time.

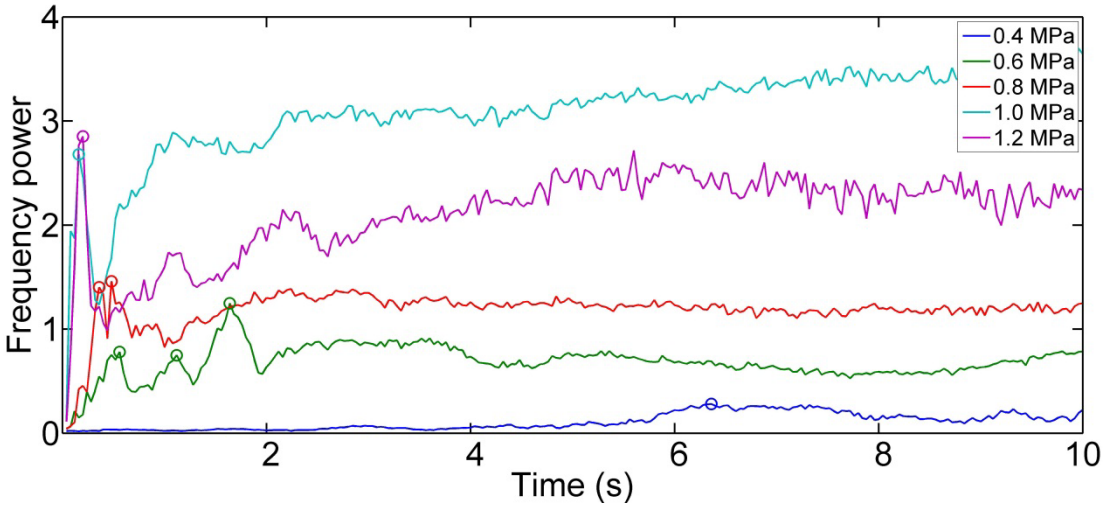


Figure 3.9 Peak emission level and time, the peaks of collapse emission are indicated by circles.

Table 3.2 Time and value of peak emission of intensity series

| Parameter | 0.4 MPa | 0.6 MPa | 0.8 MPa | 1.0 MPa | 1.2 MPa |
|---|---|---|---|---|---|
| Time of peak | 6.36 s | 1.64, 1.12, 0.56 s | 0.48, 0.36 s | 0.16 s | 0.20 s |
| Peak value | 0.2803 | 1.248, 0.7496, 0.7816 | 1.46, 1.402 | 2.681 | 2.852 |

Thirdly, after 10 seconds, emissions come from cavity behavior. The emission level increases until 1.0 MPa, and then there is a drop when the intensity increases

from 1.0 MPa to 1.2 MPa, which can be easily found in Figure 3.8 (C). With higher acoustic pressure, the amplitude of oscillation is higher so the emission level is higher. The reason that the emission of 1.2 MPa is lower than 1.0 MPa is that 1.2 MPa is too strong to collapse most of the cavities rather than let them experience stable oscillation, which can be proved by the noise like emission signals around 4 MHz and 1 MHz. Since the emission level is averaged between 1.5 MHz and 2.5 MHz, lack of oscillation activities will reduce the total amount of emission. The second thing about cavity behavior is that there are significant increases in nonlinearity of oscillation of cavities when intensity increases from 0.4 MPa to 0.8 MPa. Especially for ultraharmonic emission frequencies, such as 1, 3, and 5 MHz, the increase can be easily found in the contour in Figure 3.8 (B). Such increase of ultraharmonic emissions stops when intensity reaches 1.0 MPa, and ultraharmonic signals are even close to disappear at 1.2 MPa. Here again, the collapse of cavities, though weak, is the reason. So collapse of cavities appears when intensity increases from 0.8 MPa to 1.0 MPa, and oscillation of cavities become weaker when intensity reaches 1.2 MPa. By looking into Figure 3.8 (D), such change in cavity behavior is more obvious. When intensities are above 0.4 MPa, the frequency peaks are about the same. Only at 9 MHz, the ultraharmonic signal comes out at 0.6 MPa and 0.8 MPa, indicating a slightly increased nonlinearity in cavity oscillation. However, such nonlinearity disappears after 1.0 MPa.

#### 3.3.2.2 Pulse duration series

Two pulse duration series were tested at different PRF frequencies of 5 kHz and 500 Hz. The pulse duration series at 500 Hz was chosen here. In pulse duration series, 5 pulse durations from 5 μs to 500 μs were tested. The intensity is 0.8 MPa, the irradiation time is 60 seconds, and the PRF is 500 Hz. The results are shown in Figure 3.9.

Figure 3.10 (A) and Figure 3.10 (B) are contour plots of all 5 pulse durations, where Figure 3.10 (A) shows the first 10 seconds, i.e. from 0 to 10 seconds and Figure 3.10 (B) shows the third 10 seconds, i.e. from 30 to 40 seconds. Figure 3.10 (C) shows averaged emission level of all 5 pulse durations represented by the interval

of 1.5 to 2.5 MHz over all the 60 seconds irradiation time. Figure 3.10 (D) shows the frequency magnitude of 5 pulse durations, from 0 to 10 MHz, averaged over all the 60 seconds irradiation time.

In Figure 3.10 (A), collapse signals can be seen in all 5 cases. The case of 5 μs is different from the other 4 cases because the collapse signal is weaker. The laser diode results show that after 10 second the microbubble concentration, though dropping with time, is still high so the collapse behavior is weak. The case of 10, 20, 50 μs are similar with a collapse signal and harmonic emissions at 4, 6 MHz. The case of 500 μs shows much noise like emissions and ultraharmonics.

In Figure 3.10 (B), except for the 5 μs case, the microbubble concentrations for other 4 cases are negligible. During 30 to 40 second, the case of 5 μs is still has high microbubble concentration so the emissions still show weak collapse signal. The case of 10, 20, 50 μs show stable harmonic emission signals at $2f_0$, $3f_0$. The case of 500 μs still shows clear collapse signals and very strong emissions at both harmonic and ultraharmonic frequencies.

The emission level shown in Figure 3.10 (C) is different from that of intensity series in Figure 3.9 (C). During the collapse of microbubbles, there are still peaks after sharp increasing. For cavities behavior after the collapse, the difference among 10, 20, 50 μs is little and the emission levels for all these 3 cases are stable but the case of 500 μs is totally different: the emission level changes dramatically, i.e. there are alternative increases and decreases.

Figure 3.10 (D) also shows that the case of 5 μs has only weak harmonic emissions. The cases of 10, 20, 50 μs are quite similar, showing strong harmonic emissions but the ultraharmonic emission of 50 μs case is stronger than the other 2 cases. The case of 500 μs has the strongest emissions among all 5 cases, no matter at harmonic, ultraharmonic or even broadband signals. With increasing pulse duration, more frequencies are coming out.

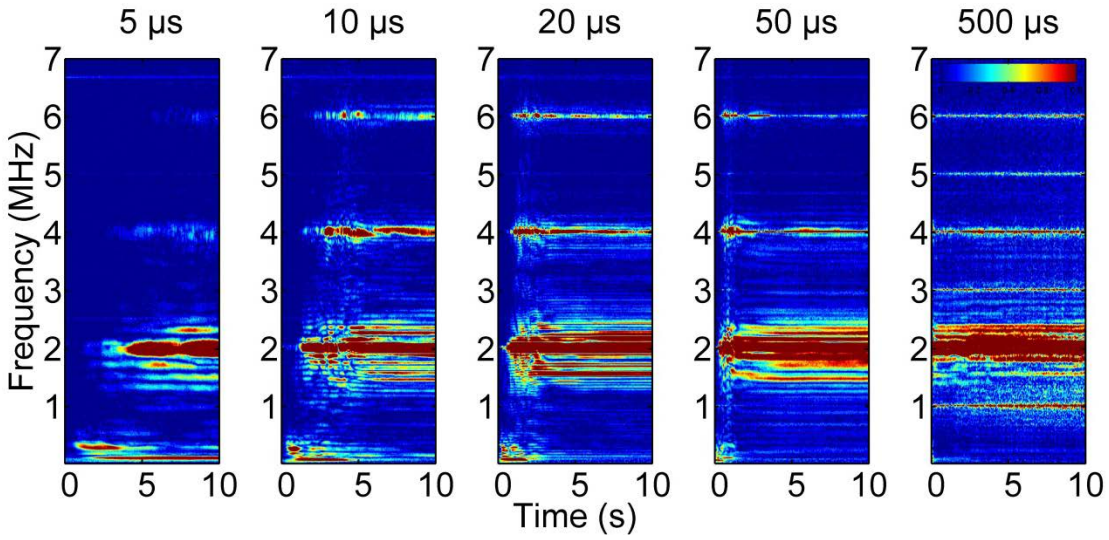
5 μs
10 μs
20 μs
50 μs
500 μs
Frequency (MHz)
Time (s)

(A)

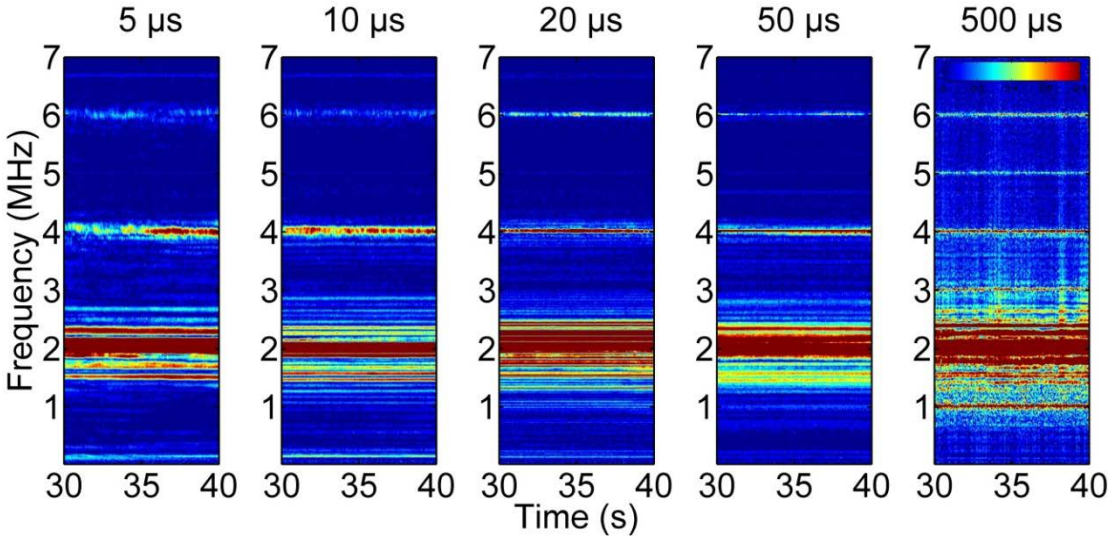
5 μs
10 μs
20 μs
50 μs
500 μs
Frequency (MHz)
Time (s)

(B)

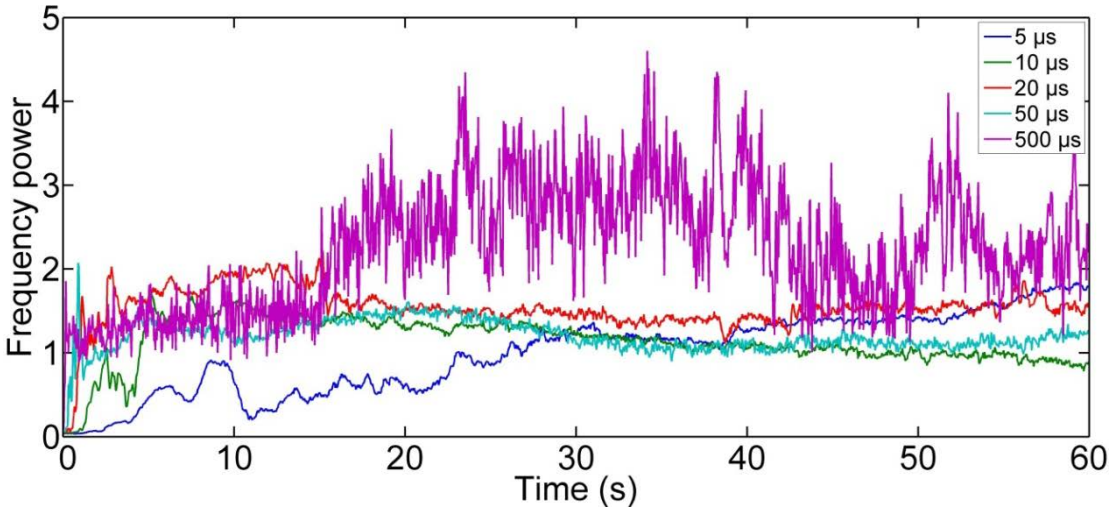


(C)

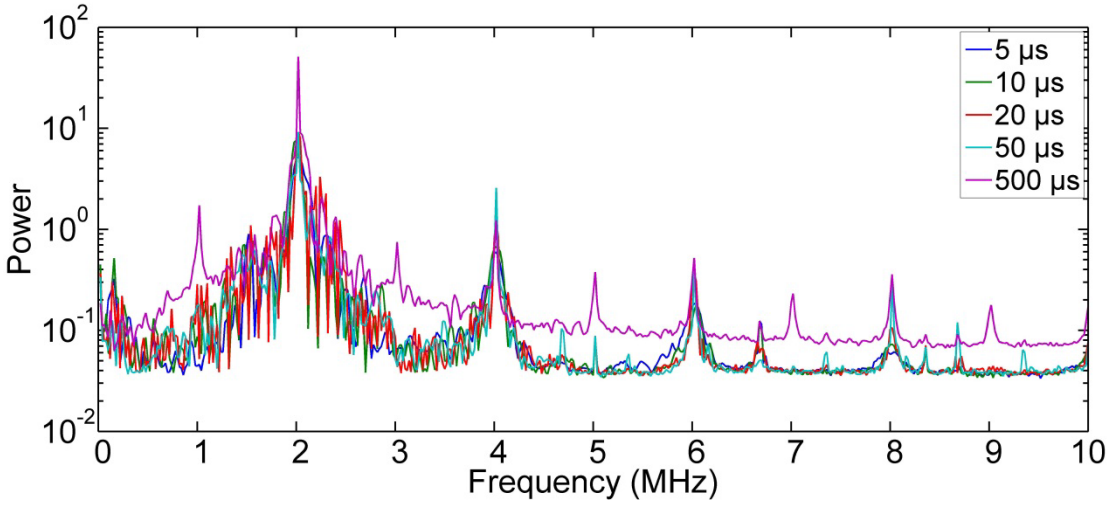


(D)

Figure 3.10 Influence of pulse duration on cavitation noise, (A) frequency contour during the first 10 seconds of irradiation; (B): frequency contour during the 3rd 10 seconds (from 30 to 40 second) of irradiation; (C): the noise emissions averaged over frequency interval of 2 to 3 MHz; (D): the noise emission spectra averaged over 30 to 40 second. The intensity is 0.8 MPa; the irradiation time is 60s; and the PRF is 0.5 kHz. Color bar is the value of the power of frequencies after FFT with limited value range.

Similarly, to discuss the influence of pulse duration on bubble radial behavior, the results from laser diode measuring will also be used.

For shelled bubble behavior, the case of 5 μs is totally different from other cases, where weak oscillation of shelled bubbles dominates cavitation activity. For all other 4 cases, violent collapse of microbubbles happens. Using the same method described by Figure 3.9, the time when peak emission appears and the value of the peak emission are listed in Table 3.3. As pulse duration increases from 10 μs to 50 μs, the time when peak emission appears decreases and the peak emission value increases, which means that the intensity of collapse increases. The collapse of microbubbles in 500 μs case is extremely quick while the peak emission level is smaller than 50 μs case. So for shelled bubbles, as pulse duration increases, the intensity of collapse also increases but similarly as what intensity series has shown, such increase gradually plateaus.

Table 3.3 Time and value of peak emission of pulse duration series

| Parameter | 10 μs | 20 μs | 50 μs | 500 μs |
|---|---|---|---|---|
| Time of peak | 2.52 s | 1.12 s | 0.88 s | 0.16 s |
| Peak value | 1.059 | 1.677 | 2.073 | 1.855 |

For cavity behavior, from 10 μs to 50 μs, the changes in emission level or emission pattern is not significant, all the 3 cases only show horizontally stable emission from oscillation. But from 50 μs to 500 μs, the change is dramatic. Firstly, the nonlinearity of oscillation increases, showing by the appearance of strong emission from both harmonic and ultraharmonic signals. It is also very clear that 1 MHz signal appears in 500 μs case. As that introduced in Figure 2.2, with increasing pulse duration, the response of cavity radius becomes more and more nonlinear. Within one ultrasound wave cycle, the cavity neither collapse nor drops to its minimum size. So in the coming next wave cycle, the cavity continues to response with a large radius, so emissions at half driving frequency, in other words, subharmonic signals, come out. Also in Figure 3.10 (D), the 1 M Hz signal showing only in the 500 μs case results in combination frequencies of further ultraharmonic

frequencies, such as 7 MHz and 9 MHz. Such an increase in frequency values is shown in Figure 3.11. The first 5 seconds of 50 μs case show weak signals of harmonics while the last 5 seconds of 500 μs case show strong signals of emission of both harmonics and ultraharmonics. One more point about the 500 μs is that collapse of cavities, indicated by the jigsaw like pattern emission level curve in Figure 3.10 (C), appears only in this case. To make the case of 500 μs more special, such strong collapse of cavities is not found in either case in intensity series.

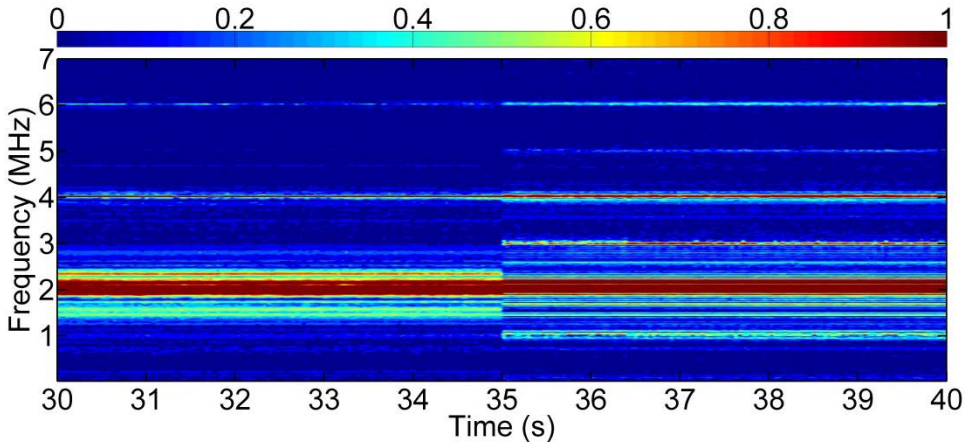


Figure 3.11 Increase in emission frequency when pulse duration changes from 50 μs to 500 μs. From 30 to 35 second belongs to the case of 50 μs and from 35 to 40 second belongs to 500 μs

### 3.3.2.3 PRF series

In PRF series, 8 intensities from 50 Hz to 50 kHz were tested. The intensity is 0.8 MPa, the duty ratio is 10%, and the irradiation time is 60 seconds. The noise data are shown in Figure 3.12.

Figure 3.12 (A) and Figure 3.12 (B) are contour plots of all 7 PRFs, where Figure 3.12 (A) shows the first 10 seconds, i.e. from 0 to 10 seconds and Figure 3.12 (B) shows the third 10 seconds, i.e. from 30 to 40 seconds. Figure 3.12 (C) shows averaged emission level of 5 selected PRFs represented by the interval of 1.5 to 2.5 MHz over all the 60 seconds irradiation time. Figure 3.12 (D) shows the frequency magnitude of 5 selected PRFs averaged over all the 60 seconds irradiation time.

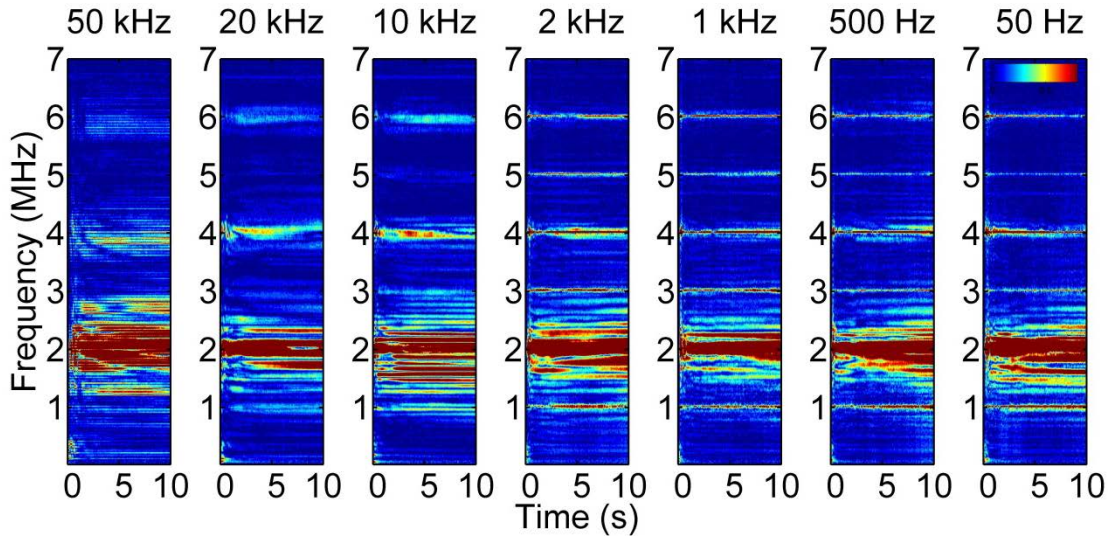
50 kHz
20 kHz
10 kHz
2 kHz
1 kHz
500 Hz
50 Hz
Frequency (MHz)
Time (s)

(A)

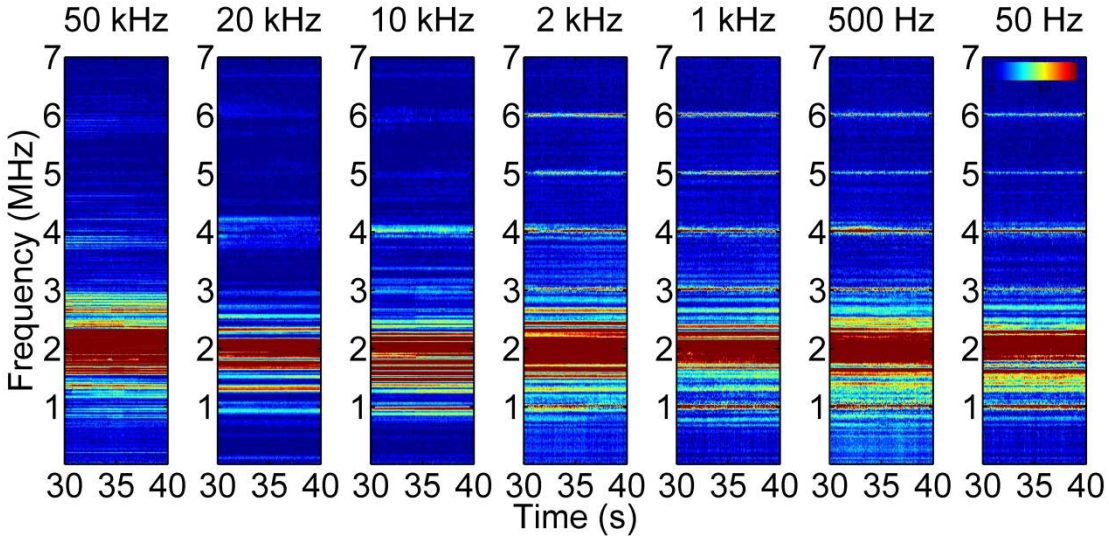
50 kHz
20 kHz
10 kHz
2 kHz
1 kHz
500 Hz
50 Hz
Frequency (MHz)
Time (s)

(B)

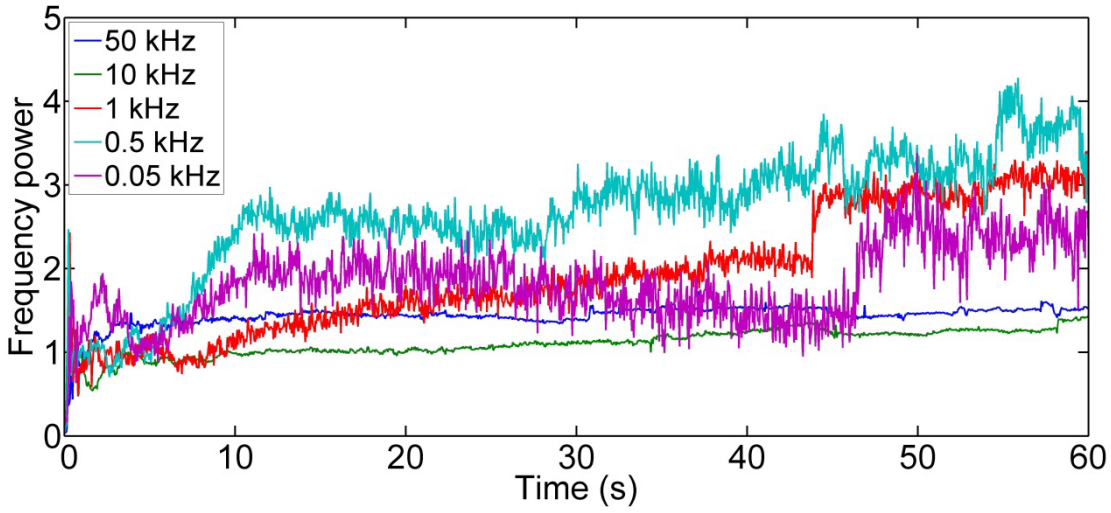


(C)

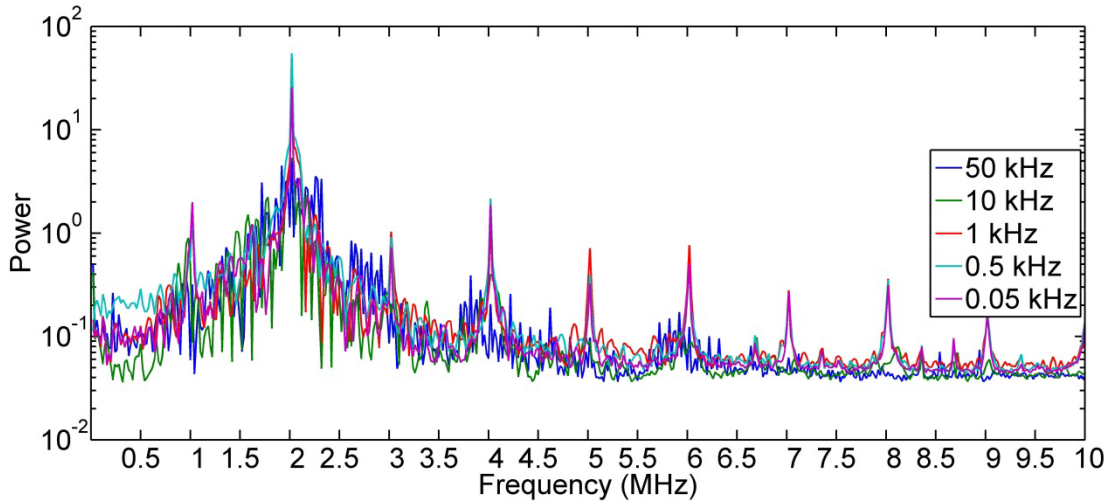


(D)

Figure 3.12 Influence of PRF on cavitation noise, (A) frequency contour during the first 10 seconds of irradiation; (B): frequency contour during the 3rd 10 seconds (from 30 to 40 second) of irradiation; (C): the noise emissions averaged over frequency interval of 2 to 3 MHz; (D): the noise emission spectra averaged over 30 to 40 second. The intensity is 0.8 MPa; the irradiation time is 60s; and the duty ratio is 10%. Color bar is the value of the power of frequencies after FFT with limited value range.

Strong microbubble collapse signals can be seen in all 7 cases shown in Figure 3.12 (A). For all 7 cases, the collapse speed is very fast. The intensity of collapse is compared using the same method as described by Figure 3.9. The time when peak emission of collapse appears and the peak emission level for 7 PRF cases are shown in Table 3.4. The difference of the time when peak emission comes among 7 cases are small except for the case of 20 kHz, where the microbubbles collapse, although very fast, a little bit slower than other 6 cases. For peak emission values, the cases of 50 kHz, 50 kHz, and 10 kHz have smaller peaks than other 4 cases, indicating that longer pulse duration, though with the same constant energy, can collapse microbubbles more violent.

Table 3.4 Time and value of peak emission of PRF series

| Parameter | 50 kHz | 20 kHz | 10 kHz | 2 kHz | 1 kHz | 500 Hz | 50 Hz |
|---|---|---|---|---|---|---|---|
| Time of peak | 0.4 s | 0.76 s | 0.44 s | 0.44 s | 0.32 s | 0.24 s | 0.4 s |
| Peak value | 1.04 | 0.8742 | 1.294 | 2.228 | 2.432 | 2.47 | 1.848 |

The difference of cavity behavior shown in Figure 3.10 (B) is clearer. The cases of 50 kHz and 20 kHz show very weak oscillation signals; the case of 2 kHz shows harmonic emissions; and from 2 kHz to 50 Hz, strong emission signals at both strong harmonic and ultraharmonic frequencies are shown. The time-averaged emission level shown in Figure 3.10 (D) also indicates that only low PRF cases with long pulse durations have strong emissions at ultraharmonic frequencies. For shelled bubble behavior, the difference among all 7 cases is very small, while the difference between cavity behaviors is easier to be seen. Especially in Figure 3.12 (C), the shapes of different emission level curves are clearly different. The jigsaw shape becomes more obvious as PRF decreases. To better compare such difference, the time period beginning from 30 s ending at 40s when for all 7 cases the microbubble concentration can be negligible is taken out and the emission level for all 7 cases are plotted in Figure 3.13. The changes in values of emission level become clearer as PRF

decreases. To evaluate such changes in emission levels, the mean value and standard deviation of emission level of all 7 cases during 30 to 40 second are listed in Table 3.5. It can be found that the emission level falls into two groups: the three high PRF cases have relatively lower emission level while the 4 low PRF cases have relatively higher emission level and that unlike the emission level the standard deviation increases as PRF decreases. In intensity series and pulse duration series, only one case of 500 μs has shown similar dramatic changes in emission level during the same period. The mean value and standard deviation of 500 μs case calculated by the same method are 2.9257, 0.5641 respectively. The standard deviation of this 500 case is thus the largest.

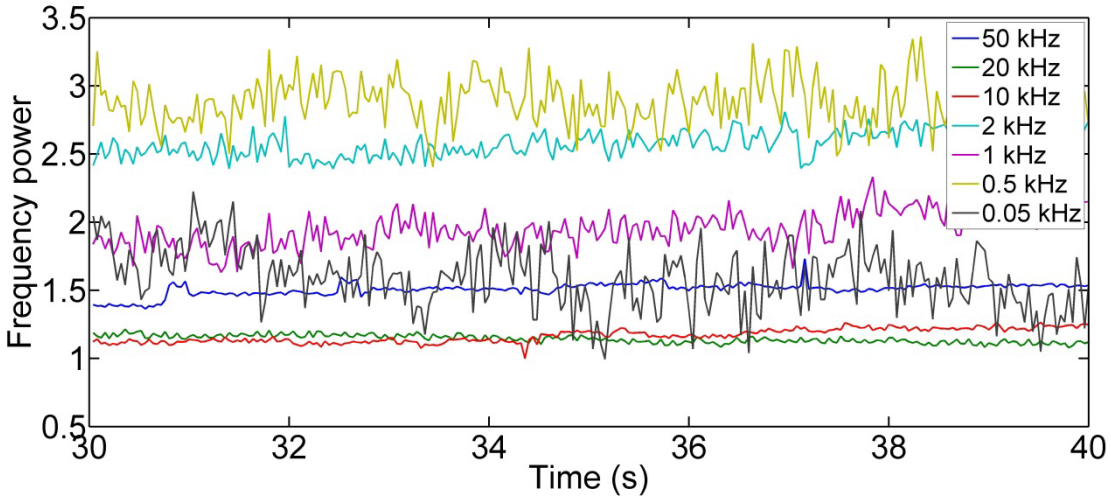


Figure 3.13 The emission level of all 7 PRF cases during 30 to 40 second

Table 3.5 Emission level comparing during 30 to 40 second of PRF series

| Parameter | 50 kHz | 20 kHz | 10 kHz | 2 kHz | 1 kHz | 500 Hz | 50 Hz |
|---|---|---|---|---|---|---|---|
| Mean | 1.5074 | 1.1432 | 1.1672 | 2.578 | 1.9553 | 2.8721 | 1.5931 |
| Standard deviation | 0.0452 | 0.0286 | 0.0487 | 0.094 | 0.1352 | 0.1818 | 0.2279 |

## 3.4 Summary of bubble behavior

The influences of intensity, pulse duration and PRF on bubble radial dynamics are examined by measuring the concentration change of microbubbles using laser diode unit, and also by recording the noise from cavitation using focused hydrophone. The parametric differences are summarized from two parts: on artificially added microbubbles with lipid shells and on cavities generated in the liquid itself.

One part is influence of parameters on microbubbles.

Parametric influence on shelled bubbles can be very straightly seen. The first kind is weak oscillation pattern dominant where bubbles collapse very slowly and the concentration remains high after 10 seconds. The other kind is quick collapse pattern dominant, where most of the microbubbles collapsed within 10 seconds. For such a kind of collapse, the differences are discussed by comparing the collapse time and peak emission signal from collapse.

When intensity increases from 0.3 MPa to 0.4 MPa, the microbubbles behavior changes from weak collapse and oscillation to violent collapse. As intensity increases, microbubbles collapse quickly and more violent, but such increase gradually plateaus when intensity reaches the value of 1.0 MPa.

The influence of pulse duration on microbubbles behavior is somehow similar to that of intensity. At 5 μs length pulse duration, weak oscillation and collapse happen and as pulse duration becomes longer, violent collapse dominants. In a short range of 10 μs to 50 μs, the collapse process does not change much but when the pulse duration becomes long enough such as 500 μs, the microbubbles collapse extremely quickly.

The influence of PRF on microbubble behavior is not very directly output since in all 7 cases, collapse dominants and the collapse processes are all very quick and violent.

The other part is influence of parameters on cavities.

Parametric influences on cavities are discussed by both the amplitude of emission and the nonlinearity from emission. The total emissions amount averaged from the frequency interval of 1.5 MHz to 2.5 MHz have been discussed one parameter by one parameter. Here to compare together, frequencies values of 1 MHz

to 7 MHz from all 3 parameter series averaged between 30 to 40 second are plotted in Figure 3.14. The values of ultraharmonic signals, such as 1 MHz, 3 MHz, and 5 MHz reflect the nonlinearity of cavity oscillation; especially the 1 MHz signal also partly reflects the cavity collapse.

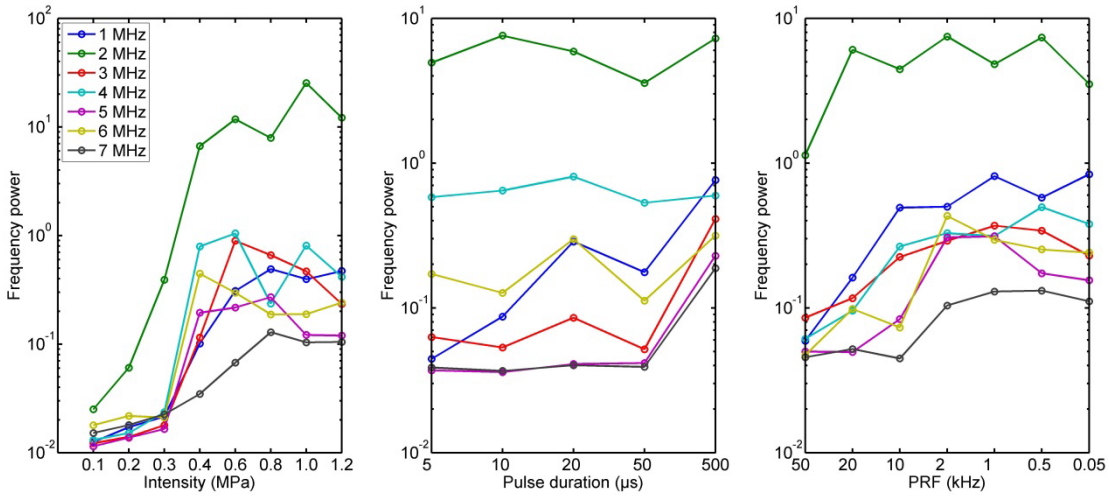


Figure 3.14 Frequency power of 1 to 7 MHz signal of all 3 parameters averaged between 30 to 40 second

As intensity increases, the oscillation amplitude of cavities increases until 1.0 MPa. The nonlinearity of oscillation of cavities increases until 0.8 MPa. For the 1.0 MPa and 1.0 MPa cases, weak collapse of cavities can be seen.

When pulse duration is less than 50 μs, the difference of oscillation of cavities are not very clear but when pulse duration increases to 500 μs, the nonlinearity increases dramatically and strong collapse of cavities can be found.

With the same intensity and energy, lower PRF cases with longer pulse duration show stronger oscillation signals. As PRF decreases, the changes of the intensity of bubble behavior, either oscillation or collapse, becomes clearer.

# Chapter 4. Ultrasond-mediated delivery *in vitro*: parametric studies on sonoporation efficiency

## 4.1 Introduction

### 4.1.1 Delivery via sonoporation *in vitro*

The pores created during sonoporation have long been used for the delivery of drugs as well as genes. Since the ultrasound-mediated delivery technic still has a long way to go before going clinical, as introduced in Chapter 1 much work has been done both *in vitro* and *in vivo*. *In vivo* experiments with animals would be more close to clinical reality, but it is time consuming and usually has relatively lower productivity. Here we focus on mechanism and parametric influence of sonoporation, requiring much experimental work, so the delivery experiments in this study are carried out *in vitro*. To show successful accomplishment of sonoporation, fluorescent markers with large molecular weight which won't be internalized unprompted were delivered into cultured cells. Various parameter arrangements that are identical to experiments done with bubble behavior are tested on their influences on the delivery efficiency as well as the cell viability.

### 4.1.2 Difference between cell statuses

The mechanisms involved in sonoporation include shear stress and microstreaming induced by stable cavitation and shockwave and jetting induced by inertial cavitation. These mechanisms are affected to parameters, to make the effects of these mechanisms more clear, the cells were irradiated in both attachment and suspension status in this chapter. The reason why the same cell type was irradiated in two different statuses is that the behaviors of cells will be different when subjected to either stable or inertial cavitation whether they are free in liquids or attached to a rigid wall. The difference mainly comes from two factors. The first one is the mechanical factor. When cells are in a suspension status, they are free. Liquid won't hold shear

stress, so does the cells suspending in it. For a cell suspending in the medium, shear stress and microstreaming will have few effects on it since it will translate in the liquid when subjected to such stress. Such comparison can then help understanding not only the parametric influence but also mechanisms on sonoporation process. The second one is the bubble factor. Cells suspending in liquid will have much more contrast agents, as well as cavities in the liquid around them since they are immersing into liquid and have larger volume of liquid around them than the cells attached to the bottom of the plate.

## 4.2 Materials

The ultrasound exposure system is the same one as that used for microbubble behavior study. The medium in wells of the 24-well plate changed and cultured cells were applied as an *in vitro* model. FITC-Dextran is chosen as the marker for sonoporation.

### 4.2.1 Cell line

Mouse embryonic fibroblast cells (NIH3T3), adherent, were incubated as monolayer at 37°C under a humidified atmosphere of 5% $CO_2$ in 55 $cm^2$ tissue culture dishes containing Dulbecco's modified Eagle's medium (DMEM) supplemented with 10% v/v fetal bovine serum (FBS) and 1% v/v antibiotics (Penicillin-Streptomycin and L-Glutamine). All of the reagents were purchased from Invitrogen (Carlsbad, CA). The double time of cells is 18 h and to avoid completely confluent of cells subcultures (also called passage) are needed. The passage of cells is carried out every three days. During passage, the cells are detached using trypsin and parts of them are transferred to a standard commercial 24-well plate and left to grow to ~ 90% confluence before being irradiated.

A view of NIH3T3 cells cultured is shown in Figure 4.1. NIH3T3 cells have a long and narrow morphology and turn to form cluster by adhering to each other. The main body is less than 20 μm in size for most cells.

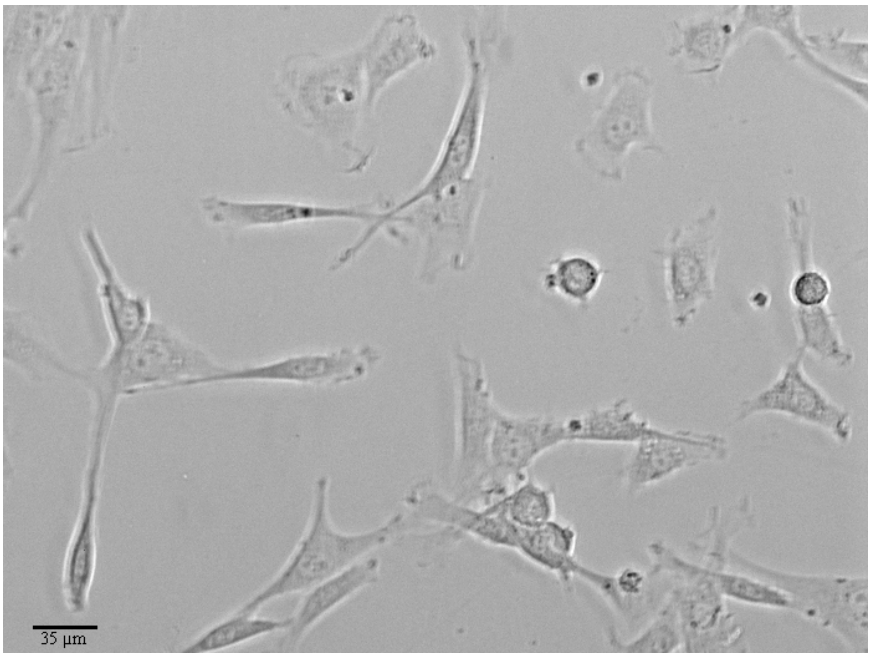


Figure 4.1 Appearance of cultured NIH3T3 cells

### 4.2.2 FITC-Dextran

Sonoporation is characterized by pores on the cell membrane and the pores are validated by the uptake of large molecules which usually can't be internalized by the cell itself. The indicator of internalization used is FITC (Fluorescein isothiocyanate) – Dextran, purchased from Sigma-Aldrich (St. Louis, MO).

Dextran is a complex, branched glucan (polysaccharide made of many glucose molecules) composed of chains of varying lengths (from 3 to 2000 kilo Daltons), shown in Figure 4.2 (A). FITC is the original fluorescein molecule functionalized with an isothiocyanate reactive group, replacing a hydrogen atom on the bottom ring of the structure. The coupled dextran with FITC is shown in Figure 4.2 (B).

The molecular weight of FITC-Dextran used in this study is 20 kDa. It appears to be a yellow powder. It is dissolved in phosphate buffered saline (PBS), giving a yellow solution. The concentration of the solution is set to be 5 mg/ml. In the solution, the approximate Stokes' radius for FITC-dextran with a MW of 20 kDa is 33 Angstroms.

Toxicity of FITC-Dextran to cells is considered to be negligible. In studies in

mice, FITC-dextrans were found to be tolerated well when injected intravenously or intraperitoneally in doses up to 6g/kg bodyweight. Their toxicity patterns follow those of the parent dextrans (tested by the manufacturer).

The excitation maximum of FITC-dextran is 490 nm. The emission maximum is 520 nm.

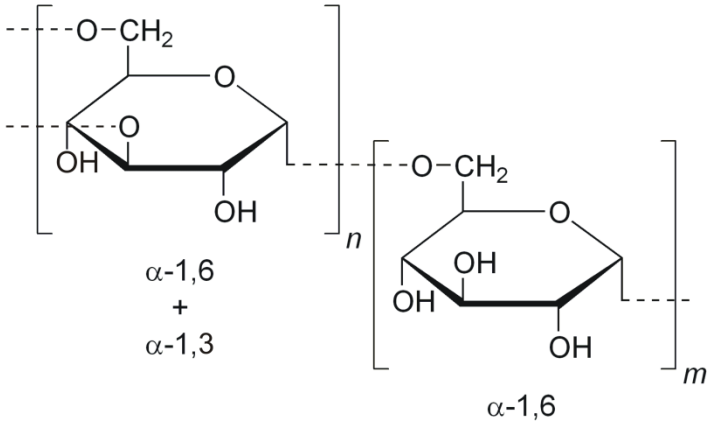


(A)

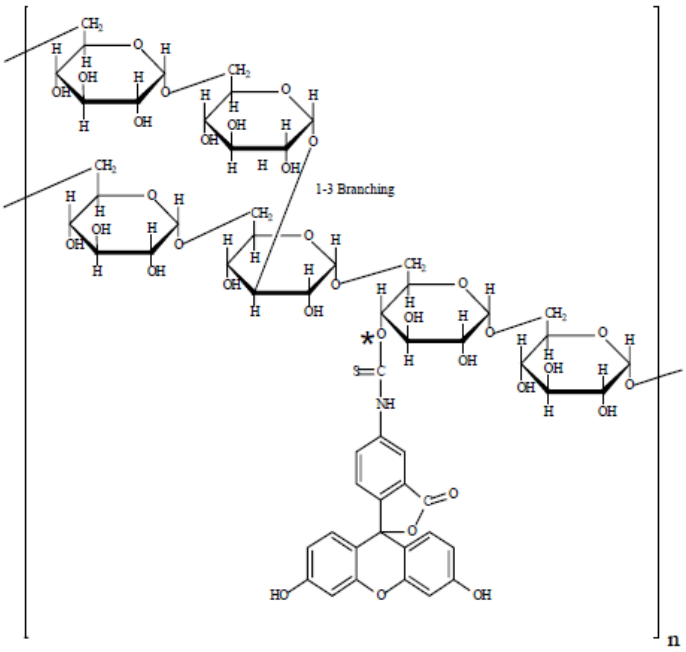


(B)

Figure 4.2 Structural formulas of dextran (A) and FITC-Dextran (B). The data are offered by the manufacturer, Sigma-Aldrich.

## 4.3 Methods

### 4.3.1 Irradiation protocol of attachment status

The ultrasound exposure system is the same one with that used in bubble radial movements study.

During passage, cells were transferred to 24-well pates with a density of $1\times10^5/cm^2$. The plates were incubated for 24 h and then the cells were exposed to ultrasound. The cells reached approximately 100% confluent when irradiated.

For a single well in the 24-well plate, a total volume of 0.8 ml of mixed medium is injected. The mixed medium contains 0.08 ml of Sonazoid$^{TM}$, 0.72 ml of DMEM, and 8 μl of FITC-dextran solution. The volume concentration of microbubbles is 10%, corresponds to a count of $1.7\times10^5$/ml. The density of FITC-Dextran is 50 μg/ml. The medium is pre-mixed and then injected to wells one by one.

Before irradiation, the plate was taken out from the incubator. DMEM in wells were piped out and the cells were rinsed once by PBS. The mixture of microbubbles, FITC-Dextran and DMEM was then injected to wells and cells were exposed to ultrasound at various configurations. After exposure, the plate was placed back to the incubator and incubated for 10 min without changing the medium inside the wells. Then the plate was taken out again for analyzing. The mixture inside wells was piped out and the cells were rinsed twice by a mixture of PBS and anti-dye (A889, Invitrogen, Carlsbad, CA). A volume of 0.1 ml of Trypsin-EDTA was then injected to each well to detach cells. The plate was incubated for 2 min to allow full detachment of cells. A volume of 0.9 ml of DMEM was then injected to each well and was carefully pipetted for three to five times. The total volume of 1 ml mixture in each well was transferred to a 1.5 ml tube. A volume of 10 μl out of the 1 ml mixture was transferred to another 1.5 ml tube for viability analysis. The tubes containing 1 ml mixture were centrifuged for 5 min at 2000 rpm and 4 °C. After centrifugation, the cells deposited to the bottom of the tubes and the upper medium was piped out. A volume of 0.4 ml of PBS was then injected to each tube and careful pipetting was carried out for three to five times to make sure all the cells in the tube will suspend into PBS. The cell suspended PBS was then injected to a tube with mesh and flowed

in a cytometer. All the manipulations were carried out in a clean bench except for centrifuge.

### 4.3.2 Cell preparing for suspension status

NIH3T3 is natural adherent cells. During passage, a portion of cells were transferred to 24-well plates and were then irradiated in attachment status. At the same passage, cells were transferred to dishes with the same density of $1\times10^5/cm^2$. After incubation for 24 h, the cells in the dishes were harvested by trypsin-EDTA and transferred to plates and then soon irradiated while they were suspending in the medium.

Since the medium for culture are the same, identical proliferation is expected after 24 h. The area of a single well in 24-well plate and a dish is 1.883 and 55 $cm^2$, respectively. In order to make sure that cells in a single well irradiated in two statuses have an identical population, (188.3/55) % of cells in the dish were transferred to a well in a new 24-well plate. In this new plate, cells were irradiated in suspension status. The volume of medium inside a dish is 5 ml in all passages, so the volume of cell suspension that will be transferred to a single well is thus 5 × (188.3/55) % ml, which is, 171.2 µl.

### 4.3.3 Irradiation protocol of suspension status

For a single well in the 24-well plate, a total volume of 0.8 ml of mixed medium is injected. The mixed medium contains 0.08 ml of Sonazoid$^{TM}$, 171.2 µl of cell suspension from dishes, 0.55 ml of DMEM, and 8 µl of FITC-dextran solution. The medium is pre-mixed and then injected to wells one by one.

The cells were immediately irradiated after they were injected to the well. After irradiation, a volume of 0.2 ml mixture of PBS and anti-dye was injected to each well. The total volume of 1 ml of the mixture of cells and medium in the well were transferred to a 1.5 ml tube after careful pipetting. The tubes were centrifuged for 5 min at 2000 rpm and 4 °C. After centrifugation, the cells deposited to the bottom of the tubes and the upper medium was piped out. A volume of 1 ml of DMEM was then injected to each tube and careful pipetting was carried out for three to five times to

make sure all the cells in the tube will suspend into DMEM. A volume of 10 μl out of the 1 ml mixture was transferred to another 1.5 ml tube for viability analysis. The tubes were then again centrifuged for 5 min at 2000 rpm and 4 °C. After centrifugation, the cells deposited to the bottom of the tubes and the upper medium was piped out. A volume of 0.4 ml of PBS was then injected to each tube and careful pipetting was carried out for three to five times to make sure all the cells in the tube will suspend into PBS. The cell suspended PBS was then injected to a tube with mesh and flowed in a cytometer. All the manipulations were carried out in a clean bench except for centrifuge.

### 4.3.4 Flow cytometry and viability analysis

The confirmation of FITC-dextran delivery to cells was done by flow cytometer (FACS Verse, BD, Franklin Lakes, New Jersey). Flow cytometry is a laser based technology employed in cell counting, sorting, and biomarker detection, by suspending them in a stream of fluid and passing them by an electronic detection apparatus. Cells in suspension pass laser beam one by one and excitation signals are recorded.

In our test, forward scatter (FSC), side scatter (SSC) and FITC signals were applied. FSC and SSC signals were used to gate cells out from dirt and other impurities in the suspension. After the cells were labeled out, FITC signal was used to gate the cell with FITC-Dextran inside out from all the cells.

The delivery rate is then defined as

$$\text{Delivry rate} = \frac{\text{Number of FITC- Dextran positive cells}}{\text{Number of total cells}} \qquad (4\text{-}1)$$

For a single well, at least 10, 000 cells were counted.

The cell viability is measured by TC10™ Automated Cell Counter (BIO-RAD, Hercules, CA), shown in Figure 4.3. It is an automated device that provides a total count of mammalian cells and a live/dead ratio in one step.

Figure 4.3 TC10™ Automated Cell Counter, picture from the manufacturer

A volume of 10 µl of trypan blue dye was added into the 10 µl suspension in the 1.5 ml tube and mixed carefully by pipetting for about 10 times. A small portion of the mixture was then loaded to the slide, and the slide was then inserted into the automated counter where the total number of cells as well as the viability will be obtained.

As described in the irradiation protocol, the cells irradiated in attachment status were rinsed before cytometry test. So dead cells floating in the medium were rinsed out, which would add inaccuracy to the viability data. To compensate this inaccuracy, a well with cultured cells was used. The medium inside this well was unchanged during the whole process so influence from ultrasound and mixed medium was absent. The cell viability of a tested well for cells irradiated in attachment is define as

$$\text{Cell viability} = \frac{\text{Total numer of cells in the tested well}}{\text{Total numer of cells in the cultured well}} \times \text{viablity of the tested well} \quad (4\text{-}2)$$

For cells irradiated in suspension status, the cell viability is just the viability measured by the cell counter.

All the data of delivery rate and cell viability are averaged from three independent replicates (12 samples) and shown as the mean +/- standard deviation.

## 4.4 Results and discussions

### 4.4.1 Influence of intensity

The influence of acoustic intensity on both delivery rate and cell viability was studied. The cell behaviors of 8 intensities together with a control case were shown in Figure 4.4 (A). The initial microbubble concentration is 0.1 (10% volume to volume). The other parameters were set as: the irradiation time is 60s; PRF is 5 kHz and the pulse duration is 20 μs.

The delivery rate increases while cell viability decreases as intensity increases. No delivery was found in control case without ultrasound irradiation, which agrees with literature very well [51] [34]. The increase trend of delivery rate is slow under 0.3 MPa, becomes quicker between 0.3 and 0.8 MPa and turns to plateau from 0.8 MPa. The increase in sonoporation efficiency from 0.3 MPa to 0.4 MPa is extremely sharp. There are large drops of cell viability when intensity increases from 1.0 MPa to 1.2 MPa.

There is a pattern shift of shelled bubble behavior between 0.3 MPa and 0.4 MPa, as shown in Chapter 3. To test the influence of this pattern shift on delivery rate and cell viability, minor intensity increments on both delivery rate and cell viability were tested between these two intensities and the results were shown in Figure 4.4 (B). The other parameters were set as: the irradiation time is 60 s; PRF is 5 kHz and the pulse duration is 20 μs.

Still, the delivery rate increases while cell viability decreases as intensity increases. There is obvious increase of delivery rate when intensity increases from 0.32 MPa to 0.34 MPa. For cell viability, the decrease appears to be in a gradual way.

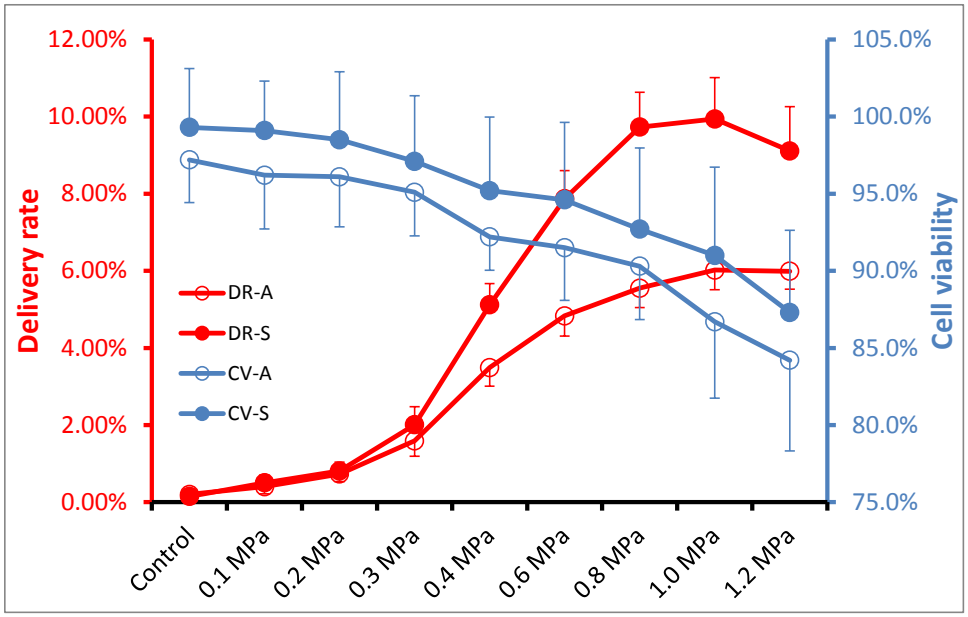


(A)

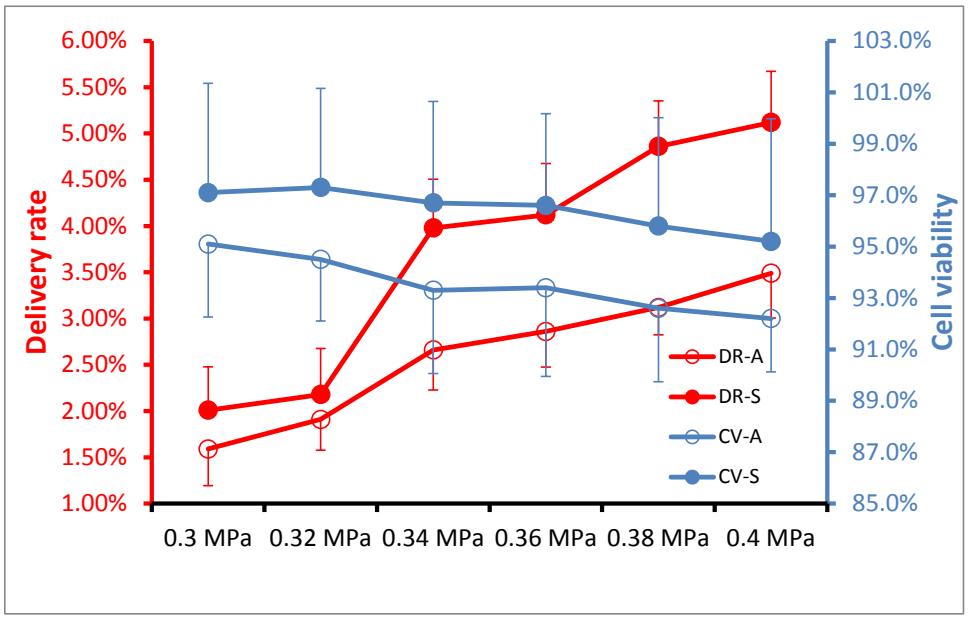


(B)

Figure 4.4 Effects of ultrasound intensity on the delivery rate and cell viability for cells irradiated in both attachment and suspension statuses. (B) is done with small increment. DR is short for delivery rate; CV is short for cell viability; and A, V indicate attachment and suspension status, respectively. No ultrasound was applied in the case of control. The irradiation time is 60s; PRF is 5 kHz and the pulse duration is 20 μs. The data is averaged from 4 independent replicates (12 samples) and shown as the mean +/- standard deviation.

To discuss parametric influence on sonoporation, the results of parametric influence on bubble radial movements will be applied. In Chapter 3, the influence of intensity on bubble behavior has been summarized from two sides.

The first one is on microbubbles: when intensity increases from 0.3 MPa to 0.4 MPa, the microbubbles behavior changes from weak collapse and oscillation to violent collapse. As intensity increases, microbubbles collapse quickly and more violent, but such increase gradually plateaus when intensity reaches the value of 1.0 MPa. The other one is on cavities: as intensity increases, the oscillation amplitude of cavities increases until 1.0 MPa. The nonlinearity of oscillation of cavities increases until 0.8 MPa. For the 1.0 MPa and 1.0 MPa cases, weak collapse of cavities can be seen.

Here the sharp increase in sonoporation efficiency when intensity increases from 0.3 MPa to 0.4 MPa is the result of the change in cavitation pattern. Figure 4.4 (B) further shows that such a pattern shift happens when intensity increases from 0.32 MPa to 0.34 MPa. Beginning from 0.4 MPa to 0.8 MPa, the reason of the rise in sonoporation efficiency cannot be clearly concluded here since the intensity of microbubble collapse and cavity oscillation both increases. Beginning from 0.8 MPa, the reason of the plateau in sonoporation efficiency is interesting. In Table 3.2, it has been shown that the microbubble collapse at 1.0 MPa and 1.2 MPa is more violent than that of 0.8 MPa. In Figure 3.8 (C), it has been shown that the cavity oscillation is stronger than that of 0.8 MPa. The limited increase in sonoporation efficiency from 0.8 MPa to 1.0 MPa indicates that cavitation behavior at 0.8 MPa, either from shelled bubbles or cavities, is strong enough to sonoporate cells. Further increase in cavitation intensity will not result in the increase in sonoporation efficiency but the decrease in cell viability. But still, the reason for such a plateau can comes from either microbubbles or cavities. From 1.0 MPa to 1.2 MPa, the drop in sonoporation efficiency for cells irradiated in suspension is due to the sharp decrease in cell viability. Even sonoporated, the death of cell causes the breakdown of cell membrane and the fluorescent markers will such flow out of the cell.

As for cell viability, the trend is much easier. The increase in either microbubble collapse intensity or cavity oscillation intensity will cause decrease in cell viability.

One more thing needed attention is that the difference between two statuses. This topic is not a main point of this thesis and further arrangements of experiments are needed to come to any conclusions. However, here the reason for such difference is briefly discussed. For all cases tested, both the sonoporation efficiency and cell viability of cells irradiated in suspension status are higher than those irradiated in attachment status. Since the cell population and microbubble density are identical for both statuses, it is obvious that when cells are suspending in the mixture there are more microbubbles around them. Besides when cells are attached to the bottom only parts of their surface area are open to microbubbles. Adding these two points together, the possibility that cells in attachment status be influenced by microbubble cavitation activities is lower than the cells in suspension status. What's more, as introduced in section 4.3, the preparation methods are different for two different statuses. The time that cells are out of incubator is different for two statuses which may result in a difference in the cells themselves. Such difference may be the difference in cells capability of keeping its intactness or even the difference in cells viability.

### 4.4.2 Influence of irradiation time

The influence of irradiation time on both delivery rate and cell viability was studied. The cell behaviors under 6 different time lengths of 3 different cases together with a control group were shown in Figure 4.5. The initial microbubble concentration is 0.1 (10% volume to volume). The other parameters were set as: the acoustic intensity is 0.8 MPa; PRF is 5 kHz and pulse duration is 20 μs (case 6) for (A); PRF is 0.05 kHz and pulse duration is 2,000 μs (case 15) for (B); and the acoustic intensity is 0.8 MPa; PRF is 0.5 kHz and pulse duration is 500 μs (case 23) for (C).

For all 3 cases: the delivery rate increases while cell viability decreases as irradiation time increases. Within 20 s, the delivery rate reaches more than 50% of the value of 60 s. In Figure 4.5 (A), the increase trend of delivery rate is obvious under 30 s and plateaus after that. The decrease of cell viability presents a gradual style over all irradiation time lengths. While in Figure 4.5 (B) and (C), the increase trend of delivery rate is still obvious under 30 s but unlike in Figure 4.5 (A) the plateau does not appear: the delivery rate keeps increasing as irradiation time increases, though the

speed of increasing is slower than the speed of under 30 s. The cell viability, similarly as that shown in Figure 4.5 (A), decreases as irradiation time increases.

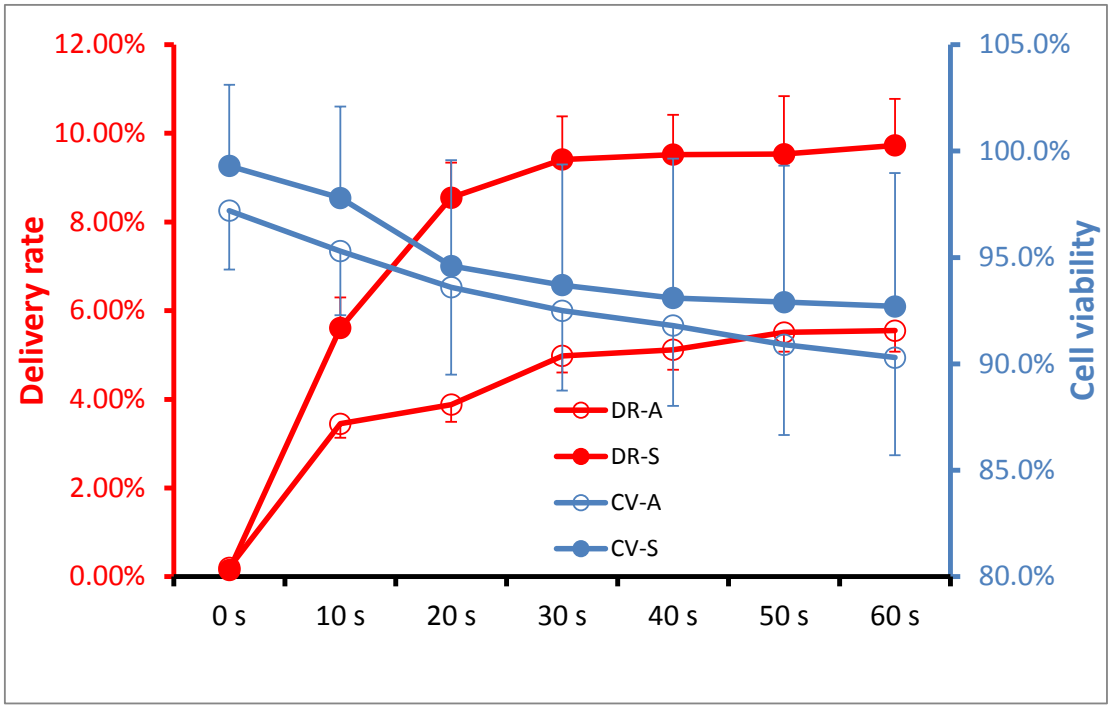
12.00%
10.00%
8.00%
6.00%
4.00%
2.00%
0.00%
Delivery rate
105.0%
100.0%
95.0%
90.0%
85.0%
80.0%
Cell viability
0 s
10 s
20 s
30 s
40 s
50 s
60 s
DR-A
DR-S
CV-A
CV-S

(A)

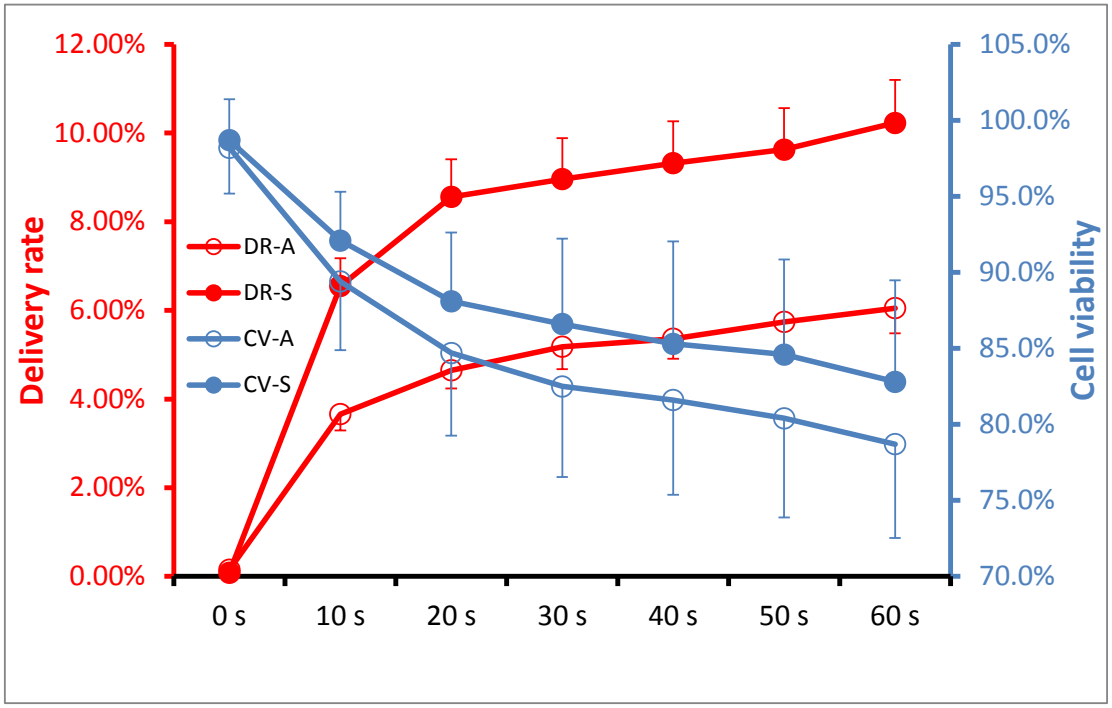
12.00%
10.00%
8.00%
6.00%
4.00%
2.00%
0.00%
Delivery rate
105.0%
100.0%
95.0%
90.0%
85.0%
80.0%
75.0%
70.0%
Cell viability
0 s
10 s
20 s
30 s
40 s
50 s
60 s
DR-A
DR-S
CV-A
CV-S

(B)

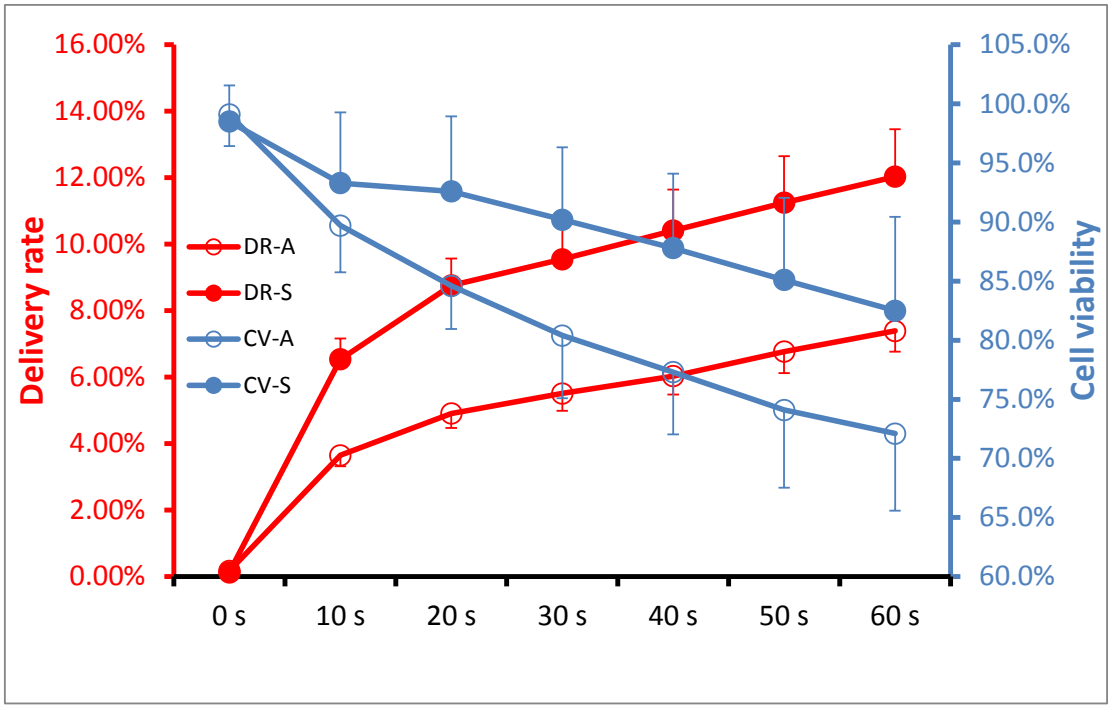


(C)

Figure 4.5 Effects of total irradiation time on the delivery rate and cell viability for cells irradiated in both attachment and suspension statuses. DR is short for delivery rate; CV is short for cell viability; and A, V indicate attachment and suspension status, respectively. No ultrasound was applied in the case of 0 s. The acoustic intensity is 0.8 MPa. PRF is 5 kHz and pulse duration is 20 μs (case 6) for (A); PRF is 0.05 kHz and pulse duration is 2,000 μs (case 15) for (B); and The acoustic intensity is 0.8 MPa; PRF is 0.5 kHz and pulse duration is 500 μs (case 23) for (C). The data is averaged from 4 independent replicates (12 samples) and shown as the mean +/- standard deviation.

To understand the difference between the irradiation series of 3 cases, the method used in discussion in Part 3.3.2 is applied. The emission levels averaged over the frequency interval of 1.5 MHz to 2.5 MHz and the noise spectra of 3 cases tested are shown in Figure 4.6. The most obvious difference among these 3 cases is the irregularity of the curve, especially for the curve after 10 seconds. The curve of case 6 is smooth; the curves of case 15 and 23 are serrate while the saw tooth in case 23 is sharper and deeper. To evaluate the difference quantitatively, as described in Part 3.3.2.3, the mean value and standard deviation of the emission level values during 30 to 40 second are listed in Table 4.1. The mean level difference between case 6 and 15 is minor but the deviation difference is large while both the mean level and deviation of case 15 are far larger than case 6 and 15. The spectra figure shows that for 3 cases most of the frequencies from emission are the same only that the values are different: the emission from 500 μs case is stronger. So here such values shown in Table 4.1, in other words the stableness of emission level, as well as the level of nonlinearity of oscillation can both be applied to judge the cavity behavior. The difference is that the frequency spectrum is a time averaged result so it lacks information from the collapse of cavities which is transient while the ‘stability’ of emission level is a combination since all the emissions are recorded together. In Figure 3.10 (B), it is found that collapse of cavities also happened in the 500 μs case. Here the ‘unstableness’ values in Table 4.1 count oscillation and collapse together.

The results from laser diode have shown for all these 3 cases, the microbubble concentrations after 10 s are negligible. So during first 10 seconds, using the same method as described in Part 3.3.2.1, the intensity of microbubble collapse of 3 cases is compared in Table 4.2. The main difference between case 6 and 15 is the peak emission value while the main difference between case 15 and 23 is the time took to reach peak emission.

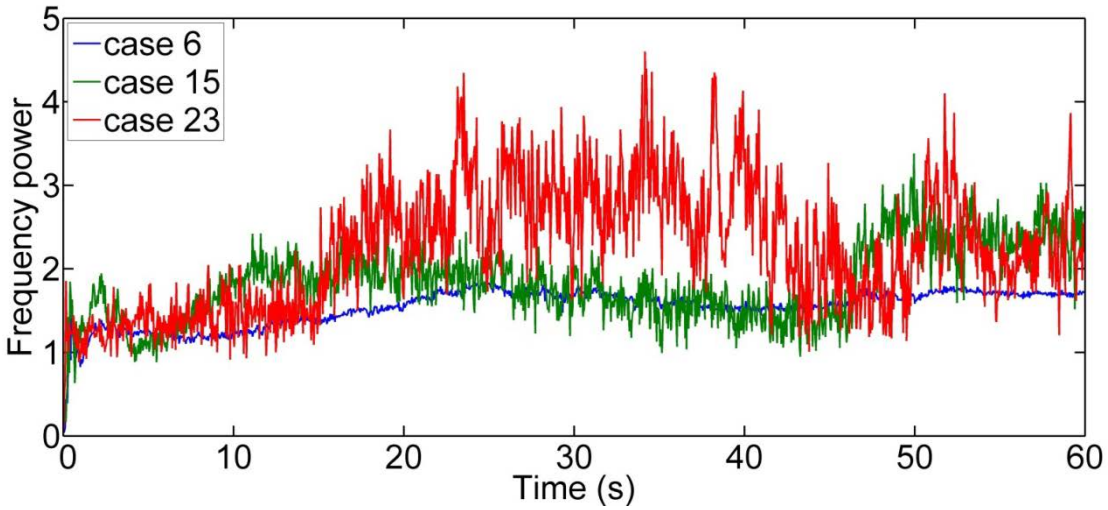


(A)

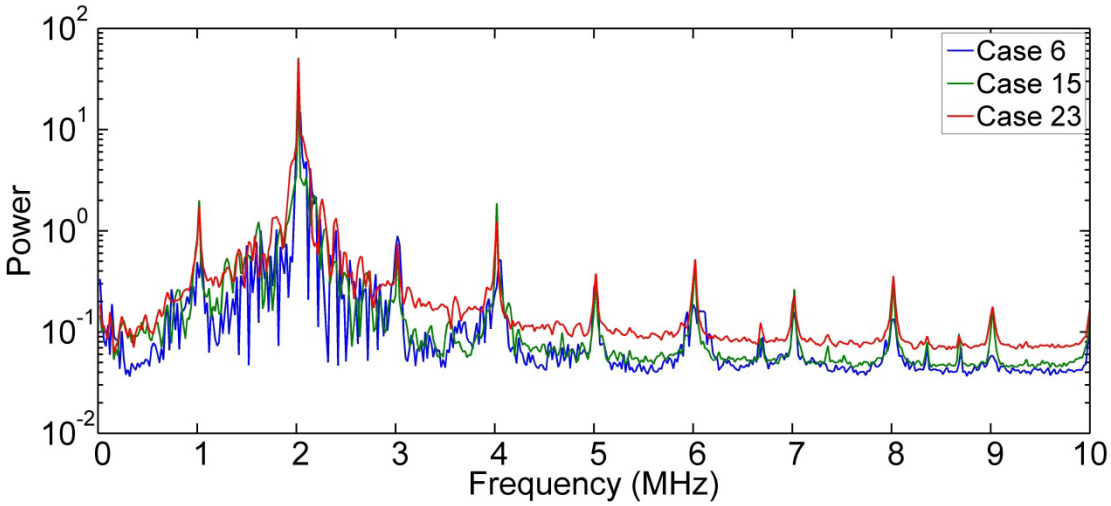


(B)

Figure 4.6 Cavitation noise of 3 case, (A) Noise emissions averaged over frequency intervals; (B) the noise emission spectra averaged over 30 to 40 second. The acoustic intensity is 0.8 MPa, PRF is 5 kHz and pulse duration is 20 μs (case 6); PRF is 0.05 kHz and pulse duration is 2,000 μs (case 15); and PRF is 0.5 kHz and pulse duration is 500 μs (case 23).

Table 4.1 Emission level comparing during 30 to 40 second of 3 cases

| Parameter | Case 6 | Case 15 | Case 23 |
|---|---|---|---|
| Mean | 1.6193 | 1.5931 | 2.9257 |
| Standard deviation | 0.0766 | 0.2279 | 0.5641 |

Table 4.2 Time and value of peak emission of 3 cases

| Parameter | Case 6 | Case 15 | Case 23 |
|---|---|---|---|
| Time of peak | 0.48 s | 0.4 s | 0.16 s |
| Peak value | 1.46 | 1.848 | 1.855 |

The influence of irradiation time on sonoporation efficiency is discussed within one case as well case by case.

In the first 10 seconds that microbubbles collapse violently, the sonoporation efficiency of case 6, 15, 23 are 3.45%, 3.66%, and 3.65% for attachment status, and 5.61%, 6.55%, and 6.54% for suspension status. Within 40 seconds, the sonoporation efficiency of case 6, 15, 23 are 5.12%, 5.36%, and 6.03% for attachment status, and 9.52%, 9.32%, and 10.41% for suspension status. In the first 10 seconds, sonoporation efficiency in case 23 is about the same with case 15, a little bit larger than case 6. But after 40 seconds, the efficiency in case 23 is much larger than both case 6 and case 15. So the difference happens while cavity behavior dominates cavitation.

To find the difference from cavity behavior, the discussion is done within one case. In case 6, the sonoporation efficiency increase from 20 s to 30 s is smaller than that from 10 s to 20 s. From 30 s, the sonoporation efficiency plateaus. But in case 15 and 23, from 30 s, although the increase is not as large as that within 30 s, the sonoporation efficiency is still increasing as irradiation time increases. And the increase is more obvious in case 23 than that of case 15. Together as that shown in Figure 4.6, the deeper and sharper saw tooth causes such increase while smooth curve

is not capable. In other words, the alternatively changes in emission from cavity behavior is much more effective than stable emission in sonoporating cells. Since such alternative change in emission is caused either by collapse of cavities or changing in nonlinearity of cavity oscillation while stable emission is caused by stable oscillation of cavity, collapse of cavity is much more effective in sonoprating cells than stable oscillation of cavity.

One more thing is that for all 3 cases, the increase of sonoporation efficiency in first 20 seconds is quicker than the increase from 20 s to the end. Majority of sonoporated cells are caused by the collapse of shelled bubbles. In other words, the collapse of shelled bubbles is more effective in sonoporating cells than the collapse of cavity.

### 4.4.3 Influence of pulse duration

The influence of pulse duration on both delivery rate and cell viability was tested at two different PRFs. The results during irradiation of 4 pulse durations at 5 kHz PRF and during irradiation of 6 pulse durations at 0.5 kHz PRF were shown in Figure 4.7. The initial microbubble concentration is 0.1 (10% volume to volume). The other parameters were set as: the acoustic intensity is 0.8 MPa and the irradiation time is 30 s. At 5 kHz RPF, pulse durations of 5, 10, 20, and 50 μs correspond to duty ratios of 2.5, 5, 10, and 25%. At 500 Hz RPF, pulse durations of 5, 10, 20, 50, 200, and 500 μs correspond to duty ratios of 0.25, 0.5, 1, 2.5, 10, and 25%.

For both PRFs, the delivery rate increases while cell viability decreases as pulse duration increases. At 5 kHz PRF, the increase trend of delivery rate is obvious under 20 μs and becomes slower after that. The decrease of cell viability presents a gradual style over all irradiation time lengths. At 500 Hz PRF, the increase trend of delivery rate is more gradual. The cell viability decreases slightly when pulse duration is less than 200 μs and suddenly drops largely at 500 μs.

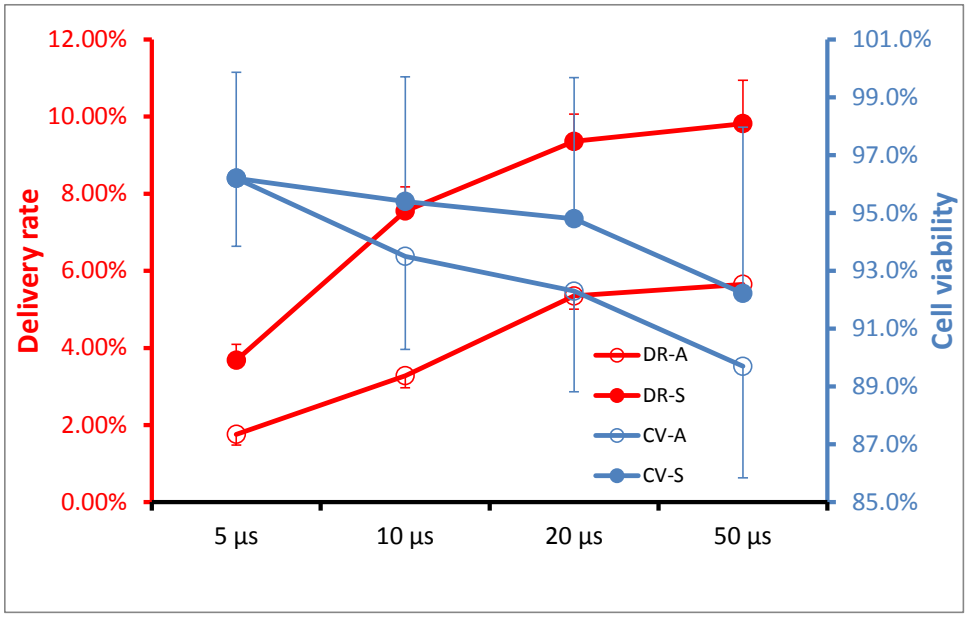


(A)

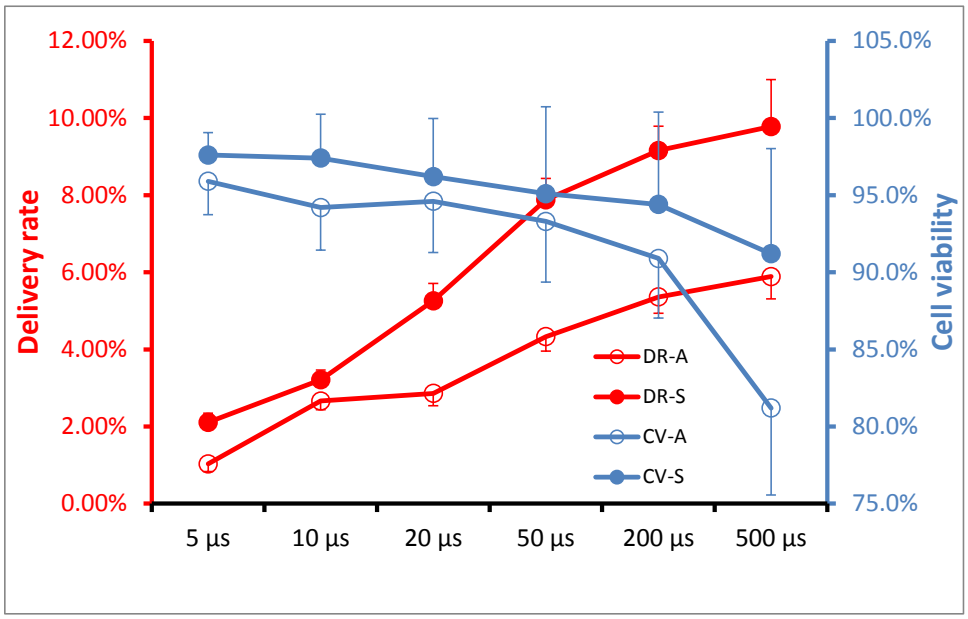


(B)

Figure 4.7 Effects of pulse duration on the delivery rate and cell viability for cells irradiated in both attachment and suspension statuses. PRF of (A) and (B) is 5 kHz, and 500 Hz, respectively. DR is short for delivery rate; CV is short for cell viability; and 'A', and 'V' indicate attachment and suspension status, respectively. The acoustic intensity is 0.8 MPa; and the irradiation time is 30 s. The data is averaged from 4 independent replicates (12 samples) and shown as the mean +/- standard deviation.

The 2 pulse duration series at 5 kHz and 0.5 kHz PRF are similar and the discussion will use the series of 0.5 kHz which contains more cases.

The case of 5 μs is the same type as cases in intensity series when intensity is smaller than 0.3 MPa where weak oscillation of microbubbles dominates. From 10 μs to 50 μs, the intensity of microbubble collapse increases as shown in Table 3.3 in Part 3.3.2.3. But at the same time, the difference in cavity behavior among these 3 pulse durations is extremely small as shown in Figure 3.10 (C). So the reason of the increase in sonoporation efficiency is the increase in the intensity of shelled bubble collapse. The case of 500 μs shows violent collapse of shelled bubbles, strong nonlinearity in cavity oscillation and collapse of cavity can also be found. Since all these 3 behaviors are strong, the sharp drop of cell viability is thus understandable.

### 4.4.4 Influence of PRF

Burst settings, as introduced in Part 2.2.2, including pulse duration and pulse repetition frequency (PRF). Different burst settings have different total ‘on’ time of ultrasound and thus have different total energy.

The influence of PRF on both delivery rate and cell viability was tested. The cell behaviors during irradiation of 8 PRF values together with continuous wave case were shown in Figure 4.8. The initial microbubble concentration is 0.1 (10% volume to volume). The other parameters were set as: the acoustic intensity is 0.8 MPa; the duty cycle is kept at 10%; and the irradiation time is 30 s except for the continuous case where the irradiation time is 20 s.

There is no clear trend of increase of decrease for either delivery rate or cell viability as PRF changes. Delivery rates of continuous case, 20 kHz and 50 kHz are smaller than other 6 cases. Cell viability of continuous case, 50 Hz, 20 kHz and 50 kHz are lower than other 5 cases.

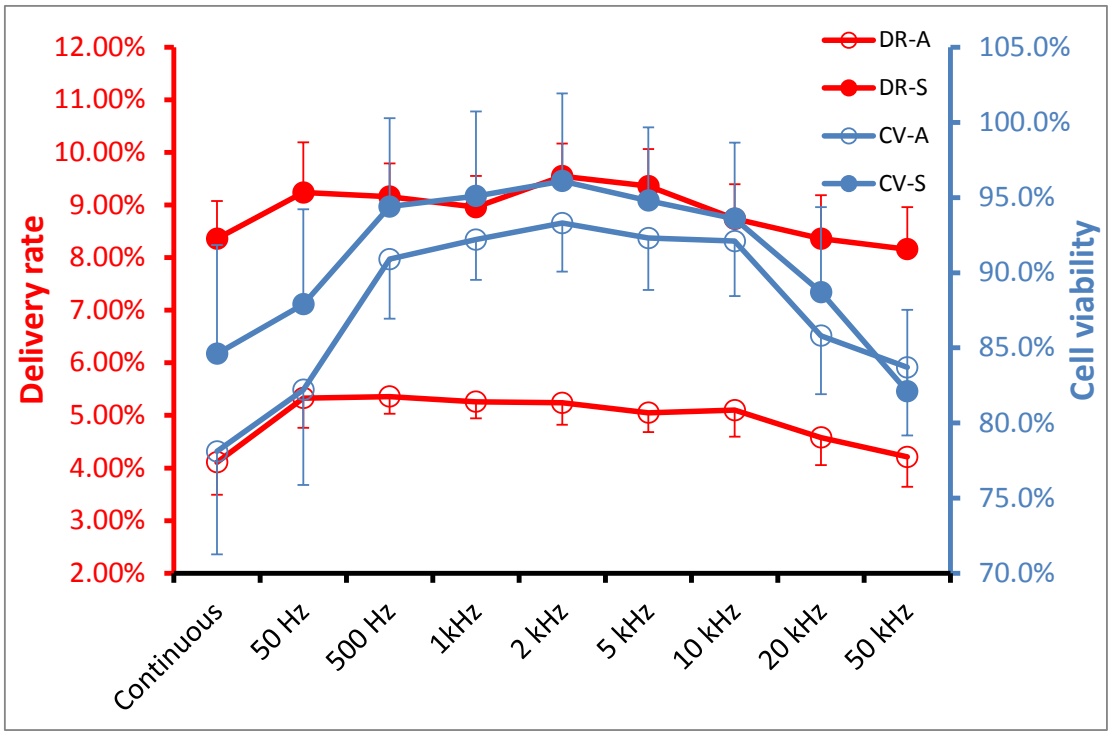


Figure 4.8 Effects of PRF on the delivery rate and cell viability for cells irradiated in both attachment and suspension statuses. DR is short for delivery rate; CV is short for cell viability; and A, V indicate attachment and suspension status, respectively. The acoustic intensity is 0.8 MPa; the duty cycle is kept at 10%; and the irradiation time is 30 s. The data is averaged from 4 independent replicates (12 samples) and shown as the mean +/- standard deviation.

The results from bubble radial dynamics have proved that for shelled bubbles, there is little difference in the intensity of collapse among all PRF cases. For cavity, cases with lower PRF have relatively higher deviation of emission level, which has been proved to cause sonoporation. However, the irradiation time is only 30 s and within 30 s, as discussed in Part 4.4.2, the increase in sonoporation efficiency comes mainly from shelled bubble behavior. So for all cases, the sonoporation efficiency difference is small. The cell viability for the case of continuous, 50 Hz, 20 kHz and 50 kHz is lower than the other 4 cases. The case of 50 Hz has stronger cavity behavior so the low cell viability is understandable. The low cell viability of 20 kHz and 50 kHz is somehow puzzling since neither shelled bubble nor cavity behavior are stronger than other cases. For the results obtained in this thesis, no clear explanation

can be given. But one possible explanation is the happening of resonant vibration of cells (http://www.ccmr.cornell.edu/education/ask/index.html?quid=734). The PRF is high enough to cause cells vibrate mechanically and further disruption of cell membrane resulting in the cell death.

## 4.5 Correlation between bubble and cell behaviors

As known, cavitation activities are believed to play very important role in sonoporation. The results in Chapter 2 and 3 have shown the parametric influence on bubble behavior and here in Part 4.4 such influence on cell behaviors is discussed. Since cell behaviors are the results of cavitation of bubbles, to get a more comprehensive understanding on such relationship, the correlation between bubble and cell behaviors will be discussed together here based on the parametric influences on both bubble and cell behaviors.

It must be noticed that size of the cell we used, NIH3T3, is around 30 μm while the averaged diameter of the contrast agents are around 3 μm. Cell is a much larger object compared to contrast agent, which is also true for human cells whose size are around 30-100 μm. Weak action of cavitation bubbles does not destroy the intactness of the membrane while strong action causes cell lysis and disintegration. Here what is focused in sonoporation is the sublethal damage to the cell membrane which opens the membrane structure for a short time while keeps the cell itself alive.

The relationship between bubble and cell behavior is complicated by the fact that several kinds of bubble behaviors can cause cell behaviors that also have two sides, repairable pores and death.

The first kind of bubble behavior is oscillation or collapse of cavities generated in the medium itself. One point to be carefully mentioned here is that such cavity behavior is the after phase of contrast agents, in other words, after the shelled bubbles have collapsed to a negligible concentration. Stable oscillation of such cavities is too weak to cause sonoporation behavior even at very high ultrasound intensity, as shown in Figure 4.5 (A) after 30 seconds. And surprisingly, here the effect of oscillation comes not from the amplitude but from the nonlinearity. With higher nonlinearity,

sonoporation and cell death both increase from cavity behavior. Then it is understandable that collapse of cavities which is naturally high nonlinear, causes both repairable pores as well as cell death. For oscillation of cavity, the parameters are more burst settings dependent than intensity. Either high duty ratio or long pulse duration is needed to reach a high nonlinear move of cavities. Since in none of the cases tested, continuous collapse of cavities is achieved, there is no clear conclusion on the parameters settings that causes collapse of cavities. But it is obvious that as the oscillation goes more and more nonlinear, the collapse of cavities will finally take place. So for cavity behavior, the threshold for causing damage on cells is much higher than that of contrast agent behavior.

For contrast agents, the results on bubble radial dynamics have shown that beginning from 0.2 MPa the shelled bubbles begin to response to ultrasound by starting to oscillate and from around 0.34 MPa they begin to collapse. At 0.2 MPa, both repairable pores and cell deaths are significant, which indicate relatively low thresholds for membrane damage. It also proves that stable oscillation of shelled bubbles, unlike that of cavities, is also able to cause cell behavior. This ability, however, is quite weak compared to collapse of shelled bubbles since beginning from 0.3 MPa the increase of sonoporated cells and decrease of dead cells both become much sharper. This is understandable because the population of contrast agents around a cell is large and the possibility of cell behavior is surely higher than that from cavities. At 0.4 MPa the cavitation of contrast agents is collapse dominant but cell behaviors are still far from its maximum intensity. The number of sonoporated cells nearly doubles and the dead cells also increases as intensity goes to 0.8 MPa. Since increase in intensity causes more violent collapse of contrast agents, with the same amount of shelled bubbles around a cell, stronger activities of individual bubbles cause stronger cell behavior. Stronger activities result in larger pores, as well as longer opening time [93] and thus benefit the internalization process. But such increase partly stops when intensity reaches 0.8 MPa: the cell death continues while sonoporation nearly stops, indicating that there is a number limit of the total effective contrast agents. Considering that a cell has only limited area and also can only bear limited area of pores otherwise it dies, the existence of intensity plateau is natural.

The only question is to what intensity the pores can last for the longest time without causing cell death. This self-sealing time is studied to be only a few seconds [94] for pores caused by shear stress at a very low intensity. For high intensity shock wave caused pore cases and a large number of cells, the time may be longer. As seen for most cases, the violent collapse of shelled bubbles stops within 10 seconds, but the rapid increase lasts till 30 s. The self-sealing time is here believed to be no shorter than 10 seconds.

The results shown in Figure 4.5 compare the difference between cell behaviors caused by cavity and shelled bubbles very well. Even with high nonlinear oscillation and occasional collapse in Figure 4.5 (C), cavity activities is still much weaker compared to shelled bubble activities.

## 4.6 Therapeutic ratio

The delivery rate and cell viability for all cases including cells irradiated in both attachment and suspension status are shown in Figure 4.9. The data from 8 series discussed above, including intensity, irradiation time for 3 different settings, PRF, pulse duration for 2 different settings are presented as a scatter plot. The legends in italic font indicating hollow markers are for cells irradiated in suspension. The overall trend for both cells irradiated in attachment status and suspension status is that increases in transfection efficiency are associated with decreased cell viability. With similar cell viability, the delivery rate of cells irradiated in suspension is higher than that of cells irradiated in attachment status.

For attachment status, the highest delivery rate obtained is 7.39%. The experiment condition for it is: 0.8 MPa intensity, 60 s irradiation time, 0.5 kHz PRF, and 500 μs pulse duration. The cell viability at this condition is 78.7%.

For suspension status, the highest delivery rate obtained is 12.03%. The experiment condition is the same as that in attachment status. The cell viability at this condition is 82.5%.

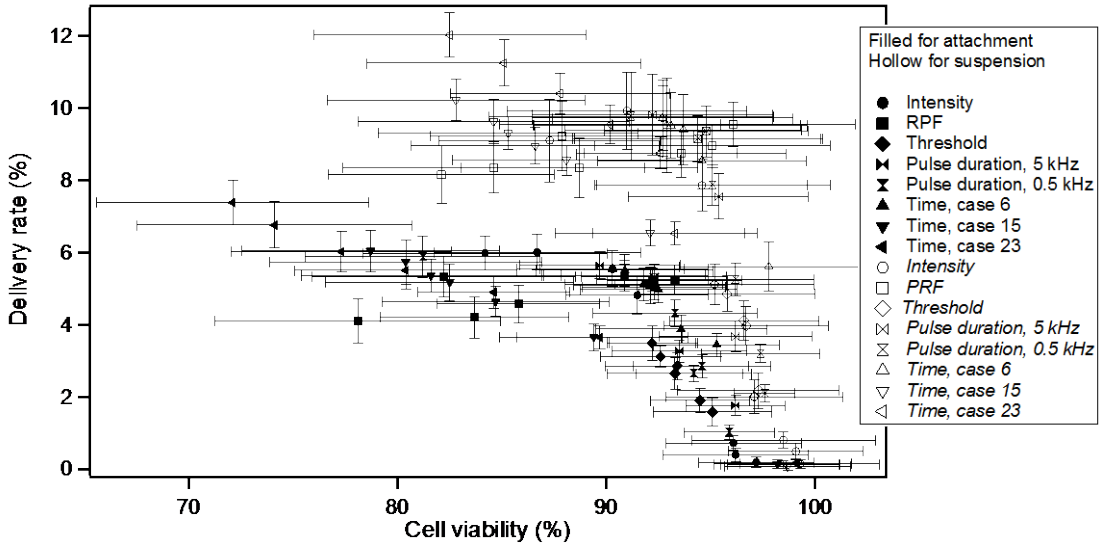


Figure 4.9 Delivery efficiency and cell viability of all cases for both cells irradiated in attachment and suspension status. The filled markers are for attachment status, and the blank markers with italic font legend are for cells irradiated in suspension.

To quantitatively assess delivery rate and cell viability together, the therapeutic ratio [44] (defined as the ratio of delivered cells to dead cells) for all cases including cells irradiated in both attachment and suspension status are shown in Figure 4.10. For cells irradiated in both statuses, the delivery rate of case 15 and case 23 in irradiation time series are clearly higher than other series. However, the therapeutic ratios for both 2 cases are not very high due to the lower cell viability.

For attachment status, there are two close therapeutic ratio peak values. One is 0.78. The experiment condition for it is: 0.8 MPa intensity, 60 s irradiation time, 2 kHz PRF, and 50 μs pulse duration. The delivery rate at this condition is 5.24% and the cell viability is 93.3%. The other one is 0.73. The experiment condition for it is: 0.8 MPa intensity, 10 s irradiation time, 5 kHz PRF, and 20 μs pulse duration. The delivery rate at this condition is 3.45% and the cell viability is 95.3%.

For cells irradiated in attachment status, the highest therapeutic ratio comes from the combination of delivery rate and cell viability while the second highest therapeutic ratio comes mainly from the high cell viability.

For suspension status, there are also two close therapeutic ratio peak values. One is 2.55. The experiment condition for it is: 0.8 MPa intensity, 10 s irradiation time, 5

kHz PRF, and 20 μs pulse duration. The delivery rate at this condition is 5.61% and the cell viability is 97.8%. The other one is 2.45. The experiment condition for it is: 0.8 MPa intensity, 60 s irradiation time, 2 kHz PRF, and 50 μs pulse duration. The delivery rate at this condition is 9.55% and the cell viability is 96.1%.

For cells irradiated in suspension status, the highest therapeutic ratio comes mainly from the high cell viability while the second highest therapeutic ratio comes from the combination of delivery rate and cell viability.

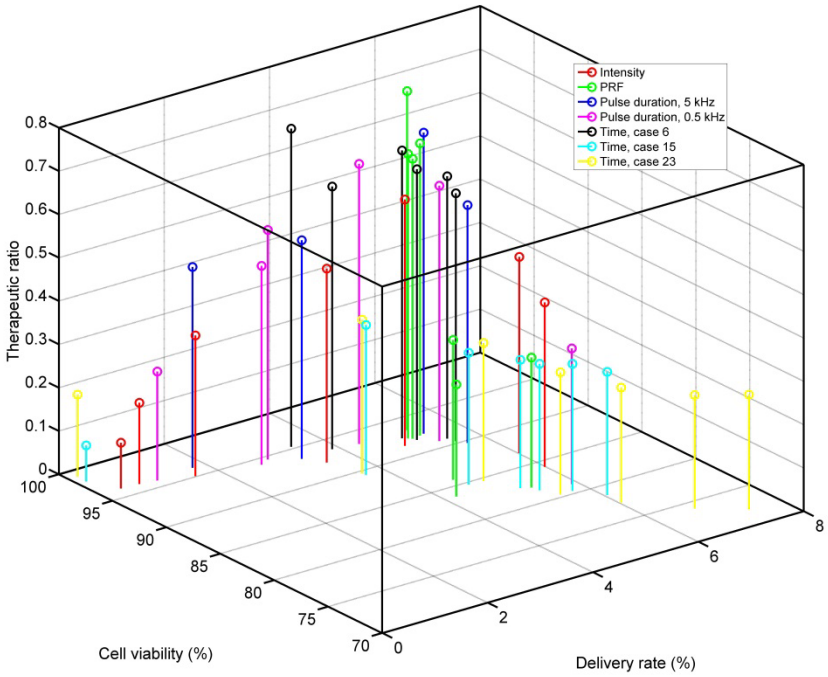


(A)

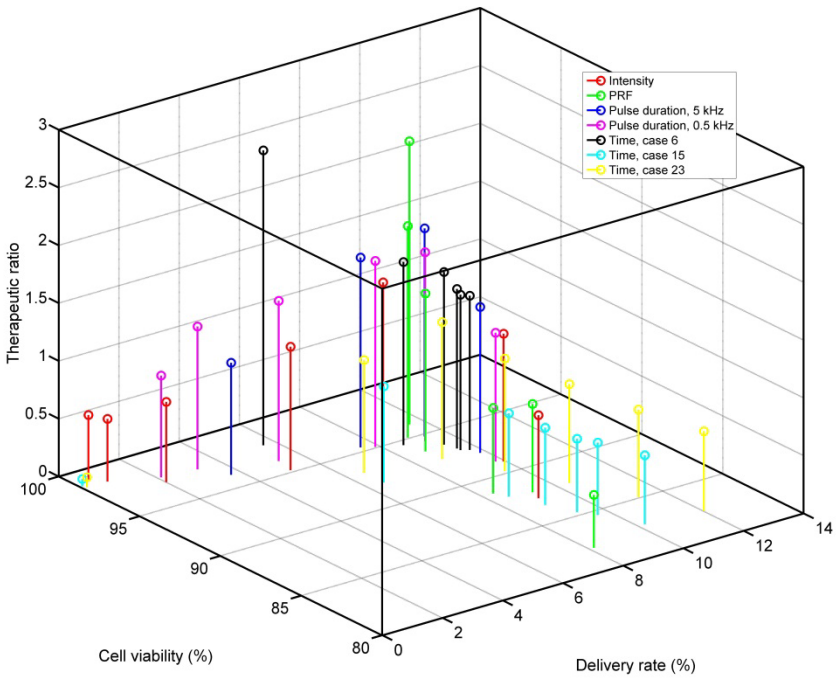


(B)

Figure 4.10.Therapeutic ratio for all cases. (A) is the result for cells irradiated in attachment status and (B) is the result for cells irradiated in suspension status.

## 4.7 Summary

FITC-dextran was delivered to cultured NIH3T3 cells via sonoporation in the presence of microbubbles. Influences of ultrasonic parameters, including intensity, irradiation time, PRF and pulse duration, on both delivery rate and cell viability were studied. The cells were irradiated in both attachment and suspension status.

As intensity increases, sonoporation efficiency increases but cell viability decreases. The difference in increasing between 0.3 MPa and 0.4 MPa is large. The increase of efficiency plateaus from 0.8 MPa but cell viability keeps decreasing.

As irradiation time increases, sonoporation efficiency increases but cell viability decreases. For case 6, the increase of sonoporation plateaus from 30 s. As pulse duration increases, sonoporation efficiency increases but cell viability decreases. The cell viability of 500 μs case is very low. The difference in sonoporation efficiency among different PRF values is small. The cell viability at 50 Hz, 20 kHz, and 50 kHz is lower than other cases.

As for the correlation between cavitation behavior and sonoporation efficiency: weak oscillation of shelled bubbles can cause sonoporation but is very ineffective; stable oscillation of cavity does not sonoporate cells; collapse of both shelled bubbles and cavities are effective in sonoporating cells while the first one is more effective. The self-sealing time of cells is around 10 seconds.

The highest delivery rate obtained is 7.39%, 12.03% for attachment and suspension status, respectively. The corresponded cell viability is 78.7%, 82.5%, respectively. The experiment condition is: 0.8 MPa, 60 s irradiation time, 0.5 kHz PRF, and 500 μs pulse duration. For attachment status, there are two close therapeutic ratio peaks. One is 0.78. The experiment condition is: 0.8 MPa, 60 s irradiation time, 2 kHz PRF, and 50 μs pulse duration. The delivery rate at this condition is 5.24% while the cell viability is 93.3%. The other one is 0.73. The experiment condition is: 0.8 MPa, 10 s irradiation time, 5 kHz PRF, and 20 μs pulse duration. The delivery rate at this condition is 3.45% while the cell viability is 95.3%. For suspension status, there are also two close therapeutic ratio peaks. One is 2.55. The experiment condition is: 0.8 MPa, 10 s irradiation time, 5 kHz PRF, and 20 μs pulse duration. The delivery rate at this condition is 5.61% while the cell viability is 97.8%. The other one

is 2.45. The experiment condition is: 0.8 MPa, 60 s irradiation time, 2 kHz PRF, and 50 μs pulse duration. The delivery rate at this condition is 9.55% while the cell viability is 96.1%.

# Chapter 5. Conclusions and future directions

Towards higher delivery efficiency from sonoporation, experimental studies from two sides were carried out. The overall aim is deeper understanding of sonoporation mechanism and thus methods to improve sonoporation efficiency. Totally 23 experiment conditions were carried out for both bubble behavior and delivery of markers into cells with identical settings. Ultrasonic parameters' influence, including intensity, pulse duration, PRF on both bubble radial dynamics and cell behaviors are discussed. The bubble behavior is separately discussed on both oscillation and collapse of both cavities generated in the liquid itself and artificially added contrast agents from the results of laser diode concentration test and cavitation noise analysis. The cell behaviors including the sonoporation and cell death measured by flow cytometry and automated counter are listed by parameters.

The results of bubble behavior are very briefly listed as following. Shelled bubble oscillations appear at low intensities and dominant bubble behavior under 0.3 MPa. Between 0.3 MPa and 0.4 MPa, oscillation and collapse of shelled bubbles coexist. From 0.4 MPa, collapse of shelled bubble dominates and collapse becomes quicker as intensity and pulse duration increase. There is a threshold intensity of 0.34 MPa, where microbubble behavior changes from oscillation dominant to collapse dominant. For shelled bubbles, pulse duration is leading influencing factor rather than rest time when pulse duration is longer than 10 μs. Pulse duration and PRF also influence cavity behavior. With longer pulse duration, the oscillation of cavity becomes more nonlinear. At high PRFs oscillations of cavities are stronger. Collapses of cavities are obvious at high pulse durations and low PRFs.

The results of cell behavior are briefly listed as following. Sonoporation efficiency increases but cell viability decreases when intensity increases. The difference in increasing between 0.3 MPa and 0.4 MPa is large. The increase of efficiency plateaus from 0.8 MPa but cell viability keeps decreasing. Sonoporation efficiency increases but cell viability decreases when pulse duration increases. As

pulse duration increases, sonoporation efficiency increases but cell viability decreases. The cell viability of 500 μs case is very low. The difference in sonoporation efficiency among different PRF values is small. The cell viability at 50 Hz, 20 kHz, and 50 kHz is lower than other cases. The sonoporation efficiency reaches more than 60% of its final value at 60 s during first 20 seconds. After 20 seconds, the increasing in efficiency is small. But such small increase is more obvious with an unstable emission level.

The relationship between cavitation behavior and sonoporation efficiency is quite complicated and is briefly listed as following. Weak oscillation of shelled bubbles can cause sonoporation but is very ineffective; stable oscillation of cavity does not sonoporate cells; collapse of both shelled bubbles and cavities are effective in sonoporating cells while the first one is more effective. The self-sealing time of cells is around 10 seconds.

One continuing work is refilling of microbubbles. Since the collapse of shelled bubbles is most effective and happens very quickly, refilling of bubbles would improve sonoporation efficiency directly. Even with the same amount of bubbles, rupture them step by step is a better choice. Further future work may include two parts. The first one is to carry out sonoporation experiments in a more microscopic way. For example, to observe the pores directly will help to form theory on pore formation process which is now one of the most difficult topics in sonoporation research. The other one is to apply the parametric influence to *in vivo* cases. Delivery with animal experiments applying the conclusions in this study is very necessary before clinical settings of sonoporation delivery therapy.

# Bibliography

[1] A. I. Freeman and E. Mayhew, "Targeted drug delivery," *Cancer,* vol. 58, no. S2, pp. 573-583, 1986.

[2] T. Friedmann and R. Roblin, "Gene therapy for human genetic disease?," *Science,* vol. 175, pp. 949-955, 1972.

[3] T. Friedmann, "Progress toward human gene therapy," *Science,* vol. 244, pp. 1275-1281, 1989.

[4] R. C. Scott, D. Crabbe, B. Krynska, R. Ansari and M. F. Kiani, "Aiming for the heart: targeted delivery of drugs to diseased cardiac tissue," *Expert Opinion on Drug Delivery,* vol. 5, no. 4, pp. 459-470, 2008.

[5] R. H. Muller and C. M. Keck, "Challenges and solutions for the delivery of biotech drugs – a review of drug nanocrystal technology and lipid nanoparticles," *Journal of Biotechnology,* vol. 113, no. 1-3, p. 151–170, 2004.

[6] J. K. Mills and D. Needham, "1275-1281," *Expert Opinion on Therapeutic Patents,* vol. 9, no. 11, pp. 1499-1513, 1999.

[7] T. M. Allen and P. R. Cullis, "Drug Delivery Systems: Entering the Mainstream," *Science,* vol. 303, pp. 1818-1822, 2003.

[8] Y. H. Bae and P. K, "Targeted drug delivery to tumors: Myths, reality and possibility," *Journal of Controled Release,* vol. 153, no. 3, p. 198–205, 2011.

[9] O. Pillai, A. B. Dhanikula and R. Panchagnula, "Drug delivery: an odyssey of 100 years," *Current Opinion in Chemical Biology,* vol. 5, p. 439–446, 2001.

[10] V. P. Torchilin, "Drug targeting," *European Journal of Pharmaceutical Sciences,* vol. 11, no. S2, p. S81–S91, 2000.

[11] L. R, "New Methods of Drug Delivery," *Science,* vol. 249, pp. 1527-1533, 1990.

[12] Y. Li, F. Chen, M. M. Cona, Y. Feng, U. Himmelreich, R. Oyen, A. Verbruggen and Y. Ni, "A review on various targeted anticancer therapies," *Targeted Oncology,* vol. 7, pp. 69-85, 2012.

[13] M. R. Prausnitz, S. Mitragotri and R. Langer, "Current status and future potential of transdermal drug delivery," *Nature Reviews Drug Discovery,* Vols. 115-124, p. 3, 2004.

[14] A. Bianco, K. Kostarelos and M. Prato, "Applications of carbon nanotubes in drugdelivery," *Current Opinion in Chemical Biology,* vol. 9, no. 6, p. 674–679, 2005.

[15] J. Dobson, "Magnetic nanoparticles for drug delivery," *Drug Development Research,* vol. 67, no. 1, pp. 55-60, 2006.

[16] N. A. Kootstra and I. M. Verma, "Gene therapy with viral vectors," *Annual Review of Pharmacology and Toxicology,* vol. 43, pp. 413-439, 2003.

[17] A. L. Dunehoo, M. Anderson, S. Majumdar, N. Kobayashi, C. Berkland and S. T. J, "Cell Adhesion Molecules for Targeted Drug Delivery," *Journal of Pharmaceutical Sciences,* vol. 95, no. 9, pp. 1856-1872, 2006.

[18] C. M. Newman, A. Lawrie, A. F. Brisken and D. C. Cumberland, "Ultrasound gene therapy: on the road from concept to reality," *Echocardiography,* vol. 18, pp. 339-347, 2001.

[19] D. L. Miller, S. V. Pislaru and J. F. Greenleaf, "Sonoporation: mechanical DNA delivery by ultrasonic cavitation," *Somatic Cell and Molecular Genetics,* vol. 27, pp. 115-134, 2002.

[20] W. G. Pitt, G. A. Husseini and B. J. Staples, "Ultrasonic drug delivery-a general review," *Expert Opinion on Drug Delivery,* vol. 1, pp. 37-56, 2004.

[21] G. R. ter Haar and C. C. Coussios, "High intensity focused ultrasound: past, present and future," *International Journal of Hyperthermia,* vol. 23, pp. 85-87, 2007.

[22] G. R. ter Haar and C. C. Coussios, "High intensity focused ultrasound: physical principles and devices," *International Journal of Hyperthermia,* vol. 23, pp. 89-104, 2007.

[23] F. A. Duch, "Hazards, risks and safety of diagnostic ultrasound," *Medical Engineering & Physics,* vol. 30, no. 10, p. 1338–1348, 2008.

[24] V. F. Humphrey, "Ultrasound and matter—Physical interactions," *Progress in Biophysics and Molecular Biology,* vol. 93, pp. 195-211, 2007.

[25] C. E. Brennen, Cavitation and Bubble Dynamics, New York: Oxford University Press, 1995.

[26] S. Barnett, "Nonthermal issues: cavitation—its nature, detection and measurement," *Ultrasound in Medicine and Biology,* vol. 24, p. S11–S21, 1998.

[27] J. Wu and W. L. Nyborg, "Ultrasound, cavitation bubbles and their interaction with cells," *Advanced Drug Delivery Reviews,* vol. 60, pp. 1103-1116, 2008.

[28] J. Wu, "Theoretical study on shear stress generated by microstreaming surrounding contrast agents attached to living cells," *Ultrasound in Medicine and Biology,* vol. 28, no. 1, pp. 125-129, 2002.

[29] D. Willian and J. O'brien, "Ultrasound–biophysics mechanisms," *Progress in Biophysics and Molecular Biology,* vol. 93, p. 212–255, 2007.

[30] W. Lauterborn, T. Kurz, R. Geisler, D. Schanz and O. Lindau, "Acoustic cavitation, bubble dynamics and sonoluminescence," *Ultrasonics Sonochemistry,* vol. 14, pp. 484-491, 2007.

[31] H.-D. Liang, J. Tang and Halliwell, "Sonoporation, drug delivery, and gene therapy," *Proceedings of the Institution of Mechanical Engineers, Part H: Journal of Engineering in Medicine,* vol. 224, pp. 343-361, 2010.

[32] Y. Zhao, Y. Luo, C. Lu, J. Xu, J. Tang, M. Zhang, Y. Zhang and H. Liang, "Phospholipids-based microbubbles sonoporation pore size and reseal of cell membrane

cultured in vitro," *Journal of Drug Targeting,* vol. 16, no. 1, pp. 18-25, 2008.

[33] R. K. Schlicher, H. Radhakrishna, T. P. Tolentino, R. P. Apkarian, V. Zarnitsyn and M. R. Prausnitz, "Mechanism of intracellular delivery by acoustic cavitation," *Ultrasound in Medicine and Biology,* vol. 32, no. 6, pp. 915-924, 2006.

[34] Y. Zhang, R. Tachibana, A. Okamoto, T. Azuma, A. Sasaki, K. Yoshinaka, Y. Tei, S. Takagi and Y. Matsumoto, "Ultrasound-Mediated Gene Transfection in vitro: Effect of Ultrasonic Parameters on Efficiency and Cell Viability," *International Journal of Hyperthermia,* vol. 28, no. 4, pp. 290-299, 2012.

[35] D. J. Wells, "Electroporation and ultrasound enhanced non-viral gene delivery in vitro and in vivo," *Cell Biol Toxicol,* vol. 26, pp. 21-28, 2010.

[36] S. Mehier-Humbert and R. H. Guy, "Physical methods for gene transfer: Improving the kinetics of gene delivery into cells," *Advanced Drug Delivery Reviews,* vol. 57, no. 5, pp. 733-753, 2005.

[37] J. Pepe, M. Rincón and J. Wu, "Experimental comparison of sonoporation and electroporation in cell transfection applications," *Acoustics Research Letters Online,* vol. 5, no. 2, pp. 62-67, 2004.

[38] P. J. Canatell, J. F. Karr, J. A. Petros and M. R. Prausnitz, "Quantitative Study of Electroporation-Mediated Molecular Uptake and Cell Viability," *Biophysical Journal,* vol. 80, no. 2, pp. 755-764, 2001.

[39] K. Ng and Y. Liu, "Therapeutic ultrasound: Its application in drug delivery," *Medicinal Research Reviews* , vol. 22, no. 2, pp. 204-223, 2002.

[40] M. Fechheimer, C. Denny, M. F. Murphy and D. L. Taylor, "Measurement of cytoplasmic pH in Dictyostelium discoideum by using a new method for introducing macromolecules into living cells," *European Journal of Cell Biology,* vol. 40, no. 2, pp. 242-247, 1986.

[41] M. Fechheimer, J. F. Boylan, S. Parker, J. E. Sisken, G. L. Patel and S. G. Zimmer, "Transfection of mammalian cells with plasmid DNA by scrape loading and sonication loading," *Proceedings of the National Academy of Sciences,* vol. 84, no. 23, pp. 8463-8467 , 1987.

[42] S. Bao, B. D. Thrall and D. L. Miller, "Transfection of a reporter plasmid into cultured cells by sonoporationin vitro," *Ultrasound in Medicine and Biology,* vol. 23, no. 6, p. 953–959, 1997.

[43] H. J. Kim, J. F. Greenleaf, R. R. Kinnick, J. T. Bronk and M. E. Bolander, "Ultrasound-mediated transfection of mammalian cells," *Human Gene Therapy,* vol. 7, pp. 1339-1346, 1996.

[44] R. Karshafian, P. D. Bevan, R. Willams, S. Samac and B. P. N, "Sonoporation by ultrasound-activated microbubble contrast agents: effect of acoustic exposure parameters on cell membrane permeability and cell viability," *Ultrasound in Medicine and Biology,* vol. 35,

pp. 847-860, 2009.

[45] L. C. Phillips, A. L. Klibanov, B. R. Wamhoff and J. A. Hossack, "Localized ultrasound enhances delivery of rapamycin from microbubbles to prevent smooth muscle proliferation," *Journal of Controlled Release*, vol. 154, no. 1, p. 42–49, 2011.

[46] J. M. Escoffre, J. Piron, A. Novell and A. Bouakaz, "Doxorubicin Delivery into Tumor Cells with Ultrasound and Microbubbles," *Molecular Pharmaceutics,* vol. 8, no. 3, p. 799–806, 2011.

[47] M. Kinoshita and K. Hynynen, "A novel method for the intracellular delivery of siRNA using microbubble-enhanced focused ultrasound," *Biochemical and Biophysical Research Communications*, vol. 335, p. 393–399, 2005.

[48] L. Reslan, J.-L. Mestas, S. Herveau, J.-C. Béra and C. Dumontet, "Transfection of cells in suspension by ultrasound cavitation," *Journal of Controlled Release*, vol. 142, pp. 251-258, 2010.

[49] K. Koshiyama, T. Yano and T. Kodama, "Self-Organization of a Stable Pore Structure in a Phospholipid Bilayer," *Physical Review Letters*, vol. 105, no. 1, p. 018105 (4), 2010.

[50] A. Choubey, M. Vedadi, K. Nomura, R. K. Kalia, A. Nakano and P. Vashishta, "Poration of lipid bilayers by shock-induced nanobubble collapse," *Applied Physics Letters,* vol. 98, p. 023701(3), 2011.

[51] S. Mehier-Humbert, T. Bettinger, F. Yan and R. H. Guy, "Plasma membrane poration induced by ultrasound exposure: Implication for drug delivery," *Journal of Controlled Release*, vol. 104, p. 213–222, 2005.

[52] Z. Fan, R. E. Kumon, J. Park and C. X. Deng, "Intracellular delivery and calcium transients generated in sonoporation facilitated by microbubbles," *Journal of Controlled Release,* vol. 142, pp. 31-39, 2010.

[53] P. Marmottant, M. Versluis, N. de Jong, S. Hilgengeldt and D. Lohse, "High-speed imaging of an ultrasound-driven bubble in contact with a wall: “Narcissus” effect and resolved acoustic streaming," *Experiments in Fluids*, vol. 41, no. 2, pp. 147-153, 2006.

[54] A. van Wamel, K. Kooiman, M. Harteveld, M. Emmer, F. J. ten Cate, V. Michel and N. de Jong, "Vibratingmicrobubblespokingindividualcells: Drugtransfer into cellsviasonoporation," *Journal of Controlled Release*, vol. 112, no. 2, pp. 149-155, 2006.

[55] Z. Y, K. Yang, J. Cui, J. Y. Ye and C. X. Deng, "Controlled permeation of cell membrane by single bubble acoustic cavitation," *Journal of Controlled Release,* vol. 157, pp. 103-111, 2012.

[56] C.-D. Ohl, M. Arora, R. Ikink, N. de Jong, M. Versluis, M. Delius and D. Lohse, "Sonoporation from Jetting Cavitation Bubbles," *Biophysical Journal,* vol. 91, pp. 4285-4295, 2006.

[57] B. Krasovitski and E. Kimmel, "Shear stress induced by a gas bubble pulsating in an

ultrasonic field near a wall," *IEEE Transactions on Ultrasonics, Ferroelectrics and Frequency Control,* vol. 51, no. 8, pp. 973-979, 2004.

[58] J. Collis, R. Manasseh, P. Liovic, P. Tho, A. Ooi, K. Petkovic-Duran and Y. Zhu, "Cavitation microstreaming and stress fields created by microbubbles," *Ultrasonics,* vol. 50, pp. 273-279, 2010.

[59] P. F. Davies, "Flow-mediatedendothelialmechanotransduction," *Physiological Reviews,* vol. 75, no. 3, pp. 519-560, 1995.

[60] J. Park, Z. Fan and C. X. Deng, "Effects of shear stress cultivation on cellmembrane disruption and intracellular calcium concentration in sonoporation of endothelial cells," *Journal of Biomechanics,* vol. 44, pp. 164-169, 2011.

[61] S. Mitragotri, "Healing sound: the use of ultrasound in drug delivery and other therapeutic applications," *Nature Reviews Drug Discovery ,* vol. 4, pp. 255-260, 2005.

[62] K. Koshiyama, T. Kodama, T. Yano and S. Fujikawa, "Structural change in lipid bilayers and water penetration induced by shock waves: molecular dynamics simulations," *Biophysical Journal,* vol. 91, pp. 2198-2205, 2006.

[63] S. Y. Chen, R. V. Shohet, R. Bekeredjian, P. Frenkel and P. A. Grayburn, "Optimization of ultrasound parameters for cardiac gene delivery of adenoviral or plasmid deoxyribonucleic acid by ultrasound-targeted microbubble destruction," *Journal of the American College of Cardiology,* vol. 42, pp. 301-308, 2003.

[64] V. G. Zarnitsyn and M. R. Prausnitz, "hysical parameters influencing optimization of ultrasound-mediated DNA transfection," *Ultrasound in Medicine and Biology,* vol. 30, pp. 527-538, 2004.

[65] H. D. Liang, Q. L. Lu, S. A. Xue, M. Halliwell, T. Kodama, D. O. Cosgrove, H. J. Stauss, T. A. Partridge and M. K. Blomley, "Optimisation of ultrasound-mediated gene transfer (sonoporation) in skeletal muscle cells," *Ultrasound in Medicine and Biology,* vol. 30, pp. 1523-1529, 2004.

[66] A. Rahim, S. L. Taylor, N. L. Bush, G. R. ter Haar, J. C. Bamber and C. D. Porter, "Physical parameters affecting ultrasound/microbubblemediated gene delivery efficiency in vitro," *Ultrasound in Medicine and Biology,* vol. 32, pp. 1269-1279, 2006.

[67] J.-P. Franc and J.-M. Michel, "Fundamentals of Cavitation," *Fluid Mechanics and Its Applications,* vol. 76, pp. 1-306, 2005.

[68] M. S. Plesset and A. Prosperetti, "Bubble dynamics and cavitation," *Annual Review of Fluid Mechanics,* vol. 9, pp. 145-185, 1977.

[69] W. P. Mason, Physical Acoustics, Vol. 1-B, New York: Academic Press, 1964.

[70] T. Faez, M. Emmer, K. Kooiman, M. Versluis, A. van der Steen and N. de Jong, "20 Years of Ultrasound Contrast Agent Modeling," *IEEE Transactions on Ultrasonics, Ferroelectrics and Frequency Control,* vol. 60, no. 1, pp. 7-20, 2013.

[71] J. S. Allen, D. J. May and K. W. Ferrara, "Dynamics of therapeutic ultrasound contrast agents," *Ultrasound in Medicine and Biology,* vol. 28, no. 6, pp. 805-816, 2002.

[72] M. Ashokkumar, J. Lee, S. Kentish and F. Grieser, "Bubbles in an acoustic field: An overview," *Ultrasonics Sonochemistry,* vol. 14, p. 470–475, 2007.

[73] M. Liebler, T. Dreyer and R. E. Riedlinger, "Modeling of interaction between therapeutic ultrasound propagation and cavitation bubbles," *Ultrasonics,* vol. 44, p. e319–e324, 2006.

[74] A. H. Lo, O. D. Kpipfgans, P. L. Carson and J. B. Fowlkes, "Spatial control of gas bubbles and their effects on acoustic fields," *Ultrasound in Medicine and Biology,* vol. 32, no. 1, p. 95–106, 2006.

[75] A. A. Doinikov and S. T. Zavtrak, "On the mutual interaction of two gas bubbles in a sound field," *Physics of Fluids,* vol. 7, no. 8, pp. 1923-1930, 1995.

[76] É. S. Nasibullaeva and I. S. Akhatov, "Dynamics of a bubble cluster in an acoustic field," *Acoustical Physics,* vol. 51, no. 6, pp. 705-712, 2005.

[77] P. C. Sontum, "Physicochemical Characteristics of Sonazoid™, A New Contrast Agent for Ultrasound Imaging," *Ultrasound in Medicine & Biology,* vol. 34, no. 5, pp. 824-833, 2008.

[78] J. D. Ingle and S. R. Crouch, Spectrochemical Analysis, New Jersey : Prentice Hall, 1988.

[79] P. Misra and M. Dubinskii, Ultraviolet Spectroscopy and UV Lasers, New York: CRC Press, 2002.

[80] T. G. Leighton, The acoustic bubble, San Diego: Academic Press, 1994.

[81] 松本洋一郎 , 吉澤晋,“気泡の非線形振動,”*機械の研究,* 第 巻54, 第 1, pp. 108-113, 2002.

[82] E. A. Neppiras, "Acoustic cavitation," *Physics Reports* , vol. 61, pp. 159-251, 1980.

[83] A. J. Walton and G. T. Reynolds, "Sonoluminescence," *Advances in Physics* , vol. 33, no. 6, pp. 595-660, 1984.

[84] K. Negishi, "Experimental Studies on Sonoluminescence and Ultrasonic Cavitation," *Journal of the Physical Society op Japan,* vol. 16, pp. 1450-1465, 1961.

[85] S. Paliwal and S. Mitragotri, "Ultrasound-induced cavitation: applications in drug and gene delivery," *Expert Opinion on Drug Delivery,* vol. 3, no. 6, pp. 713-726, 2006.

[86] V. Kamath and A. Prosperetti, "Numerical integration methods in gas-bubble dynamics," *The Journal of the Acoustical Society of America,* vol. 85, pp. 1538-1548, 1989.

[87] W. Lauterborn, "Cavitation bubble dynamics - new tools for an intricate problem," *Applied Scientific Research,* vol. 38, pp. 165-178, 1982.

[88] A. L. Klibanov, "Microbubble contrast agents: targeted ultrasound imaging and ultrasound-assisted drug-delivery applications," *Investigative Radiology,* vol. 41, no. 3, pp. 354-362, 2006.

[89] K. Ferrara, R. Pollard and M. Borden, "Ultrasound microbubble contrast agents:

fundamentals and application to gene and drug delivery," *Annual Review of Biomedical Engineering*, vol. 9, pp. 415-447 , 2007.

[90] D. M. Hollow, A. D. Mahajan, T. E. McCutchen and M. R. Prausnitz, "Measurement and correlation of acousticcavitation with cellular bioeffects," *Ultrasound in Medicine and Biology*, vol. 32, no. 7, pp. 1111-1122, 2006.

[91] Y. Qiu, Y. Luo, Y. Zhang, W. Cui, D. Zhang, J. Wu, J. Zhang and J. Tu, "The correlation between acoustic cavitation and sonoporation involved in ultrasound-mediated DNA transfection with polyethylenimine (PEI) in vitro," *Journal of Controlled Release*, vol. 145, pp. 40-48, 2010.

[92] W. S. Chen, T. J. Matula, A. A. Brayman and L. A. Crum, "A comparison of the fragmentation thresholds and inertial cavitation doses of different ultrasound contrast agents," *Journal of the Acoustical Society of America*, vol. 113, no. 1, pp. 643-651, 2003.

[93] D. L. Miller and J. Quddus, "Lysis and sonoporation of epidermoid and phagocytic monolayer cells by diagnostic ultrasound activation of contrast agent gas bodies," *Ultrasound in Medicine and Biology*, vol. 27, no. 8, pp. 1107-1113, 2001.

[94] F. Yang, N. Gu, D. Chen, X. Xi, D. Zhang and J. Wu, "Experimental study on cell self-sealing during sonoporation," *Journal of Controlled Release*, vol. 131, no. 3, pp. 205-210, 2008.

# List of Figures

Figure 1.1 An atomic force microscopy image of pores on the cell membrane [32] ..... 8
Figure 1.2 An example of intracellular delivery by ultrasound. (a) Confocal micrographs showing a nonsonicated DU 145 cell exposed to calcein (A1) and sonicated cells exhibiting uptake of calcein (A2), bovine serum albumin (A3) and 150 (A4), 500 (A5) and 2,000 kDa (A6) dextrans. Scale bars are 1 μm [33] ..... 9
Figure 1.3 An example of intracellular delivery of plasmid DNA via sonoporation [34] ..... 9
Figure 1.4 An example of parametric studies on sonoporation efficiency and cell viability, PRF stands for pulse repetition frequency [34] ..... 13
Figure 1.5 Sonoporation studied in this dissertation, mainly two parts: bubble behavior including concentration change and broadband noise, and cell behavior including marker uptake and cell viability ..... 14
Figure 2.1 The radial oscillations for a 2.5 μm agent with a 500 nm triacetin shell driven at 1.6 MPa, 2.5 MHz [71] ..... 20
Figure 2.2 The radial oscillations for a 2.5 μm agent with a 5 nm triacetin shell driven at 1.6 MPa, 2.5 MHz [71] ..... 20
Figure 2.3 A microscopic view of Sonazoid™ suspension ..... 23
Figure 2.4 Number (open squares) and volume (filled squares) size distributions of Sonazoid™ suspension, data from manufacturer, GE Health [77] ..... 23
Figure 2.5 Diagram of Beer–Lambert absorption ..... 25
Figure 2.6 Diagram of ultrasound exposure system, all the pictures of instuments are provided by their manufacturers except for E) and G) ..... 27
Figure 2.7 A chart of typical burst wave applied for most experimental cases ..... 28
Figure 2.8 Laser diode units used to measuring the voltage of transmitted light. (A) is a photo of laser and diode unit, in which the left one is laser unit and the right one is diode unit; (B) is a diagram showing the position of this laser diode system, the diameter of laser beam is about 3 mm. ..... 30
Figure 2.9 Fit curve of bubble concentration and intensity of transmitted light. Red dots are measured data with known concentration; blue curve is the fit curve calculated from Beer-Lambert law. ..... 32
Figure 2.10 Hydrophone position for measuring ultrasound wave absorption and reflection ..... 33
Figure 2.11 Acoustic pressure field measured with needle hydrophone. (A) Hydrophone placed 3 mm away from the transducer. The unit is Mega Pascal and the total area is 15mm×15 mm. (B) Hydrophone placed 6 mm away from the transducer. +: 24-well plate positioned between the hydrophone and the transducer; –: no 24-well plate positioned between the hydrophone and the transducer. ..... 34

Figure 2.12 (A) Effects of ultrasound intensity on the microbubble concentration; (B) the time took for the microbubble to reach a concentration of 0.015; and (C) the minimum concentration of microbubbles during exposure. No ultrasound was applied in the case of control. The irradiation time is 60s; PRF is 5 kHz and the pulse duration is 20 μs. The data in (B) and (C) are averaged from three independent replicates and shown as the mean ± standard deviation. ..... 39
Figure 2.13( A) Effects of ultrasound intensity on the microbubble concentration with small intensity increments; (B) the time took for the microbubble to reach a concentration of 0.015; and (C) the minimum concentration of microbubbles during exposure. No ultrasound was applied in the case of control. The irradiation time is 60s; PRF is 5 kHz and the pulse duration is 20 μs. The data in (B) and (C) are averaged from three independent replicates and shown as the mean ± standard deviation. ..... 41
Figure 2.14 (A) Effects of pulse duration on the microbubble concentration, the data after 25 seconds were not shown; (B) the time took for the microbubble to reach a concentration of 0.015; and (C) the minimum concentration of microbubbles during exposure. The acoustic intensity is 0.8 MPa; PRF is 5 kHz and the irradiation time is 60 s. The data in (B) and (C) are averaged from three independent replicates and shown as the mean ± standard deviation. ..... 45
Figure 2.15 (A) Effects of pulse duration on the microbubble concentration with smaller PRF; (B) the time took for the microbubble to reach a concentration of 0.015; and (C) the minimum concentration of microbubbles during exposure. The acoustic intensity is 0.8 MPa; PRF is 5 kHz and the irradiation time is 60 s. The data in (B) and (C) are averaged from three independent replicates and shown as the mean +/- standard deviation. ..... 47
Figure 2.16 Pulse number scaled concentration change from different pulse lengths. The details of the waves are shown by the legend with μs unit. The acoustic intensity is 0.8 MPa; the duty cycle is kept at 10%; and the irradiation time is 60 s. ..... 49
Figure 2.17 (A) Effects of PRF on the microbubble concentration, the data after 20 seconds were not shown; (B) the time took for the microbubble to reach a concentration of 0.015; and (C) the minimum concentration of microbubbles during exposure. The acoustic intensity is 0.8 MPa; the duty cycle is kept at 10%; and the irradiation time is 60 s. The data in (B) and (C) are averaged from three independent replicates and shown as the mean ± standard deviation. ..... 51
Figure 3.1 Sources of acoustic emission [80] ..... 56
Figure 3.2 An example of broadband noise [81]. The upper one is the radius time curve, the middle one is the corresponding emitted sound signal due to the radial oscillation, and the lower one is the frequency domain characteristics of the signals. ..... 57
Figure 3.3 An example plot of ‘visible noise’ [87] ..... 59
Figure 3.4 Experimental setup for cavitation noise recording system. (A) is the diagram plot; (B) is a photo of the system; and (C) is a photo of focused PVDF hydrophone and preamplifier, in which the lower unit is the focused hydrophone, the middle unit is the preamplifier, and the upper unit is the power supply for the preamplifier. ..... 63
Figure 3.5 Noise spectrum processing method. The time domain signal (A) is obtained and then transformed to frequency domain in (B). ..... 65

Figure 3.6 Cavitation noise spectrum contour of case 15 over the whole irradiation time. (A): control case without microbubbles; (B): tested case. The irradiation time is 60s; PRF is 0.05 kHz and the duty ratio is 10%. Color bar is the value of the power of frequencies after FFT with limited value range. ..... 70
Figure 3.7 Averaged emission level of case 15 over the whole irradiation time. (A): control case without microbubbles; (B): tested case. The value of frequency power is averaged value over a frequency interval, indicating by the legend. The irradiation time is 60s; PRF is 0.05 kHz and the duty ratio is 10%. ..... 71
Figure 3.8 Influence of intensity on cavitation noise, (A) frequency contour during the first 10 seconds of irradiation; (B): frequency contour during the 3rd 10 seconds (from 30 to 40 second) of irradiation; (C): the noise emissions averaged over frequency interval of 1.5 to 2.5 MHz; (D): the noise emission spectra averaged over 30 to 40 second. The irradiation time is 60s; PRF is 5 kHz and the duty ratio is 10%. Color bar is the value of the power of frequencies after FFT with limited value range. ..... 75
Figure 3.9 Peak emission level and time, the peaks of collapse emission are indicated by circles. 77
Figure 3.10 Influence of pulse duration on cavitation noise, (A) frequency contour during the first 10 seconds of irradiation; (B): frequency contour during the 3rd 10 seconds (from 30 to 40 second) of irradiation; (C): the noise emissions averaged over frequency interval of 2 to 3 MHz; (D): the noise emission spectra averaged over 30 to 40 second. The intensity is 0.8 MPa; the irradiation time is 60s; and the PRF is 0.5 kHz. Color bar is the value of the power of frequencies after FFT with limited value range. ..... 81
Figure 3.11 Increase in emission frequency when pulse duration changes from 50 μs to 500 μs. From 30 to 35 second belongs to the case of 50 μs and from 35 to 40 second belongs to 500 μs 83
Figure 3.12 Influence of PRF on cavitation noise, (A) frequency contour during the first 10 seconds of irradiation; (B): frequency contour during the 3rd 10 seconds (from 30 to 40 second) of irradiation; (C): the noise emissions averaged over frequency interval of 2 to 3 MHz; (D): the noise emission spectra averaged over 30 to 40 second. The intensity is 0.8 MPa; the irradiation time is 60s; and the duty ratio is 10%. Color bar is the value of the power of frequencies after FFT with limited value range. ..... 85
Figure 3.13 The emission level of all 7 PRF cases during 30 to 40 second ..... 87
Figure 3.14 Frequency power of 1 to 7 MHz signal of all 3 parameters averaged between 30 to 40 second ..... 89
Figure 4.1 Appearance of cultured NIH3T3 cells ..... 93
Figure 4.2 Structural formulas of dextran (A) and FITC-Dextran (B). The data are offered by the manufacturer, Sigma-Aldrich. ..... 94
Figure 4.3 TC10™ Automated Cell Counter, picture from the manufacturer ..... 98
Figure 4.4 Effects of ultrasound intensity on the delivery rate and cell viability for cells irradiated in both attachment and suspension statuses. (B) is done with small increment. DR is short for delivery rate; CV is short for cell viability; and A, V indicate attachment and suspension status, respectively. No ultrasound was applied in the case of control. The irradiation time is 60s; PRF

is 5 kHz and the pulse duration is 20 μs. The data is averaged from 4 independent replicates (12 samples) and shown as the mean +/- standard deviation. .....100
Figure 4.5 Effects of total irradiation time on the delivery rate and cell viability for cells irradiated in both attachment and suspension statuses. DR is short for delivery rate; CV is short for cell viability; and A, V indicate attachment and suspension status, respectively. No ultrasound was applied in the case of 0 s. The acoustic intensity is 0.8 MPa. PRF is 5 kHz and pulse duration is 20 μs (case 6) for (A); PRF is 0.05 kHz and pulse duration is 2,000 μs (case 15) for (B); and The acoustic intensity is 0.8 MPa; PRF is 0.5 kHz and pulse duration is 500 μs (case 23) for (C). The data is averaged from 4 independent replicates (12 samples) and shown as the mean +/- standard deviation. .....105
Figure 4.6 Cavitation noise of 3 case, (A) Noise emissions averaged over frequency intervals; (B) the noise emission spectra averaged over 30 to 40 second. The acoustic intensity is 0.8 MPa, PRF is 5 kHz and pulse duration is 20 μs (case 6); PRF is 0.05 kHz and pulse duration is 2,000 μs (case 15); and PRF is 0.5 kHz and pulse duration is 500 μs (case 23). .....107
Figure 4.7 Effects of pulse duration on the delivery rate and cell viability for cells irradiated in both attachment and suspension statuses. PRF of (A) and (B) is 5 kHz, and 500 Hz, respectively. DR is short for delivery rate; CV is short for cell viability; and ‘A’, and ‘V’ indicate attachment and suspension status, respectively. The acoustic intensity is 0.8 MPa; and the irradiation time is 30 s. The data is averaged from 4 independent replicates (12 samples) and shown as the mean +/- standard deviation. .....110
Figure 4.8 Effects of PRF on the delivery rate and cell viability for cells irradiated in both attachment and suspension statuses. DR is short for delivery rate; CV is short for cell viability; and A, V indicate attachment and suspension status, respectively. The acoustic intensity is 0.8 MPa; the duty cycle is kept at 10%; and the irradiation time is 30 s. The data is averaged from 4 independent replicates (12 samples) and shown as the mean +/- standard deviation. .....112
Figure 4.9 Delivery efficiency and cell viability of all cases for both cells irradiated in attachment and suspension status. The filled markers are for attachment status, and the blank markers with italic font legend are for cells irradiated in suspension. .....116
Figure 4.10.Therapeutic ratio for all cases. (A) is the result for cells irradiated in attachment status and (B) is the result for cells irradiated in suspension status. .....118

# List of Tables

Table 1.1 Targeted delivery methods ..... 2
Table 2.1 Bubble volume concentration and density count ..... 24
Table 2.2 Dimensions of a single well in the 24-well plate ..... 27
Table 2.3 Parameters and ranges applied ..... 29
Table 3.1 Experiment conditions ..... 67
Table 3.2 Time and value of peak emission of intensity series ..... 77
Table 3.3 Time and value of peak emission of pulse duration series ..... 82
Table 3.4 Time and value of peak emission of PRF series ..... 86
Table 3.5 Emission level comparing during 30 to 40 second of PRF series ..... 87
Table 4.1 Emission level comparing during 30 to 40 second of 3 cases ..... 108
Table 4.2 Time and value of peak emission of 3 cases ..... 108

# Biography

Yiwei ZHANG (张 祎伟) was born on February 15th, 1986 in the Province of Hubei, China. He graduated from the first high school in Xiaochang, Xiaogan, Hubei in 2003, and started study in the Department of Thermal Engineering in Beijing Jiaotong University in Beijing, China in the same year. He graduated with a Bachelor's degree in July, 2007 and then from September began graduate study in Tsinghua University in Beijing, China. He was under the supervision of Professor Shuhong LIU and Yulin WU in the Department of Thermal Engineering, and focused his research on lithotripsy. He graduated from Tsinghua University in 2009 with a Master' degree, and then flied to Japan to do his PhD research. His research work was supervised by Prof. Yoichiro MATSUMOTO in the Department of Bioengineering in The University of Tokyo, and was sponsored by a Japanese Government Sponsorship from the Ministry of Education, Culture, Sports, Science and Technology of Japan. In 2010 he went for a two month internship to the Prof. Charles Lin's group in the Wellman center for photomedicine, Massachusetts General Hospital.

# Publications

**Journal articles**

1. Y. Zhang, R. Tachibana, A. Okamoto, T. Azuma, A. Sasaki, K. Yoshinaka, K. Osada, K. Kataoka, S. Takagi, and Y. Matsumoto, “Ultrasound-Mediated Gene Transfection In vitro: Enhanced Efficiency by Complexation of Plasmid DNA”, *Japanese Journal of Applied Physics*, vol. 51, no. 7, pp. 07GF29, 1- 5, 2012.
2. Y. Zhang, R. Tachibana, A. Okamoto, T. Azuma, A. Sasaki, K. Yoshinaka, Y. Tei, S. Takagi, and Y. Matsumoto, “Ultrasound-Mediated Gene Transfection in vitro: Effect of Ultrasonic Parameters on Efficiency and Cell Viability”, *International Journal of Hyperthermia*, vol. 28, no. 4, pp. 290-299, 2012.
3. K. Yoshinaka, Y. Zhang, A. Okamato, R. Tachibana, T. Azuma, A. Sasaki, S. Takagi, Y. Tei, and Y. Matsumoto, “Microbubble-Mediated Gene Transfection by Ultrasound (マイクロバブルを用いた超音波遺伝子導入)”, *Ultrasonic Technology (超音波テクノ)*, vol. 23, no. 5, pp. 85-90, 2011. (in Japanese)

**Conference publications**

1. Y. Zhang, T. Azuma, K. Yoshinaka, A. Sasaki, S. Takagi, and Y. Matsumoto, “Effect of ultrasonic parameters on microbubble concentration during irradiation,” *2012 International Society for Therapeutic Ultrasound Symposium*, Heidelberg, 2012, No. A-329.
2. Y. Zhang, T. Azuma, K. Yoshinaka, A. Sasaki, S. Takagi, and Y. Matsumoto, “Complex Micelles Applied Ultrasound-Mediated Gene Transfection,” *32nd Symposium Ultrasonic Electronics*, Kyoto, 2011, No. 3E5-5.
3. Y. Zhang, A. Okamoto, K. Yoshinaka, A. Sasaki, S. Takagi, and Y. Matsumoto, “Ultrasound-Mediated Gene Transfection: a Comparison between Cells Irradiated in Suspension and Attachment Status,” *2011 International Society for Therapeutic Ultrasound Symposium*, New York, 2011, No. 1569401685.

# Acknowledgements

In last three years' research in The University of Tokyo as a PhD student, I worked together with several laboratories and many people. All of these people have kindly helped me to shape this thesis, and here I would like to express my thanks to all of them. There are also a few people that I would thank particularly.

First of all, I would thank my professor Dr. Yoichiro MATSUMOTO for giving me this great chance to come to Japan and pursue a doctoral degree. From the oversea video interview when I was still in China, he has always been so kind to me, and his smile has always been an encouragement.

Opinions from Professor Dr. Shu TAKAGI are always instructive. I would like to thank him for giving useful suggestions during my presentation in the weekly laboratory meeting and during many discussions.

I would like to thank my two daily supervisors. The first one is Dr. Kiyoshi YOSHINAKA. He guided me to the area of sonoporation, and had given me many detailed tips when I began to do experiments. Even after he has left the university, he kept discussing with us weekly and helping our research. The second one is Dr. Takashi Azuma, who came in 2011. His rich experience in research helped me a lot in my experiments, and I also benefited from frequent discussions with him. He also helped me in many detailed aspects such as preparing of presentation.

My thanks also go to Rie TACHIBANA and Akio OKAMOTO, two graduated master students who had been work together with me on the same topic. I also thank master student Koudai HIROSE and Kenji TAKEHARA who are current working with me for helping me doing experiments.

My grateful thanks go to Naoki SENOO for so much help on my everyday life when I first arrived in Tokyo. I would also like to thank Yunqiao LIU for always being kind to offer help. I here thank Kazuyasu SUGIYAMA, Shintaro TAKEUCHI, Ikuya KINEFUCHI, Nobuya MIYOSHI, Yuta, YOSHIMOTO, Teruyuki NISHIHARA, Taiga KOMATSU, Wataru BABA, Hiroyuki USHIJIMA, and all other

past and current members in our lab that have been together with me as well as two administrative members for being so kind to an international student.

I then thank Professor Dr. Kazunori KATAOKA and his group, especially Dr. Kensuke OSADA for helping us make polymers and for reviewing and correcting our manuscripts.

I also thank Prof. Ichiro MANABE and his group in The University of Tokyo Hospital for providing facilities for our *in vitro* and animal experiments. Many thanks go to Jack WANG, Sahohime MATSUMOTO, Michiko HAYASHI, and Ayami ONO, who not only gave lessons on cell passage and cytometry but also gave so many suggestions dealing with cells from their years' experience. Especially I would like to thank Jack WANG who carried out animal experiment together with me for checking the grammar of our manuscripts.

I would like to express my thanks to CNBI (Center for NanoBio Integration) in The University of Tokyo, which provided facilities for our experiments.

Sincere thanks to my family in China. I was sorry for going home only once in three years. While my two elder sisters and elder brother shouldered my parents, I was not responsible for my part. I wish an easier and happier life for all of them.

Finally, I would express my special thanks to wife Yun YANG for love and understanding. I hope we have a better future together.